Graduate School ETD Form 9
(Revised 01/14)

PURDUE UNIVERSITY
GRADUATE SCHOOL
Thesis/Dissertation Acceptance

This is to certify that the thesis/dissertation prepared

By Christian Eduardo Silva Salazar

Entitled
Development, Numerical Demonstration, and Experimental Verification of a Method for Model Updating of Boundary Conditions.

For the degree of Master of Science in Mechanical Engineering

Is approved by the final examining committee:

Shirley J. Dyke

Arun Prakash

Jeffrey F. Rhoads

To the best of my knowledge and as understood by the student in the *Thesis/Dissertation Agreement. Publication Delay, and Certification/Disclaimer (Graduate School Form 32)*, this thesis/dissertation adheres to the provisions of Purdue University's "Policy on Integrity in Research" and the use of copyrighted material.

Shirley J. Dyke

Approved by Major Professor(s): _____

Approved by: David Anderson 07/29/2014

Head of the Department Graduate Program Date

DEVELOPMENT, NUMERICAL DEMONSTRATION AND EXPERIMENTAL VERIFICATION OF A METHOD FOR MODEL UPDATING OF BOUNDARY CONDITIONS

A Thesis

Submitted to the Faculty

of

Purdue University

by

Christian E. Silva

In Partial Fulfillment of the

Requirements for the Degree

of

Master of Science in Mechanical Engineering

August 2014

Purdue University

West Lafayette, Indiana

ProQuest LLC.
789 East Eisenhower Parkway
P.O. Box 1346
Ann Arbor, MI 48106 - 1346

To God.

To Ximena, Tomás, Ana and María.

To my parents and sisters.

ACKNOWLEDGMENTS

Although trying to acknowledge every person that somehow has contributed to this work would be impossible, I would like to dedicate special recognition to my advisor, Dr. Shirley Dyke whose help and support beyond the academic realm have been cornerstone in conceiving, developing and finishing this thesis. I would also like to thank the faculty members of my committee who were kind enough to accept this appointment, to read and comment my thesis and to evaluate my work. A special note will be dedicated to Dr. Juan Caicedo at University of South Carolina for his contribution with the MATLAB Finite Element Toolbox used in this work, and to Dr. Arun Prakash, for his generous sharing of information for the finite element analysis.

I owe a great deal of appreciation and gratitude towards my colleagues in the IISL group; without their selfless suggestions, ideas and support, this task would have been a much heavier burden.

I will also include the SENESCYT, my home Government funding agency as an important part of this achievement. I am convinced that their commitment and support towards fellow Ecuadorian graduate students all over the globe will contribute greatly in the growth of a better Ecuador for future generations.

Special thanks will be given to the National Science Foundation, grant number NSF-CNS-1035748, the Luna-Army SBIR funding for supporting me during my studies, and the College of Engineering and the Mechanical Engineering Department at Purdue University for providing the funding for the IISL.

Finally, I will thank my family who agreed to leave everything they knew as life to embark in this adventure called Graduate School. It sure has been a learning experience for the five of us.

TABLE OF CONTENTS

Page

LIST OF TABLES

LIST OF FIGURES

Figure Page

SYMBOLS

m	mass
x	position in the horizontal axis
v	velocity
a	acceleration
ω	natural frequency
ϕ	eigenvector (mode shape)
ψ	mode shape
ζ	damping ratio
E	modulus of elasticity
I_x	second moment of area around x
I_y	second moment of area around y
I_θ	rotational inertia
G	shear modulus
k_t	linear spring constant
k_θ	rotational spring constant
β	eigenvalue (natural frequency)
A	area
w	deflection as a function of time and position
$\bar{\mathbf{k}_\mathbf{e}}$	finite element stiffness matrix
$\bar{\mathbf{m}_\mathbf{e}}$	finite element mass matrix
$\mathcal{A}$	FEM global matrix assembly

ABBREVIATIONS

kg	kilograms
m	meters
rad	radians
Hz	hertz
N	Newtons
FRF	frequency response function
IFRF	inverse frequency response function
TF	transfer function
SS	state space
FT	Fourier transform
FFT	fast Fourier transform
IFFT	inverse fast Fourier transform
DFT	Discrete Fourier transform
ERA	eigensystem realization algorithm
Re	real
Im	imaginary

ABSTRACT

Silva, Christian E. M.S.M.E, Purdue University, August 2014. Development, Numerical Demonstration and Experimental Verification of a Method for Model Updating of Boundary Conditions. Major Professor: Shirley J. Dyke, School of Mechanical Engineering.

The study of vibrations in beams has been largely addressed by authors and researchers. However, relatively few researchers have considered the case of unknown boundary conditions, as usually it is reasonable to assume the classical cases such as simply supported, clamped or free. Indeed, there are a wide variety of boundary-condition configurations, each one representing a whole different problem with its own modal characteristics.

A method for updating experimental beam models to specifically address the issue of unknown boundary conditions is proposed. This methodology takes advantage of vector comparison techniques such as the modal assurance criterion and the dot product to determine the degree of linear relationship between two mode shapes systematically and iteratively until an acceptable parametric match is found. This thesis includes the phases of development, numerical demonstration and experimental verification. In the section devoted to development, a detailed explanation of the method is given; the numerical demonstration section is intended to demonstrate the capabilities of the method using mathematical models only; and finally, in the experimental verification section, a case study example is developed using real experiment data.

At the end of this thesis, a generalized procedure is described so the method can be applied to beam-behaving structures and ultimately any engineering model in which boundary conditions have an important role.

1. INTRODUCTION

A hundred years ago, medicine relied mostly on the physical build of an individual's body and had almost no influence on one's life expectancy. However, nowadays medicine is not only a means of monitoring a person's health, but of extending a life through appropriate corrective procedures. Similarly, structures are viewed now in a different light than in the past. The life of structures can be not only monitored but also extended, if adequate monitoring techniques are used to determine a structure's condition. "The process of implementing a damage detection and characterization strategy for engineering structures is referred to as Structural Health Monitoring (SHM)" [1]. SHM utilizes techniques and results obtained from two closely related fields that work side-by-side: modal analysis and finite element model updating. "Modal analysis is the field of measuring and analyzing the dynamic response of structures when excited" [2]; and "finite element model updating is the process of ensuring that finite element analysis results in models that better reflect the measured data than the initial models" [3].

Lately, the process of building a structure, whether it is static (a building) or dynamic (a machine part), has shifted from being a one-time action that ended at the service start-date of the structure and relied mainly in the durability of the selected materials, to a more interactive process in which the initial design is one of many stages in the structure's service lifetime. Indeed, nowadays a great deal of information from the structure can be obtained which is further used for improving or correcting its behavior.

To properly predict the behavior of a structure, a suitable model must be selected. This step requires experience and some understanding of the structure's behavior. Even though many models have already been developed by engineers and researchers, no model can be picked off-the-shelf for a determined problem. Every

structure, no matter how similar it is to a previous one, has a different behavior due to uncertainties that are present from many sources: material non-homogeneities, environmental surroundings, usage, assembly discrepancies and of course, boundary conditions. Therefore, the selected model must be corrected so it can properly predict the system's behavior. This process can be a dynamic one, that is to say that the parameters of the model can be updated many times during a structure's lifespan. But to determine how much a model has to be modified or which parameter should be updated, after having some knowledge of the behavior of the structure, some sort of identification process has to be performed. Figure 1.1 shows a schematic diagram of the described processes.

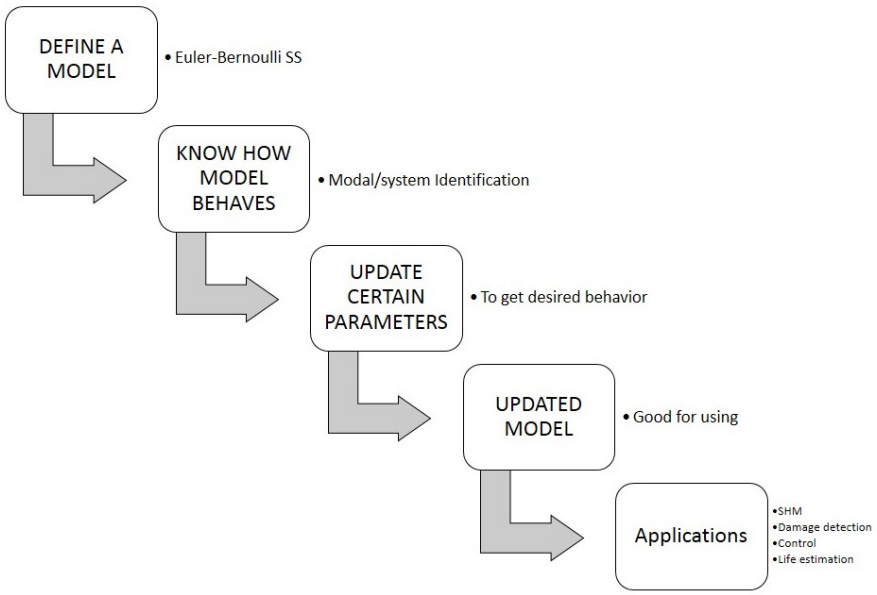

Figure 1.1. Model updating and parallel techniques.

Once a model has been selected, and the structural behavior has led to a model updating, such a structure can begin its service life and its response can start to be monitored so that its behavior is continuously compared to the predicted by the updated model. This process is called structural health monitoring, and it is among the most important subjects in civil, mechanical and aerospace engineering and has

received increasing attention from researchers and engineers in recent years. There are two different types of methodologies for health monitoring; namely, localized and global techniques [4]. Localized techniques are based on specific location analyses, such as observations and non-destructive tests performed in key locations of the structure; whereas global techniques analyze the structure as a whole, studying, for instance, its frequencies or mode shapes for determining its condition.

Modern sensor and communication technologies, as well as computational capabilities, have made it possible for an engineer to know the conditions of a structure in real-time and, therefore, since every structure is changing over time, to know with high accuracy any deviations from its intended mechanical and dynamic properties at the very moment of appearance of such deviations. The retrieved information can be used to schedule adequate and cost-effective maintenance works, to plan and execute any corrective modifications to the physical structure, and even to estimate the remaining life with a fair amount of accuracy.

Structural dynamics or modal analysis is the traditional method for obtaining dynamic properties of a given system or structure, and constitutes an important step for model updating. Several modal identification techniques have been developed, some of which will be used in the present thesis to implement the proposed method.

1.1 Overview

This project addresses the problem of a structure whose model has been partially defined. Preliminarily, a simply supported beam model has been selected, but there exist significant deviations between the model's modal information the experimental results. The idea of changing a parameter of the structure for model updating though promising, does not provide a realistic technique because of the large deviations noted above. Therefore, an alternative technique for determining a better model has to be developed beforehand.

The goal of this project is to investigate a way to provide a model updating technique that takes into account the problem of boundary conditions instead of structural parameters, and how a change in these boundary conditions will affect the behavior of the structure. The steps to achieve the proposed goal include the development of an adequate methodology for comparing modal parameters in a vectorial fashion; the verification of such a methodology with information from mathematical models only to obtain perfect matches; and, after confirming the strength of the method, the extension of the procedure to experimental data to try to obtain a mathematically close relationship between the experimental and analytical models.

The success of the present project is based in many aspects, such as the availability of analytical models already developed which only have to be compared to that of the experiment, and the vectorial form of modal parameters, either in time or frequency domain, which can be straightforwardly compared using an appropriate computer algorithm until the best match is found. Some of the assumptions made for this project are the models of the structure. A group of Euler-Bernoulli models of bending vibrations in beams are considered for the present thesis. Moreover, there are around fifty analytical cases that can be included in the comparison algorithm which constitutes a fair large analytical 'model space' to choose form. If each one of these models is tested with different parameters such as rotational inertias, linear or rotational spring stiffnesses, lumped masses, or combinations of these, the "model space" can reach several hundreds of possibilities. As any proposed technique, the methodology of this thesis is not exempt from risks and obstacles, such as the travel from the continuous domain to the discrete domain in the experimental setup. A beam is to be tested by the use of a finite number of sensors which will not replicate the continuous behavior exactly, leaving a space for uncertainties and unknown parameters. Nevertheless, the proposed method is not a model validation technique, but more of a model updating technique which instead of modifying parameters of a set model, shifts to a different model (beam model + boundary conditions) within

a reasonable error margin. For this study, four beam models have been chosen: two classical and two non-classical, which are listed below:

- Simply-supported: both ends are pinned with translation constraints in x, y and z.
- Clamped-clamped: both ends are fixed with translation and rotation constraints in x, y and z.
- Partial elastic supports: ends are pinned and have rotational springs of constant $k_{\theta i}$ on both ends $(i = 1, 2)$.
- Mixed inertial supports: pinned ends with inertial rotational masses of constant $I_{\theta i}$ on both ends $(i = 1, 2)$.

The thesis is divided in three sections: Development of the Method; Numerical Validation and Experimental Verification

The first section includes Chapters 2, 3 and 4. Chapter 2 is a short review of related literature; Chapter 3 includes some of the theoretical background on which the thesis is based; and the basics of the method are explained in Chapter 4. The second section is composed of Chapters 5 and 6. In Chapter 5, three mathematical models are developed using both analytical and finite element methods for understanding the mechanics of boundary condition changes in beams. To ensure the functionality of the method, Chapter 6 shows how the method works with data collected through simulations from analytical models. The third section includes Chapters 7 and 8. In Chapter 7 a short description of the structure designed for this study is developed, whereas Chapter 8 deals with the application of the method with an experimental example. Final chapters devoted to conclusions and future directions of research are included outside of the mentioned sections.

1.2 Purpose of Project

The specific purpose of this project is to develop a method for model updating which iteratively compares the response of a structure with the responses of a group of selected structures whose models have been preselected. The aim of such comparison is to detect the highest correlation between the case study model and any of the selected models.

The proposed method is a very interesting approach because it can be applied using a "solution space" or "model space", which can be of any finite size. All of the elements of this "model space" are compared to the specimen model (case study) one by one to construct a correlation vector or matrix which, if further analyzed, determines which model is more likely to be generating such a response. At this point, it is important to make a clarification: although the proposed method tries to correlate so-called 'models', this is indeed a model updating methodology a bit away from traditional model updating techniques inasmuch as the parameters that are tried to be correlated are boundary condition parameters, instead of a structural physical parameters. Consider for example a model with the mass, stiffness and damping matrices, $\mathbf{M}, \mathbf{C}, \mathbf{K}$ respectively are modified accordingly for model updating using a least squares approach so that the model matches some experimental behavior; the proposed technique will not change any beam structural parameters directly (such as $\mathbf{M}, \mathbf{C}$ or $\mathbf{K}$), but some boundary-condition parameters (such as a spring constants or rotational mass inertias or lumped masses at fixed points) to obtain the same desired behavior. This constitutes a novel idea since boundary conditions are more likely to be the reasons for a model deviation instead of intrinsic material structural matrices.

For the case of this thesis, only four models were studied and used as reference, two of which had variable parameters to construct a fair large model space for comparison, but in a real life case, many more can be used. Consider for example the case of a beam with a concentrated mass at midspan and a distributed load along its length: The first most intuitive model that can be considered is a simply-supported

beam with a lumped mass at midspan, but if after performing modal testing on this hypothetical structure an engineer realizes that its parameters don't match those of his first selected model, he has to repeat the modeling process over and over again until a good approximation appears, resulting in a very tedious time consuming process. On the other hand, by using the proposed method, it is only matter of running a set of correlation analysis modifying the combinations lumped mass/concentrated load until a high enough index is obtained which is an indicative of the closest mathematical match.

PART I: DEVELOPMENT

2. LITERATURE REVIEW

2.1 The Vibration of Euler-Bernoulli Beams with Different Boundary Conditions

The vibration of beams with classical boundary conditions is a topic that has been widely covered by various authors, both in books and scientific articles. However, when non-classical boundary conditions are present, the available bibliography becomes rather limited. Analytical solutions of the beam problem with simple boundary conditions such as pinned, fixed and sliding configurations were addressed in books by Meirovitch [5], Karnovsky [6], Gorman [7] and Blevins [8], just to cite a few.

Although general boundary conditions such as combinations of pinned, fixed and sliding ends appear to be simple cases, these are nothing but special cases of more complex analyses involving elastic boundary conditions in the form of springs, both linear and rotational, located either at the ends of a beam, or at intermediate points. For instance, a simply-supported beam is a special case of a beam resting on linear springs of infinite stiffness which provide the translational constraint in the x, y and z directions, and rotational springs both of zero stiffness which provide the free rotation around the y axis and rotational springs of infinite angular stiffness which provide the rotational constraints around the x and y directions. Several studies have been published on these types of constrained beams. Hibbeler [9] considered the vibration of a beam limited at both ends with rotational springs of different stiffnesses, although his results were later corrected by himself [10], and documented by several other authors like Goel [11] and Rao et al. [12]; Chun [13] derived the eigenvalues and eigenvectors of a vibrating beam with one end constrained by rotational and translational springs, and the other end free, whereas Lv et al. [14] and Kang &

Kim [15] studied general boundary condition cases. For the case of a mass-beam system, i.e., a beam with a mass at a certain distance from the origin, Goel [11] developed both analytical equations and eigenfrequency tables for different spring constant rates. Many other authors developed related works involving mass-beam systems; some examples are the publications by Register [16], Yen [17], Goel [11] and Laura et al. [18]. Maurizi, along with other researchers, developed an extensive work on vibrations of beams publishing several articles. Maurizi studied a case where a beam is constrained with a rotational spring on one end, and a translational spring on the other; i.e., mixed boundary conditions on the same beam [19]; other case was a beam with elastic constraints on both ends subjected to free or forced vibrations [20]; and he even did a review of many boundary condition cases published by previous authors [21]. All these cases are more realistic scenarios for boundary conditions to which structures are subjected on a daily basis. One good example of a problem where boundary conditions are not ideal is an emergency deployable bridge structure which is 'placed' over the connecting points without any soil or ramp preparation. In this case, no information about boundary conditions is available despite the fact that these boundary conditions are precisely the parameters which give the system its natural characteristics. Moreover, these boundary conditions will most likely change on a regular basis due to usage, weather conditions and material degradation. Another example is a beam connected to rigid supports by pins (simply-supported) in which the pin-hole assembly deviates from its design leading into unknown forcing moments. As the reader can imagine, boundary conditions are a very delicate problem that has to be addressed with the maximum of accuracy in a real-life structure.

The previous literature review dealt with general analytical and numerical methods for solving the governing equations along with the boundary condition equations. However, there is also a great deal of research regarding alternative methods for solving the problem of vibrations of beams with both classical and elastic constrained ends. One of these methods is Fourier series. A general methodology for structural

vibration problems using Fourier series was published by Greif and Mittendorf in 1976 [22]. Li [23] solved the problem of vibration of a generally supported beam by combining Fourier series and an auxiliary polynomial function. Wang [24] solved this problem in a similar way, but also using Stoke's transformations for the derivatives in the boundary conditions; and more recently, Yayli et al. [25] and [26] extended this approach for elastically-constrained ends and elastic foundation, which are not covered in the present thesis.

Other alternate methodologies, for solving the vibration problem of an Euler-Bernoulli beam subjected to various boundary condition combinations were used by Lai et al., [27] and Mao [28]. They used an Adomian decomposition to transform the governing differential equation of a beam into a recursive algebraic equation which converts the boundary conditions into simple algebraic equations suitable for symbolic computation. Although the mathematical effort to derive the frequency equations is not very straightforward, once these have been obtained, this method becomes very simple when a different boundary condition case is to be analyzed, making the overall process easier and less time consuming.

So far, the cited bibliography referred only to continuous beams. Many publications are available for the problem of vibrations of discontinuous beams. Failla and Santini [29] proposed a solution method for beams with internal translational and rotational springs whose work was based primarily in Billelo and Bergman's study of crack modeling using internal rotational and translational springs [30]. Other good examples of this approximation for cracks on beams with springs are the studies by Raffo and Carrizo which introduced the solution of an inverse problem for beams and frames under presence of cracks [31]; Wang & Qiao, who proposed a Laplace transform approach for the solution of the governing equations [32]; and Ratazzi et al., who extended their work for frames with internal hinges [33]. A variation of discontinuous beams is the case of multispan beams. Several authors covered special cases

of multi-span beams with intermediate supports. Again, Karnovsky, [6], Gorman [7] and Blevins [8] devoted separate chapters in their books for single, double, triple, quadruple and multi-span beams with combined boundary conditions and even with inter-span spring connections.

Some cases of cantilever beams are covered but as particular cases of more general ones. A rather large amount of publications have been made regarding to cantilever beams as well. Also, this literature deals with problems in which the authors use a combination of analytical and numerical methods for solving the equations. For example, in most cases, the governing partial differential equation of the beam is solved using the principle of separation of variables. However, once the equation of frequency is obtained, this is usually a transcendental equation whose solution cannot be found analytically and a numerical method like bisection or Newton-Raphson has to be used for root-finding. Moreover, approximate methods have been used also to solve the complete problem, in the form of finite element analysis. Meirovitch [5] devotes a chapter of his book for describing the finite element method as a means of modal analysis using the Rayleigh-Ritz method and both linear and higher degree interpolation functions. Other good sources for theoretical background and practical implementation of finite element analysis in vibration problems are the books by Courant [34], Huebner [35] and Zienkiewicz & Taylor [36].

2.2 Modal Analysis

Modal analysis is a foundational section of system identification. "It is a process of analysis of the vibratory behavior of structures and systems by means of theoretical or technical techniques. The ultimate goal is the determination of a structure or system modal parameters for further constructing a mathematical model of such a system," [37] with the objective of "determining, improving and optimizing dynamic characteristics of engineering systems and structures" [38]. It has spread so widely

that numerous methods for modal identification have been developed and published by authors throughout the last four decades [38] [39].

Brown & Allemang [40] considered that modal analysis is founded in two main historical scientific breakthroughs: the decomposition of solar spectrum in its color components made by Newton, and the subsequent decomposition of arbitrary functions into its simple harmonic components made by Fourier. However, it wasn't until the mid twentieth century where modal analysis started to gain academic and industrial interest due to the necessity of understanding the vibrations on airplanes, machine tools and vehicles. The introduction of the fast Fourier transform method by Cooly & Tukey [44] could be considered a turning point of the fast development and increasing popularity of modal analysis as a previous step for various applications, such as damage detection, structural health monitoring, structural control and structural design. It is not the intention of the present thesis to do a historical review of modal analysis, but to cite just a few relevant findings in the area. As a consequence of the popularity of the field, many books have been published like the ones by Mendez Maia [41], Ewins [42] and Fu & He [43].

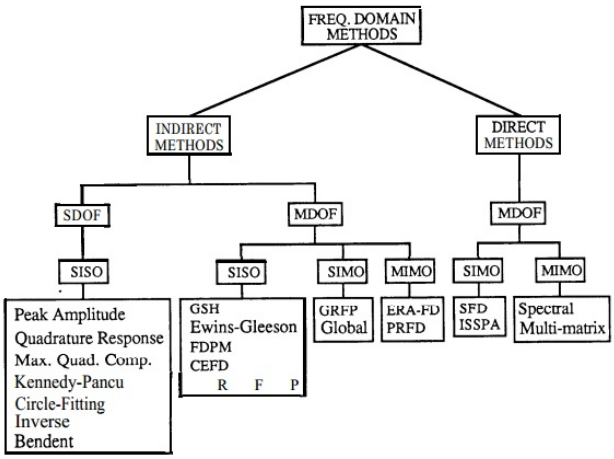

Figure 2.1. Frequency-domain methods, (from [50]).

There is a wide list of modal analysis techniques developed recently and a brief description of these will be made herein. Nevertheless, it will be helpful to provide the big picture of modal identification methods. The experimental direction frequently used by researchers is to collect acceleration, velocity or position data from a sensor (output), when an excitation (input) has been imposed to the structure to obtain, after proper analysis, an input/output relationship called transfer function (TF) which contains the modal characteristics of the structure (frequencies, mode shapes and damping ratios) or the mechanical characteristics of the system (mass and stiffness). Excitations can be as varied as ambient (traffic, wind, plant noise), impact (instrumented hammers or exciters), known functions (harmonic, step, earthquake history), etc. Modal analysis can be performed both in the time-domain and in the frequency-domain. These two main divisions can also be sub-divided into direct and indirect methods; Figures 2.1 and 2.2 depict an overall idea of most of the available methods. Frequency domain methods use the frequency response function (FRF) information and time-domain methods use finite element analysis or the inverse FRF which is nothing but the inverse fast Fourier (IFFT) transform of the FRF.

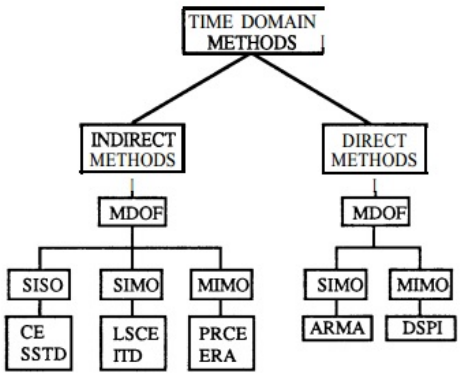

Figure 2.2. Time-domain methods, (from [50]).

2.2.1 Frequency-Domain Methods for Modal Analysis

Frequency-domain modal analysis uses a mathematical model that represents the frequency response function (FRF) data from measurements. An analytical expression of the FRF or commonly known as transfer function, as a partial fraction expansion can be given by:

$$H(\omega) = \sum_{r=1}^{N} \frac{\mathbf{A_k}}{i\omega - \beta_k} + \frac{\mathbf{A_k^*}}{i\omega - \beta_k^*} \tag{2.1}$$

where $\mathbf{A_k}$ is the modal constant matrix with components ${}_rA_{ij}$ related to components ϕ_{ik}, ϕ_{jk} of eigenvector k through the formula:

$${}_rA_{ij}a = q_k\phi_{ik}\phi_{jk} \tag{2.2}$$

and q_k is a modal participation factor. Index k indicates the k-th mode and the poles in the denominator can be obtained by solving the characteristic equation

$$\beta_k, \beta_k^* = -\omega_k\zeta_k \pm i\left(\omega_k\sqrt{1-\zeta_k^2}\right). \tag{2.3}$$

This implies that most frequency-domain methods take advantage of the information given by a transfer function to derive the modal characteristics of a linear time-invariant system. Combinations of inputs, outputs and locations lead to a set of FRF's. The most commonly used frequency-domain techniques for modal identification are peak-picking, circle fit, inverse FRF, least squares and Dobson's method.

The simplest frequency-domain method for identifying modal parameters is the peak picking method, whose idea is to manually pick the peaks of the FRF which correspond to the resonance frequencies. The damping ratios can be estimated by evaluating the sharpness of such points; and the mode shapes, from the relation between peak amplitudes in the structure [45]. This method was proposed by Bishop & Gladwell [46]. Unfortunately, this approach works fine for well separated and

clear modes whereas for complex structures that mix lateral with torsional modes may not be very efficient. Nevertheless, it is very popular due to its simplicity and implementation time. The present work utilizes also this method for mode verification and elimination of torsional modes by observations made in the imaginary part of the transfer function. This method is shown in Fig. 2.3.

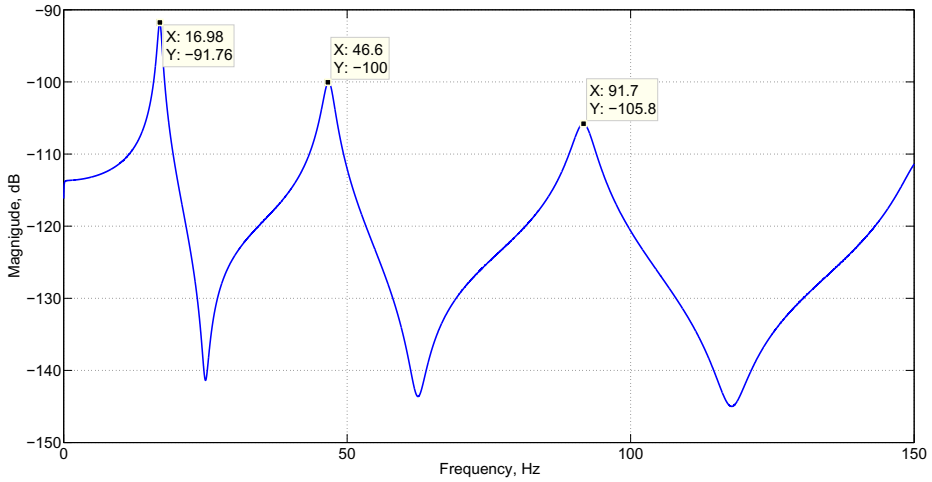

Figure 2.3. Modes manually picked from a frequency response function.

Another important method developed by Kennedy [47] is the circle fit, which uses the relationship between real and imaginary part of a transfer function around each natural frequency to identify modal parameters of the system. This method's basic idea is that the receptance FRF $\alpha(\omega)$ traces a perfect circle on the Nyquist plane, and where h is a measure of structural damping.

$$[Re(\alpha)]^2 + \left[Im(\alpha) + \frac{1}{2h}\right]^2 = \left(\frac{1}{2h}\right)^2. \tag{2.4}$$

A very interesting approach for modal estimation is derived from the properties of the inverse of the frequency response function (IFRF) which are nothing but the Bode plots presented by Dobson [48]. By plotting the real and imaginary parts of the IFRF versus frequency and after curve-fitting them, the modal parameters can

be estimated by simple inspection; indeed, the intercept point of the real part with the real axis provides the natural frequency; either the slope or the ratio of the two slopes provide both the phase and the magnitude of the modal constant; and any of the plots provide an estimate of the damping ratio. Dobson also developed a second method, this time called the "Dobson method" which takes advantage of the complex modes and corrects for neighboring ones [49]. The aforementioned methods are just to cite the few most important covering the frequency-domain direct methods. Mendez Maia in his PhD dissertation [50] presents a very thorough summary of the available indirect methods which are reproduced here for the reader's convenience: the Gaukroger-Skingle-Heron (GSH) [51], Ewins Gleeson [52], Frequency-Domain Prony (FDPM) [53], the Complex Exponential FD method [54], the Eigensystem Realization Algorithm in the Frequency Domain (ERA-FD) [55], the Rational Fraction Polynomial (RFP), the global RFP mentioned in [56], the Global Method [57] and the Polyreference Frequency Domain Method (PRFD) [58].

Among the direct-methods is a smaller number of techniques, both for single-input single-output (SISO) and multiple-input multiple output (MIMO) systems. These include the Simultaneous Frequency Domain method (SFD) introduced by Coppolino [59]; the Identification of Structural Parameters method (ISSPA) by Link [60]; the Spectral method by Klosterman [61]; and the Multi-Matrix method, developed by Leuridan [69].

2.2.2 Time-Domain Methods for Modal analysis

So far, a brief description and references of many of the available frequency-domain modal analysis methods has been provided. On the other hand, several time-domain methods are also available, some of which have gained great popularity due to current computational availability. These methods rely on time response data in the form of acceleration, velocity or displacement history. It should be noted that within

this category, many methods use the information from the inverse fourier transform (IFFT) to take advantage of the averaging of most of the frequency-domain techniques and thus reducing noise implications. Within this category the most popular direct methods are the Complex Exponential (CE) for local identification, and the Least Squares Complex Exponential (LSCE), which is an extension of the CE method for global identification, both proposed by Spitznogle and Quazi [64]. Vold and Rocklin [65] extended the previous method which is for SISO systems to a more versatile MIMO version called the Polyreference Complex Exponential Method (PRCE), whose principal improvement was the fact that it could reveal hidden modes due to input locations near nodal points. Perhaps one of the preferred time-domain methods up-to-date is the Ibrahim Time Domain Method [66], not only for its integration with the state-space representation of the equations of motion and consequently with Control Theory, but also because it was a foundation for the development of further matrix methods for modal identification such as the ERA. Among the direct methods one can find a couple of popular ones; namely the Auto Regressive Moving-Average method (ARMA), based on Gersch's [67] work; and the Direct System Parameter Identification method (DSPI) developed by Leuridan [69]; both of which include statistical analysis as an assurance criteria.

2.3 Modal Correlation

Modal testing has provided researchers the means of obtaining modal parameters from experimental information collected from a wide range of setups. However, all the collected information needs to be compared with the chosen mathematical model to define, with a fair amount of certainty, the desired behavior of the system. This comparison between observed results and expected ones is called correlation; in this particular case, modal correlation is the link that connects analytical and experimental structural dynamics and mechanical vibrations. The most popular modal parameter correlation is called modal assurance criteria (MAC), which is basically a

squared linear regression coefficient based on the Cauchy-Schwartz inequality and was first proposed by Allemang in 1980 [71]. As Allemang wrote: "The historical development of the modal assurance criteria originated from the need for a quality assurance indicator for experimental modal vectors that are estimated from measured response functions" [71], and whose intended purpose was orthogonality checks. Since then, many modal assurance methodologies have been developed depending on the specific correlation analysis that needed to be performed. These include the coordinate modal assurance criterion (COMAC), frequency response assurance criterion (FRAC), frequency-scaled modal assurance criterion (FMAC), partial modal assurance criterion (PMAC), scaled modal assurance criterion (SMAC) and reciprocal modal vector assurance criterion (RVMAC.) Some of these methods will be briefly described herein. Validation of experimentally-obtained modal parameters such as mode shape vectors or natural frequencies can be performed both in vector or scalar fashion; the former, through calculating the complex modal scale factor; and the latter, through a scalar measure of vector consistency. The vectorial correlation technique is called modal scale factor (MSF), whereas the scalar is called modal assurance criterion. These two correlation approaches are defined in Eqns. (2.5) and (2.6), for two arbitrary vectors ψ_a and ψ_b.

$$MSF = \frac{\psi_a \psi_b}{\psi_b \psi_b}. \tag{2.5}$$

$$MAC = \frac{|\psi_a \psi_b|^2}{(\psi_a \psi_a^T)(\psi_b \psi_b^T)}. \tag{2.6}$$

The COMAC utilizes both the mode shape vector and the natural frequency, called together mode pairs, to verify linear relationship between modes either experimental or analytical (similar to Chapter 6). However, its direction is more towards identifying which DOF of the measurements contribute negatively to a low value of MAC. It

was developed by Lieven [72] in 1988.

Various authors extended this methodology to the frequency-domain. Heylen & Lammens proposed a similar technique to compare, not modal vectors but frequency response function vectors using also a squared linear regression coefficient [75]; such method took the name of frequency response assurance criterion (FRAC), and later Fotsch & Ewins introduced a frequency scaling upgrade to the MAC method "such that the mode shape correlation, the degree of spatial aliasing and the frequency comparison can be displayed in a single plot" [74]. In their proposed methodology, graphical representations of the mode shape correlations with circles of diameters equal to the MAC values are compared in a chart such that related modes would appear in the form of a 45° line with big dots and non-correlated modes will appear as smaller dots spread throughout the plot. Specialized extensions of the MAC are used commonly when only a desired part of the information is needed. For such cases, Heylen & Janter proposed the partial modal assurance criterion (PMAC), and the spatial modal assurance criterion (SMAC) [75]. The former is used to correlate parts of modal vectors, and it is specially useful when computational efficiency needs to be achieved by disregarding non-relevant information; the latter compares vector spaces; that is to say that the SMAC is the least squares solution of a vector transformation equation as follows:

$$\psi_e = \psi_a \mathbf{Q} \tag{2.7}$$

where $\mathbf{Q}$ is the transformation matrix.

$$SMSF = (\psi_a^T \psi_b^T)^{-1} (\psi_a^T \psi_b^T). \tag{2.8}$$

Equation (2.8) represents the least squares solution of Eq. (2.7), minimizing $\|\psi_b - \psi_a \mathbf{Q}\|$.

When rotational degrees of freedom are used, a special scaled MAC was proposed by Brechlin et al., where the weighting matrix is such that it balances the scaling of translational and rotational DOF's in the modal vectors [76].

There is also a great deal of research on damage detection approaches using the Cauchy-Schwartz inequality. Messina proposed an assurance criterion-based method for detecting damage locations called the Damage Location Assurance Criteria (DLAC), and later upgraded his method to quantify such damage calling it the Multiple Damage Location Assurance Criteria (MDLAC) [77] [78]. Koh & Dyke extended this work by adding information from the sensitivity matrix to the formulation and used genetic algorithms in an effort to obtain a computationally-efficient algorithm for vector comparisons [79]. While both Messina's and Koh's work used natural frequency shift vectors as comparison criteria, Pandey & Biswas used mode shape information to determine location and amount of damage [80].

It is clear that the method proposed herein has a close relation to those cited above but with a different scope than to determine damage in structures. However, the conception of the proposed method in this thesis is quite similar inasmuch as both approaches propose an iterative comparison of vectors.

In the present thesis, the use of a model-correlation-based method will be used only for comparison of experimental and analytical mode shape vectors; therefore, to construct a mapping matrix between analytical and experimental mode shapes. As many of the MAC formulations use Hermitian matrices instead of transposed ones, this proposed formulation will deal only with real mode shape vectors. Should a case where complex modal vectors arise, the formulation must be corrected accordingly.

3. THEORETICAL BACKGROUND

3.1 Introduction

The identification method used for the completion of this thesis is peak-picking on FFTs. Although there is a vast variety of techniques available, such a technique was selected for its simplicity and ease of application. Also, because the identification step is not the central topic of the present work. In this section, the theoretical background of these two methods is explained in detail.

3.2 The Fourier Transform

The Fourier Transform is a basic mathematical resource in signal processing. Its essential purpose is to decompose any signal or function into sinusoidal components in an interval from $-\infty$ to $+\infty$. Since real-life signals are finite, a couple of good artifices are used to transform finite signals into infinite ones: the first is to transform the finite signal into periodic by adding itself to the right and left of the original signal; and the second, is to add zeros to the left and right of the original signal. Consider an arbitrary function $x(t)$, the Fourier transform (FT) is defined as:

$$\mathcal{F}\{x(t)\} = X(w) = \int_{-\infty}^{+\infty} x(t)e^{-i\omega_n t}dt. \tag{3.1}$$

Note that the FT is a function of the frequency ω. Subsequently, the Inverse Fourier Transform (IFT) is defined as:

$$\mathcal{F}^{-1}\{X(\omega)\} = x(t) = \frac{1}{2\pi}\int_{-\infty}^{+\infty} X(\omega)e^{i\omega_n t}dw. \tag{3.2}$$

The previous formulation is theoretical and intended for a continuous signal which is not the case in real life. For discrete signals that occur through sampling, instead

of a continuous time t, a time step $t_k = k\Delta t$ is used. The equivalent FT of such discrete system is:

$$X_n = \sum_{k_0}^{N-1} x_k e^{-i\omega t} \tag{3.3}$$

where $\omega t = \frac{2\pi}{N} nk$. The sampling frequency is defined as:

$$f_s = \frac{1}{\Delta t}. \tag{3.4}$$

Only half of the signal representation by the FT is useful due to the Nyquist-Shannon theorem which states that the maximum frequency represented by a discrete signal is equal to half the sampling frequency with which it was generated, i.e.,

$$f_s \geq 2f_c \tag{3.5}$$

where f_s is the sampling frequency, per unit of time (Hz), and f_c is the highest frequency contained in the signal. The inverse Discrete Fourier Transform (IDFT) is defined as:

$$x_k = \frac{1}{N} \sum_{n=0}^{N-1} X_n e^{i2\pi \frac{k}{N} n}. \tag{3.6}$$

For this thesis, the MATLAB function fft.m and ifft.m are used which are based on the Fast Fourer Transform, a method that breaks the DFT into smaller size DFT couples for a faster calculation.

3.3 Frequency Response Function

Consider the single degree of freedom mass-spring-dashpot system depicted in Fig. (3.1), whose equation of motion is:

$$m\ddot{x} + c\dot{x} + kx = f(t). \tag{3.7}$$

The Laplace transform of such a system is:

$$ms^2X(s) + csX(s) + kX(s) = F(s). \tag{3.8}$$

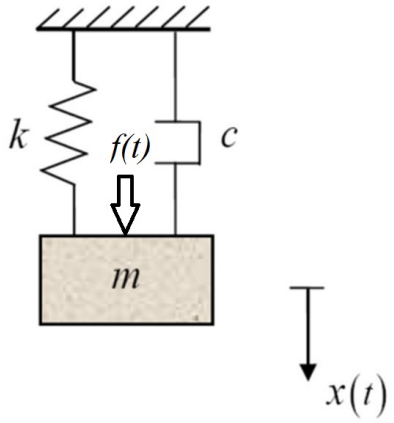

Figure 3.1. Single DOF system.

Isolating $X(s)$, yields:

$$X(s) = H(s)F(s) = \frac{1}{ms^2 + cs + k}F(s) \tag{3.9}$$

where m is the mass, c is the damping coefficient, and k is the spring stiffness. The expression of $H(s)$ in Eq. (3.9) is the frequency response function (FRF) or transfer function (TF) of the system. Assuming $s = i\omega$, one has:

$$H(i\omega) = \frac{1}{m\omega^2 + ci\omega + k}. \tag{3.10}$$

From this expression, one could obtain the original function very straightforwardly by applying the inverse Laplace transform.

$$x(t) = \mathcal{L}^{-}1\left\{\frac{1}{m\omega^2 + ci\omega + k}F(s)\right\}. \tag{3.11}$$

From the Laplace transform tables is known that for a second order system:

$$\mathcal{L}^{1}\left\{\frac{1}{(s+\alpha)(s+\beta)}\right\} = \frac{1}{\beta - \alpha}[e^{-\alpha t} - e^{-\beta t}] \tag{3.12}$$

then,

$$\begin{aligned} \alpha &= \frac{c - i\sqrt{4mk - c^2}}{2m} \\ \beta &= \frac{c + i\sqrt{4mk - c^2}}{2m}. \end{aligned} \tag{3.13}$$

Assuming an under-damped system and an impulse input [$f(t) = \delta(t) \rightarrow F(s) = 1$],

$$x(t) = \frac{1}{m(\beta\alpha)}[e^{-\alpha t} - e^{-\beta t}]. \tag{3.14}$$

Finally, defining $k = m\omega_n^2$, $c = 2m\omega_n\zeta$, and $\omega_d = \omega_n\sqrt{1-\zeta^2}$, the original function $x(t)$ is:

$$x(t) = \frac{1}{m\omega_d}e^{-\zeta\omega_n t}[\sin(\omega_n t)]. \tag{3.15}$$

The FRF describes the response of the system to arbitrary inputs.

3.4 The Peak Amplitude Method

Once the FRF of a system has been determined, and its frequency peaks are visually available, a straightforward method of modal identification is used: the peak amplitude method which takes advantage of the property of frequency domain functions to provide a single spike for each frequency content (in ideal cases). After a peak has been selected, and with the aid of the half-power method, the modal parameters can be estimated according with the following procedure:

1. The damping ratios can be estimated by evaluating the steepness of each peak, the steeper the peak, the lighter the damping ratio.

2. The natural frequency of each peak is determined by inspection of the frequency axis of the FRF plot.

3. The mode shapes can be estimated by the relative amplitudes of peaks at different locations of the structure (each sensor determines one location). Therefore, the greater the resolution, the better the mode shape estimation.

Figure (3.2) shows the half-power technique for modal parameter estimation [84], where Q represents the amplitude of the peak at the resonance frequency, points R_1 and R_2 are the half-power points used to define the bandwidth of the system.

Mode shapes are going to be estimated using the complex feature of the FRF. As a complex function, the imaginary part of such function gives useful information

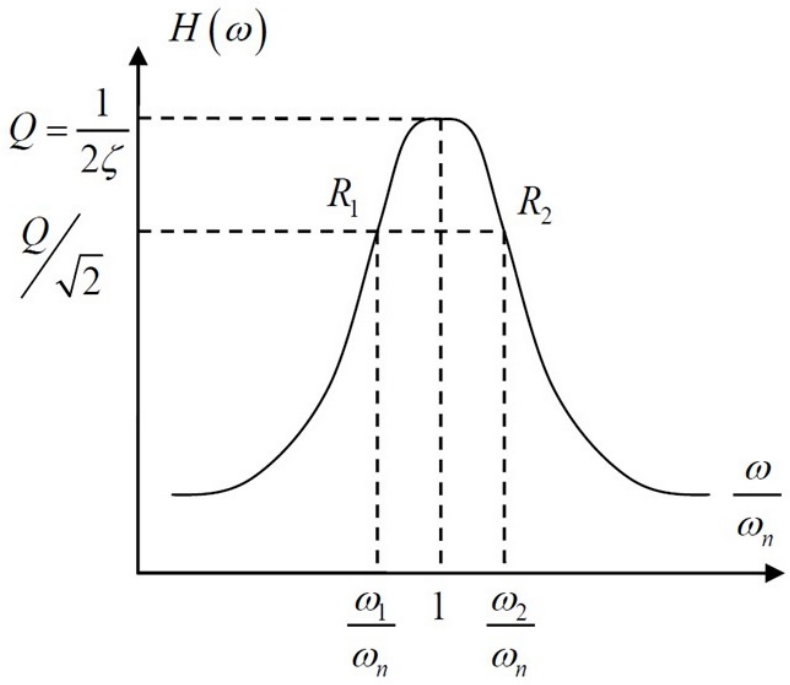

Figure 3.2. The half-power method.

about the phase and relative magnitude of the peaks in each sensor location of the structure, providing important insights about the mode of vibration at the frequencies of interest. Consider the FRF matrix row shown in Fig. 3.3 which corresponds to a cantilever beam with three accelerometers. The relative amplitude of each sensor along with its phase (above or below the horizontal axis) determine the mode shape of the first degree of freedom (corresponding to the first peak occurrence) drawn in blue. If a similar procedure is done for the second, third, and so forth set of peaks, a set of mode shape vectors is obtained. It must be noted that appropriate resolution has to be selected to determine as clear and accurate as possible mode shapes and to avoid aliasing. An alternative technique to the aforementioned is to display the imaginary part of all the transfer functions generated by each accelerometer in parallel fashion,

known as a waterfall plot. This representation allows the analyst a much clearer view of the big picture for each mode.

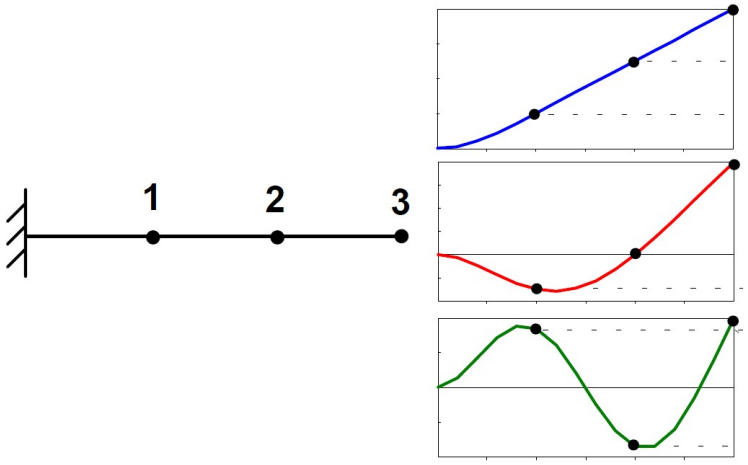

Figure 3.3. Estimation of the first three mode shapes of a cantilever beam with three sensor locations.

4. A CORRELATION METHOD

The proposed correlation technique is explained in this chapter. As stated above, the related mathematical principle used for this development is the Cauchy-Schwartz inequality, which states that for all vectors x and y of an inner-product space it is true that:

$$|\langle x, y\rangle|^2 \leq \langle x, y\rangle \cdot \langle y, y\rangle. \tag{4.1}$$

Therefore, the relationship between the left side and the right side of the inequality is always less than or equal to unity.

$$\frac{|\langle x, y\rangle|^2}{\langle x, y\rangle \cdot \langle y, y\rangle} \leq 1 \tag{4.2}$$

which can be used as a suitable correlation index between vectors x and y.

4.1 Correlation based on the Modal Assurance Criterion

The correlation method proposed herein is the application of such inequality which is a squared linear regression correlation coefficient used originally for orthogonality checks. This coefficient is very sensitive to large differences between the comparing vectors (squared error minimization) and consequently, not very sensitive to small changes. This indicator provides a means for comparing vectors originated in different sources: e.g., a FEM-originated modal vector versus an experimentally-originated one; or any other source. Therefore, no analytical model is needed for this methodology to work.

The **modal assurance criterion** is defined as the relationship between the degree of linearity between two vectors, in this case two modal vectors: one reference and one experimentally-obtained. The equation for this relationship is:

$$MAC = \frac{|\langle \psi_a \psi_e \rangle|^2}{\langle \psi_a \psi_a^T \rangle \langle \psi_e \psi_e^T \rangle} \tag{4.3}$$

where ψ_a and ψ_e are the vectors which relation is to be studied, and the T superscript refers to 'transposed'. The modal assurance criterion is a scalar value from zero to one. Zero represents no correlation whatsoever and a MAC value of unity represents a consistent correspondence. The modal assurance criterion is an indicator of consistency only, that is to say that it will indicate whether two vectors are similar or not; but it will not indicate if a given vector is correct or valid. Therefore, the use of an analytical or finite element generated reference vector is always recommended to provide a valid analysis.

The comparison procedure has two sides: on one side, the first n mode shapes along with the first $n-1$ stacked mode shapes, producing a group of $2n-1$ vectors, all obtained in an analytical or approximated fashion; on the other, the $2n-1$ vectors obtained experimentally. This will yield a $(2n-1) \times (2n-1)$ mapping matrix with elements between zero and unity.

Consider vectors ψ_1, ψ_2 and ψ_3 to be the first three mode shapes of an arbitrary structure, using r sensors as the experiment's resolution:

$$\psi_1 = \begin{Bmatrix} a_1 \\ a_2 \\ \vdots \\ a_r \end{Bmatrix} \qquad \psi_2 = \begin{Bmatrix} b_1 \\ b_2 \\ \vdots \\ b_r \end{Bmatrix} \qquad \dots \qquad \psi_n = \begin{Bmatrix} n_1 \\ n_2 \\ \vdots \\ n_r \end{Bmatrix}. \tag{4.4}$$

A pre-correlation array is formed by combining the selected number of mode shapes along with these same mode shapes successively arranged in a stacked fashion: the first stacked vector will include the first two mode shape vectors; the second stacked vector will include the first three mode shape vectors, and so forth.

$$\hat{\psi}_1 = \begin{Bmatrix} a_1 \\ a_2 \\ \vdots \\ a_r \end{Bmatrix} \; \hat{\psi}_2 = \begin{Bmatrix} b_1 \\ b_2 \\ \vdots \\ b_r \end{Bmatrix} \quad \ldots \hat{\psi}_n = \begin{Bmatrix} n_1 \\ n_2 \\ \vdots \\ n_r \end{Bmatrix} \; \hat{\psi}_{n+1} = \begin{Bmatrix} a_1 \\ a_2 \\ \vdots \\ a_r \\ b_1 \\ b_2 \\ \vdots \\ b_r \end{Bmatrix} \quad \ldots \hat{\psi}_{2n-1} = \begin{Bmatrix} a_1 \\ \vdots \\ a_r \\ b_1 \\ \vdots \\ b_r \\ \vdots \\ n_1 \\ \vdots \\ n_r \end{Bmatrix}. \tag{4.5}$$

In Eq. (4.5), $\hat{\psi}_i$ represents pre-correlation mode shape vectors. The reference array must have the same structure so a MAC calculation can be performed between the two to obtain a correlation matrix of the following structure:

$$CM = \left[\begin{array}{cccc:cccc} \psi_1 r_1 & \psi_1 r_2 & \ldots & \psi_1 r_n & 0 & 0 & \ldots & 0 \\ \psi_2 r_1 & \psi_2 r_2 & \ldots & \psi_2 r_n & 0 & 0 & \ldots & 0 \\ \vdots & \vdots & \ddots & \vdots & \vdots & \vdots & \ldots & \vdots \\ \psi_n r_1 & \psi_n r_2 & \ldots & \psi_n r_n & 0 & 0 & \ldots & 0 \\ \hdashline 0 & 0 & \ldots & 0 & \psi_{n+1} r_{n+1} & 0 & \ldots & 0 \\ 0 & 0 & \ldots & 0 & 0 & \psi_{n+2} r_{n+2} & \ldots & 0 \\ \vdots & \vdots & \ldots & \vdots & \vdots & \vdots & \ddots & \vdots \\ 0 & 0 & \ldots & 0 & 0 & 0 & \ldots & \psi_{2n-1} r_{2n-1} \end{array}\right] \tag{4.6}$$

where ψ_i and r_i are the experimental or case study and the reference pre-correlation vectors, respectively. The upper left region of the matrix corresponds to correlation between vectors of the same dimension for both the experimental and the reference modes, whereas the off-diagonal zero regions correspond to cases where no correlation

can be checked because of dimension incompatibility. Finally, the diagonal terms after the $\psi_n r_n$ term correspond to correlation between stacked mode vectors of identical dimension. A high correlation result will have values close to 1 in the entire CM matrix diagonal. A simplification of this step is to correlate only stacked vectors, leaving out of the analysis the single mode shape vectors as the latter, when analyzed individually, produce poor results due to individual mode shape similarity. Moreover, when comparing stacked-modes vectors only, the correlation matrix turns into a correlation vector much more straightforward to analyze from the analyst standpoint.

The results of the correlation matrix or vector can be presented by either the matrices themselves or bar plots, whether presented in 3D for the case of correlation matrices and in 2D for the case of vectors, which are much more easy to understand. An example of this plot for a 5 × 5 successful correlation matrix is presented in Fig. 4.1.

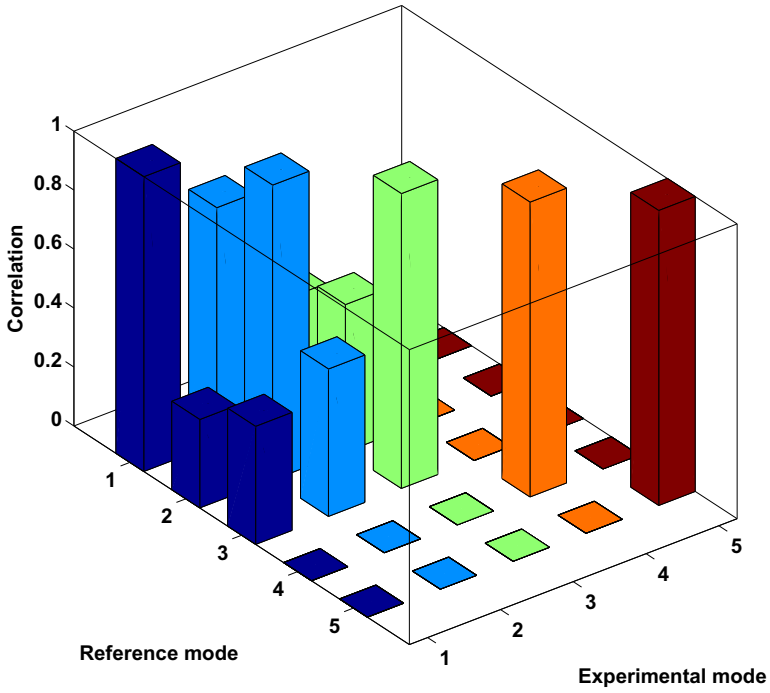

Figure 4.1. An example of a 5 × 5 correlation matrix.

Model correlation matrices are very common when a mode needs to be checked for validity in cases of computational or torsional modes. For this particular project, the benefits of the modal assurance methodologies are used with a distinct objective: to implement a methodology for verifying the closeness of a model boundary condition parameters to those of an experimental result. This is why the method will be further referred to as "MAC-based" instead of modal assurance criteria.

4.2 Resolution Study

As stated previously, the resolution chosen for data acquisition is of crucial importance in the stability of the method. Indeed, the method will become less reliable with the reduction of number of sensors; on the contrary, the higher the resolution, the better correlation results one can obtain. Three runs of the algorithm were made, using sixteen, eight and four accelerometers to determine a pattern of correlation. These analyses had to be done with analytical data to determine the sensitivity of the method to the number of sensors used without the contamination of data with external factors such as noise. The results are presented Figure 4.2, the correlation value for one of the cases where both vectors are analytical is plotted against number of accelerometers. It can be clearly observed how the correlation drops dramatically when less than eight accelerometers are used for the case of a beam of 4572 mm length. This is also confirmed by a poor approximation in the finite element model.

Setting a general rule of thumb, the stability limit occurs when the length of discretized elements of the beam is at least 1/10 of the length of the beam, so

$$\frac{L_{beam}}{L_{elements}} \leq 10. \tag{4.7}$$

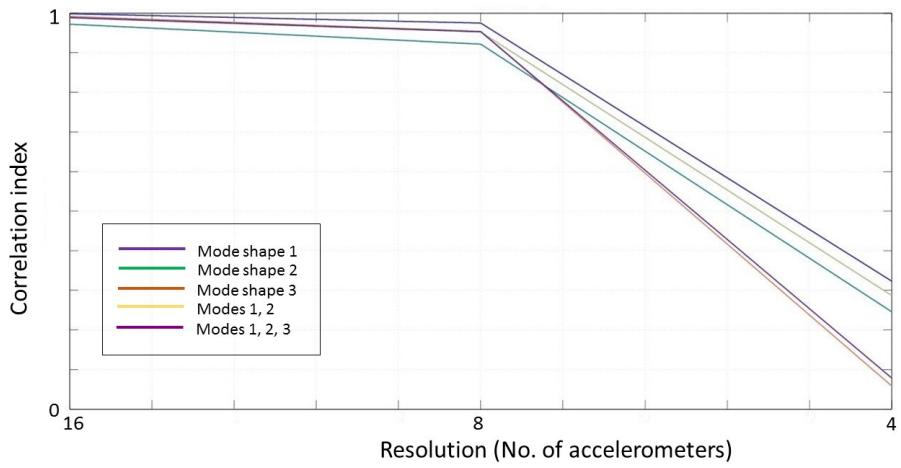

Figure 4.2. Resolution sensitivity of the proposed method.

PART II: NUMERICAL VERIFICATION

5. MATHEMATICAL MODELS

Detailed derivations of the mathematical models that were used for this work will be described herein. Both the analytical and, though approximated, the finite element method will provide insights of the "exact" solutions. Both methods will be used to prove that either approach could be used as a correlation comparison reference. This is useful specially when an analytical model cannot be obtained and a finite element approximation has to be used. Chapter 6 in addition will address the use of the method with data gathered from the models developed in this chapter. The methodology used will be thoroughly explained.

5.1 Analytical Models

The experimental setup which will be explained in detail in Chapter 7 consists of a beam-like bridge structure with four parallel beams connected by common flanges at set distances from the boundaries for simultaneous vibration of the structure. This structure was intended to behave like a continuum beam subjected to different types of boundary conditions such as pivoted (pinned), fixed (clamped), elastic (spring), or any combination of these. It should be noted that free, fixed and pivoted boundaries are commonly referred to as "classical" boundary conditions, whereas any other form is known as "non-classical". Since the purpose of this thesis is not to present extensive mathematical derivations of the solutions of all the aforementioned cases, three cases have been selected to be developed just to demonstrate the validity of the method: these cases are the more general pinned-pinned or simply-supported beam, a beam with torsional springs on both ends, and a beam with rotational masses on both ends.

Consider the two most classical cases of boundary conditions for a beam, depicted in Fig. 5.1(a) for a simply-supported beam case (pinned-pinned), and Fig. 5.1(b) for a clamped-clamped case.

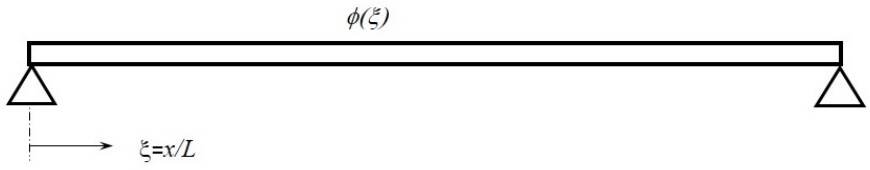

(a) Simply-supported.

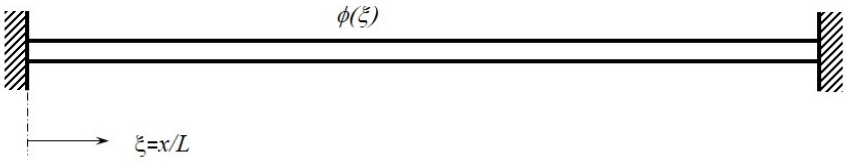

(b) Clamped-clamped.

Figure 5.1. Classic boundary conditions.

These two cases can be viewed as special cases of a beam supported both on rotational and linear springs at ends. Classical boundary conditions are those of more extensive use in engineering and the bibliography; namely, pinned, free and clamped. However, these are just particular cases of beams on elastic supports where specific values of the support spring stiffnesses are used. For instance, a beam with pinned ends and torsional supports of zero stiffness is actually a simply-supported beam.

5.1.1 Simply-Supported Beam Model

Consider a continuous beam of homogeneous material; modulus of elasticity E; second moment of area I_x; density ρ; length L; and uniform cross-sectional area A. The governing differential equation of such a beam according to the Euler-Bernoulli theory of beams can be written as:

$$-\frac{\partial^2 w(x,t)}{\partial t^2} = \frac{EI}{\rho A}\frac{\partial^4 w(x,t)}{\partial x^4}. \tag{5.1}$$

For simplicity, the effects of shear, stress and rotational inertia have been neglected in this particular case. Since Eq. (5.1) is a partial differential equation, it can be solved by the technique of separation of variables; hence, this equation has a solution of the form,

$$w(x,t) = q(t)\phi(x) \tag{5.2}$$

for a single mode, where $q(t)$ is the frequency equation and $\phi(x)$ is the mode shape equation. Substituting Eq. (5.2) into Eq. (5.1) yieds,

$$-\phi(x)\frac{d^2 q(t)}{dt^2} = \frac{EI}{\rho A}q(t)\frac{d^4\phi(x)}{\partial x^4} \tag{5.3}$$

and rearranging,

$$-\frac{1}{q(t)}\frac{d^2 q(t)}{dt^2} = \frac{EI}{\rho A}\frac{1}{\phi(x)}\frac{d^4\phi(x)}{\partial x^4}. \tag{5.4}$$

Solving this equation requires both sides to be equal to a constant which must be positive. This constant is denoted ω^2 and is the frequency parameter of the system. Now the expression can be separated into two ordinary homogeneous differential equations each one of which depends only on one variable as follows,

$$\frac{d^2 q(t)}{dt^2} + \omega^2 q(t) = 0 \tag{5.5}$$

and

$$\frac{d^4\phi(x)}{dx^4} - \omega^4\phi(x) = 0 \tag{5.6}$$

with a frequency parameter defined as

$$\beta^4 = \frac{\rho A \omega^2}{EI}. \tag{5.7}$$

The general solution for Eq. (5.5) is of the form,

$$q(t) = cos(\omega t - \alpha). \tag{5.8}$$

Similarly, the general solution for Eq. (5.5) is

$$\phi(x) = A\sin\beta x + B\cos\beta x + C\sinh\beta x + D\cosh\beta x. \tag{5.9}$$

The interest in the present analysis lies in Eq. (5.7) and Eq. (5.8). The solution of the latter, though straightforward, requires a previous determination of parameter β from the former. To complete the problem statement, boundary conditions must be defined to solve for the specific case of interest. This is a cumbersome task that requires careful mathematical manipulation along with a correct definition of boundary conditions. The boundary conditions for a simply-supported beam can be expressed as

$$\begin{aligned} &\phi(x = 0) = \phi(x = 0) = 0 \\ &\phi''(x = 0) = \phi''(x = L) = 0. \end{aligned} \tag{5.10}$$

Applying boundary conditions in Eq. (5.10) for the case of $x = 0$ into Eq. (5.9) produces,

$$\phi(x=0) = A\sin 0 + B\cos 0 + C\sinh 0 + D\cosh 0 = 0 \tag{5.11}$$

and

$$\phi''(x=0) = \beta^2(-A\sin 0 - B\cos 0 + C\sinh 0 + D\cosh 0) = 0 \tag{5.12}$$

thus giving,

$$\begin{aligned} B + D &= 0 \\ -B + D &= 0 \\ \Rightarrow B = D &= 0. \end{aligned} \tag{5.13}$$

Similarly, applying the boundary conditions corresponding to $x = L$ produces an homogeneous system of equations,

$$\begin{aligned} A\sin\beta L + C\sinh\beta L &= 0 \\ -A\sin\beta L + C\sinh\beta L &= 0. \end{aligned} \tag{5.14}$$

For a non-trivial solution to exist, the determinant of the coefficients must vanish,

$$\begin{vmatrix} \sin\beta L & \sinh\beta L \\ -\sin\beta L & \sinh\beta L \end{vmatrix} = 0 \tag{5.15}$$

which produces the following requirement,

$$\sin\beta L \sinh\beta L = 0. \tag{5.16}$$

The only possibility for Eq. (5.16) to be zero is when the values of βL are equal to $n\pi$ $(n = 1, 2, 3, ...)$. Now, the equation of mode shape along with the frequency parameter have been completely derived and can be expressed as,

$$\phi(x) = \sin\beta x \tag{5.17}$$

and

$$\beta = \frac{n\pi}{L}. \tag{5.18}$$

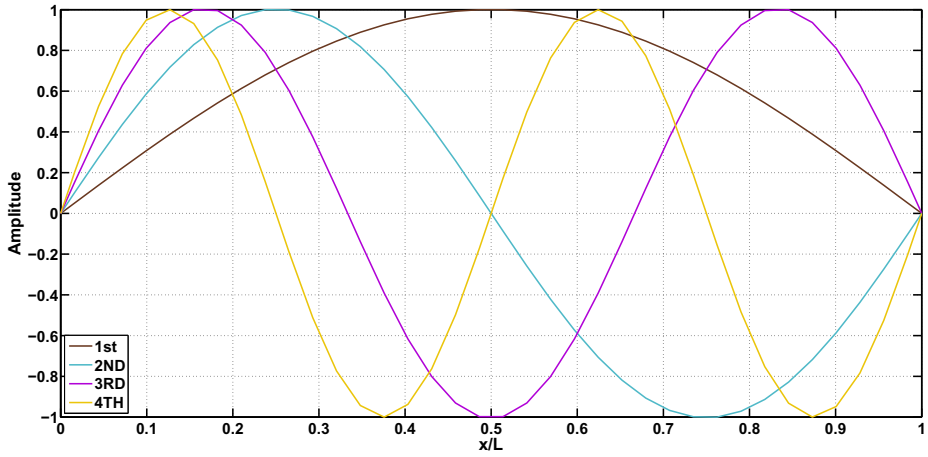

Figure 5.2. First four modes of a simply-supported beam.

This derivation produces the well known mode shape for a simply-supported beam shown in Fig. 5.2. As expected, the shape is that of a sine function whose frequency increases by a factor of one in each resonant frequency. It should be noted that at the boundaries, no slope variation is observed as no constraint is acting on those ends.

5.1.2 Beam with a Torsional Spring Support at Each End

Consider now the case of a beam shown in Fig. 5.3. The material properties are exactly the same as in Sec. 5.1.1, with the addition of two torsional springs, whose stiffnesses are $k_{\theta L}$ and $k_{\theta R}$ for the left and right side, respectively

The boundary conditions for this case are,

$$\phi(x = 0) = \phi(x = L) = 0 \tag{5.19}$$

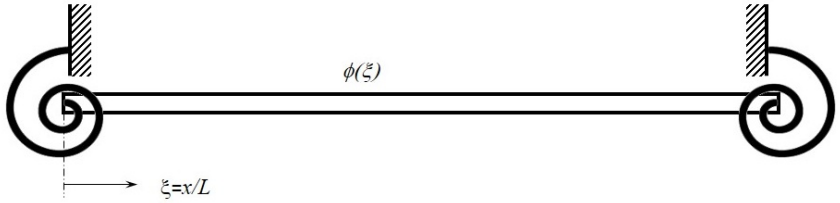

Figure 5.3. Beam on elastic supports.

for the displacement at both ends, and,

$$\frac{d^2\phi(x=0)}{dx^2} = \frac{K_{\theta L}}{EI}\frac{d\phi(x=0)}{dx}$$
$$\frac{d^2\phi(x=L)}{dx^2} = -\frac{K_{\theta R}}{EI}\frac{d\phi(x=L)}{dx} \tag{5.20}$$

for the bending moment at both ends. Substituting the boundary condition equations into the general solution [Eq. (5.9)] and after some manipulation, an expression of the frequency equation can be obtained:

$$K_1^{*2} + K_1^*\frac{\beta(1+\alpha)(\sin\beta\cosh\beta - \cos\beta\sinh\beta)}{\alpha(1-\cos\beta\cosh\beta)} + \frac{2\beta^2\sin\beta\sinh\beta}{\alpha(1-\cos\beta\cosh\beta)} = 0 \tag{5.21}$$

where $K_1^* = K_{\theta L} \times \frac{180}{\pi}$, $K_2^* = K_{\theta R} \times \frac{180}{\pi}$ and $\alpha = \frac{K_2^*}{K_1^*}$, $(0 < \alpha < 1)$.

The mode shape equation is determined,

$$\phi(\xi) = \sin\beta\xi - \sinh\beta\xi + \gamma\left[\cos\beta\xi - \cosh\beta\xi - \frac{2\beta}{K_1^*}\sinh\beta\xi\right] \tag{5.22}$$

where

$$\gamma = \frac{\sinh\beta - \sin\beta}{\cos\beta - \cosh\beta - \frac{2\beta}{K_1^*}\sinh\beta}. \tag{5.23}$$

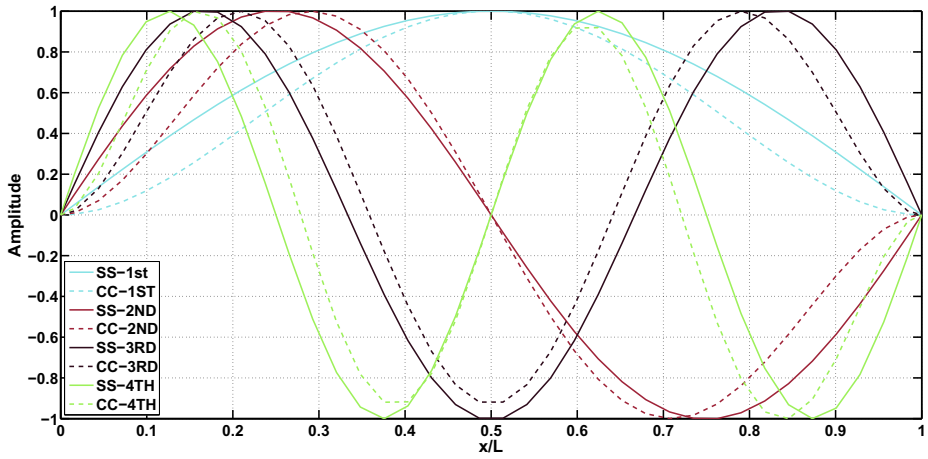

Figure 5.4. Limiting mode shapes for vibrations of a beam on elastic supports (solid lines: simply-supported; dashed lines: clamped-clamped).

This constitutes an intermediate case between the simply-supported and the clamped-clamped cases. Fig. 5.4 shows these limiting cases, the solid line represents the simply-supported case where both spring constants $K_{\theta 1}$ and $K_{\theta 2}$ are equal to zero; similarly, the dotted line represents the clamped-on-both-ends case where the spring constants are equal to infinity. Any combination of spring constants at left and right ends will yield modal parameters within these two limits, being the upper limit the clamped-clamped case; and the lower limit, the pinned-pinned case. This principle also applies for the natural frequencies, as the highest will occur for the clamped-clamped model; and the lowest, for the simply-supported model. All natural frequencies for spring supported beams will be between these two bounds.

5.1.3 Beam with Rotational Masses on Both Ends

The third model considered in the present thesis, mainly due to discrepancies in the observed modal parameters versus the ones predicted by the previous two models

is a simply-supported beam with the addition of rotational inertial masses on both ends. Consider a beam similar to that shown in Fig. 5.5

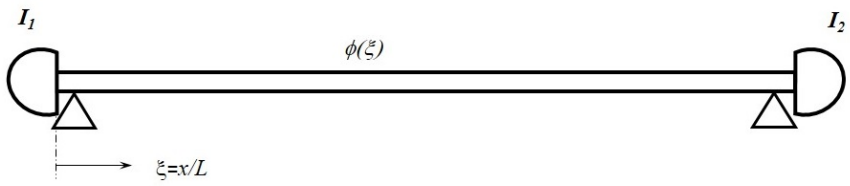

Figure 5.5. Simply-supported beam with rotational masses on both ends.

For this case, the first two boundary conditions are the same as a simply-supported case [Eq. (5.19)], whereas the second two include the effect of the rotary inertial masses:

$$\begin{aligned} \frac{d^2\phi(\xi=0)}{d\xi^2} &= \frac{-I_{o1}}{\rho AL^3}\beta^4\frac{d\phi(\xi=0)}{d\xi} \\ \frac{d^2\phi(\xi=1)}{d\xi^2} &= \frac{I_{o2}}{\rho AL^3}\beta^4\frac{d\phi(\xi=1)}{d\xi} \end{aligned} \tag{5.24}$$

where ξ is the non dimensional distance x/L. Again, solving the system of equations produced by these boundary conditions will end up giving the transcendental eigenvalue equation along with the mode shape equation:

$$I_1^{*2} + I_1^*\frac{\beta^3(1+\alpha)(\sin\beta\sinh\beta - \sin\beta\cosh\beta)}{2\alpha\sin\beta\sinh\beta} + \frac{\beta^6(1-\cos\beta\cosh\beta)}{2\alpha\sin\beta\sinh\beta} = 0 \tag{5.25}$$

where $I_1^* = I_{o1} \times \frac{180}{\pi}$, $I_2^* = I_{o2} \times \frac{180}{\pi}$ and $\alpha = \frac{I_2^*}{I_1^*}$, $(0 < \alpha < 1)$.

The mode shape equation is:

$$\phi(\xi) = \sin\beta\xi - \frac{\sinh\beta}{\sinh\beta}\sinh\beta\xi + \gamma\left[\cos\beta\xi - \cosh\beta\xi + \frac{(\cosh\beta - \cos\beta)}{\sinh\beta}\sinh\beta\xi\right] \quad (5.26)$$

where

$$\gamma = \frac{(\sin\beta/\sinh\beta) - 1}{[(\cosh\beta - \cos\beta)/\sinh\beta] - (2I_1^*/\beta^3)}. \quad (5.27)$$

Such equation has different limiting cases than those of the spring supported case (Eq. 5.4). Calculation of such limiting cases has to be performed by combining the knowledge of the current mode shape with that of previous ones; i.e., when considering the value of n for the calculation of the mode shape, some of the frequencies to consider are of previously obtained cases $(n-2)$. This is a rather delicate procedure as errors can be introduced very easily and will be explained in detail in the finite element section. The first four mode shapes for this case are shown in Fig. 5.6.

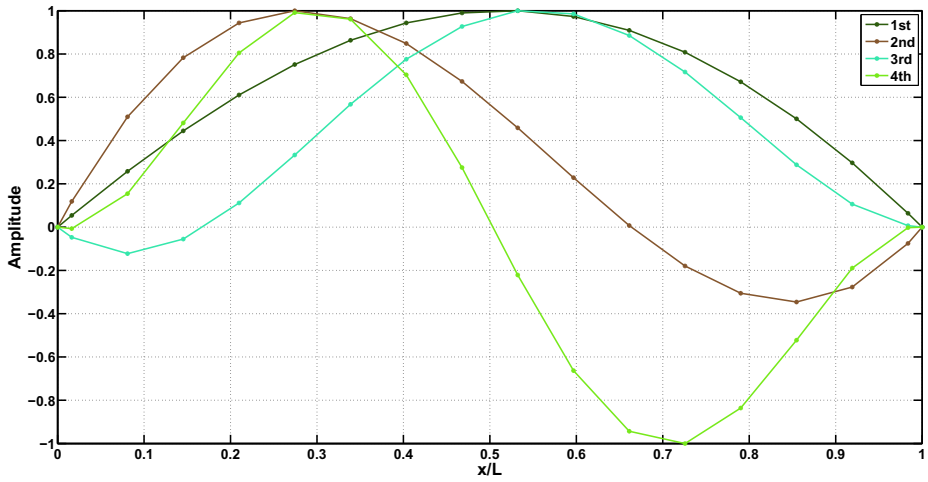

Figure 5.6. First four mode shapes of beam with rotational masses on both ends.

Note the similarity between the first and the third mode shapes; and between the second and the fourth mode shapes.

5.2 Finite Element Models

A second class of mathematical model developed for this project is a finite element approximation. A simple finite element model (FEM) was created using a toolbox developed at the Intelligent Infrastructure Systems Lab by Caicedo [4] using MATLAB [81]. Such a model was constructed with as few nodal points as possible to obtain acceptable results within a reasonable tolerance without significant computational demand. The purpose of building this model was simply to have two sources of analytical reference given that a FEM can be treated as analytical.

It should be clearly noted that the development of this type of model is a mere idealization of the real structure that will be introduced and explained in Chapter 7 and throughout this chapter, it will be considered as such.

To simulate the responses of the selected models to a variety of boundary conditions and material properties, the finite element model created consists of 72 Euler-Bernoulli beam elements connecting 76 nodes. Each beam of the structure is discretized in 17 Euler-Bernoulli beams with 18 nodes along its length. Such a model has a total of 53 degrees of freedom, provided that each node is defined with six degrees of freedom: three for translation and three for rotation, some of which are restricted to ensure a 2D behavior of the vibrations. Further discussion of the creation of the finite element model are include in the following sections.

5.2.1 Simply-Supported Beam Model

The finite element model of the structure for the simply-supported case was developed using 76 nodes and 72 beam elements. Each beam was discretized in 18 elements to replicate as close as possible the experimental setup used, which had 16 accelerometers in each beam. Since the pursued goal in this project is to study the modal behavior of the structure, the finite element toolbox used calculates simple

mass and stiffness matrices assembled from the conditions given in the input data which include:

1. Material properties such as density, modulus of elasticity and shear modulus.

2. Section and geometric properties like cross-sectional area, second moment of area in x and y directions and the St. Venant's rotational constant.

3. Nodal coordinates defined by the number of nodes chosen and their coordinates in space expressed as a 4-element vector ([node # x coord y coord z coord]). Since this is a basic toolbox, discretization has to be defined manually.

4. Boundary conditions. The toolbox calculates all the parameters using 6 degrees of freedom per node corresponding to three translational DOFs and three rotational DOFs for a total of 3 directions (x, y and z). It was of great aid to select the desired DOFs accordingly to avoid movement in unwanted directions.

5. Structural information like rigid links, lumped masses and springs.

After defining all the properties listed above, the process of construction of the model is straightforward, due to the nature of the toolbox being object-oriented. This means that what needs to be defined are objects like the material, sections, connectivities, links, masses, but all these defined as independent objects stored as such, instead of programmatic variables. A short example of definition of material parameters is given below:

```
E   = 200e9;                % Modulus of Elasticity [Pa]
nu  = 0.3;                  % Poisson coefficient
L   = 4.572;                % Beam length [m]
Iy  = 5.036e-5;             % 2nd moment of area [m^4]
Ix  = 1.550e-6;             % 2nd moment of area [m^4]
rho = 7850;                 % Material density [kg/m3]
A   = 0.004;                % Cross section area [m^2]
```

```
G   = E/(2*(1+poisson));     % Shear modulus [Pa]
J   = 2.57e-5;               % Torsional constant [m^4]
```

Section and material definition examples are also provided:

```
%%% Define Section(s) %%%
section = section('bridge',A,Ix,Iy,J);
```

In this definition, a section called 'bridge' is created and its properties are a section area A, second moments of inertia I_x and I_y, and torsional constant J.

```
%%% Define Material(s) %%%
steel    = material('steel',E,G,rho);
```

This definition on the other hand, creates a material called 'steel', whose properties are a modulus of elasticity E, a shear modulus G, and a material density of ρ.

Sections and materials can be created as needed for a given structure and assigned to different elements of the model, making it quite versatile at the moment of modeling complex structures. With all the objects defined, the toolbox calculates the mass and stiffness matrices and therefore, through solving the eigenvalue problem, the modal parameters are obtained. Fig. 5.7 shows the nodal definitions of the structure.

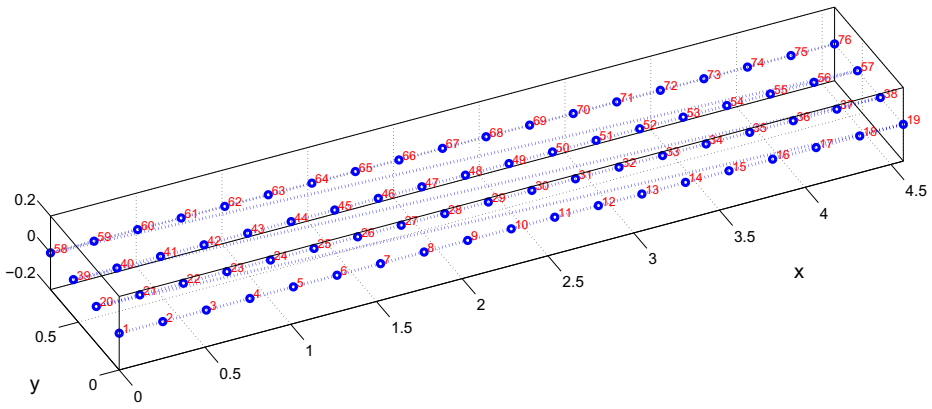

Figure 5.7. FEM node layout.

Figure 5.7 shows only the nodal points on the beams of the structure, as only these are of interest for the present analysis. Should a future need to study the implications of the piers or other connections present, these could be included without problems. The model is defined completely when the boundary conditions are set. Indeed, this is a boundary value problem. For the simply-supported case, the boundary conditions are set as,

$$y(\text{nodes } 1,\ 20,\ 39\ 58) = \begin{bmatrix} t_x = \text{constrained} \\ t_y = \text{constrained} \\ t_z = \text{constrained} \\ r_x = \text{constrained} \\ r_y = \text{free} \\ r_z = \text{constrained} \end{bmatrix} = \begin{bmatrix} 1 \\ 1 \\ 1 \\ 1 \\ 0 \\ 1 \end{bmatrix} \tag{5.28}$$

where t_x, t_y and t_z are the translational DOF's along the subscripted axis, and r_x, r_y and r_z are the rotational DOF's around the subscripted axis. The result of this definition is such that nodes $1, 20, 39$ and 58 will be restricted to translate in the three directions, and to rotate around x and z directions; whereas they will be free to rotate around the y axis. This is consistent with a pinned boundary.

Data entering for modeling in the fem toolbox uses a similar fashion as that shown in Eq. 5.28 in the sense that every element that contributes any effect on a node will have a 6-element vector associated with it. For instance, a nodal mass will have three translational and three rotational directions; a spring element acting over a node will have three translational and three rotational stiffnesses, and so on.

The results of the simulation using finite elements is shown in Table 5.1 for the first five natural frequencies. As expected, there is very good concordance between the approximate (FEM) frequencies with those of the analytical model.

For the case of the mode shapes, the output of the program is a 3D plot of each mode. For simplicity and clarity, only three 2D mode shapes are shown in Fig. 5.8.

Table 5.1. FEM frequency comparison (in Hertz).

Analytical	**FEM**
7.4869	7.4869
29.9476	29.9479
67.3821	67.3856
119.7905	119.8100
187.1726	187.2464

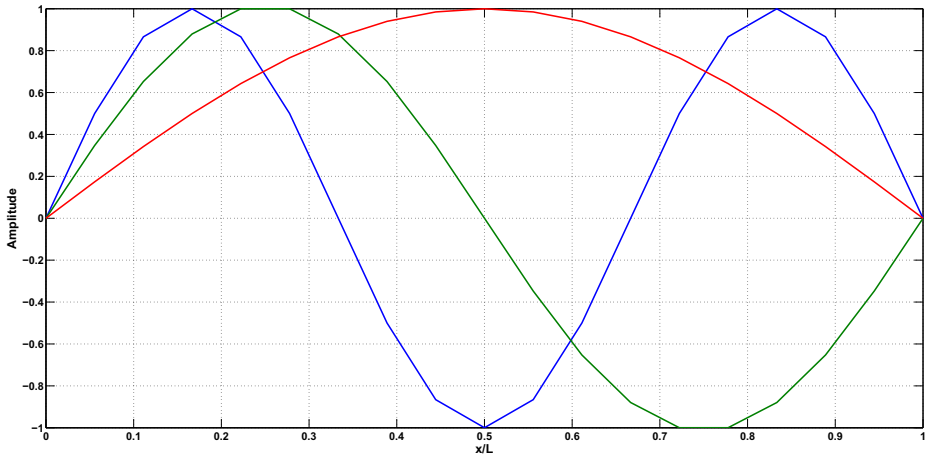

Figure 5.8. Simply-supported case mode shapes generated by FEM.

5.2.2 Beam With a Torsional Spring Support at Each End

In a similar way, the finite element method was used for modeling a beam with torsional springs at both ends. This study was done for comparing the behavior of a beam constrained in an unknown fashion at the borders. Such constraints were conceptualized as torsional springs that would prevent the system to vibrate freely. This model results in a very useful general tool to understand the vibration of similar systems from the simply-supported case, to the clamped-clamped case. Indeed, the former is nothing but a special case of a beam with torsional springs at both ends

whose stiffnesses are zero; whereas the latter is the case of a beam with springs' stiffnesses close to infinity. Any other combination of stiffnesses will lay between these two. Again, the natural frequencies and mode shapes for an intermediate value of stiffness (between zero and infinity) will be presented shortly.

The structure was discretized in a similar way as in the previous section, with the only difference being that additional nodes had to be declared for defining the springs. Springs are defined as extra elements connecting fictitious orthogonal nodes to those already existing. For the case of this investigation, springs were created for the boundaries only. Figure 5.9 depicts the element configuration of this model, including the spring elements acting over the boundaries which correspond to the vertical green lines numbered 1-8, whereas the horizontal lines between dots represent the beam elements. Rotational springs are represented this way in the model but this does not mean that they are physically as shown. This type of element is in fact conceptualized as a box having shear resistance across the faces other than the axial face. An example of the definition of these elements is:

$$k(\text{nodes } 1,\ 20,\ 39\ 58) = \begin{bmatrix} t_x \\ t_y \\ t_z \\ r_x \\ r_y \\ r_z \end{bmatrix} = \begin{bmatrix} 0 \\ 0 \\ 0 \\ 0 \\ k_i \\ 0 \end{bmatrix} \tag{5.29}$$

where k_i is the stiffness of the spring in $N\ m/rad$. The stiffness used for this example is $k_1 = 75000\ Nm^2$ which had to be transformed to units of stiffness per degree of rotation by multiplying it by $180\,/\,\pi$ and $k_2 = 45000\ Nm^2$ which is 60 % of the opposite stiffness. This difference of stiffnesses is evident when looking at the mode shape plot and by noticing that the maximum and minimum points are slightly shifted to the right due to a higher constraint at the left side causing an unsimmetric shape. If the springs were considered of equal stiffness, the plot would have been perfectly symmetric.

The boundary conditions for this model are similar to those of the simply-supported with the difference that they have an additional effect imposed by the springs.

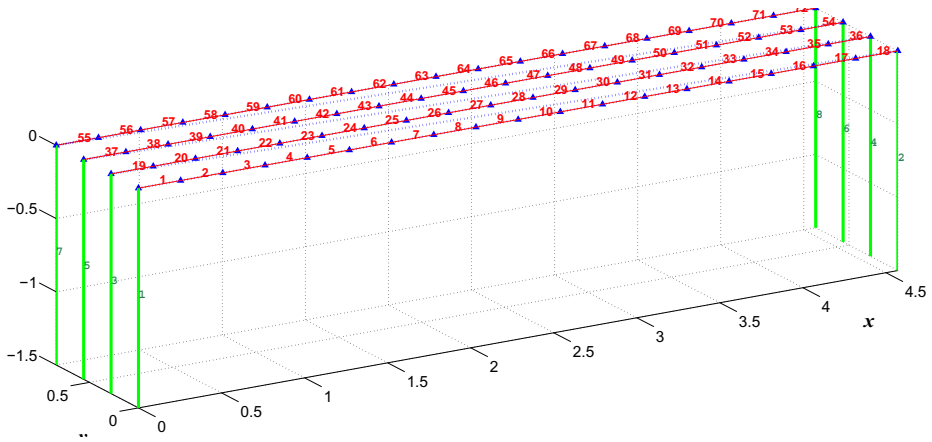

Figure 5.9. Layout of elements generated by the FEM.

The natural frequencies obtained versus those of the mathematical model are shown in Table 5.2, and the first three mode shapes in Fig. 5.10. Note that the mode shapes are somewhat similar to those of a clamped-clamped case which is expected, since the boundaries indeed have constraints in rotation.

Table 5.2. FEM frequency comparison for a system with rotational springs on both ends (in Hertz).

Analytical	**FEM**
15.4534	15.7484
42.9335	43.6126
84.7279	85.8527
140.8820	142.4655
167.3537	213.5939

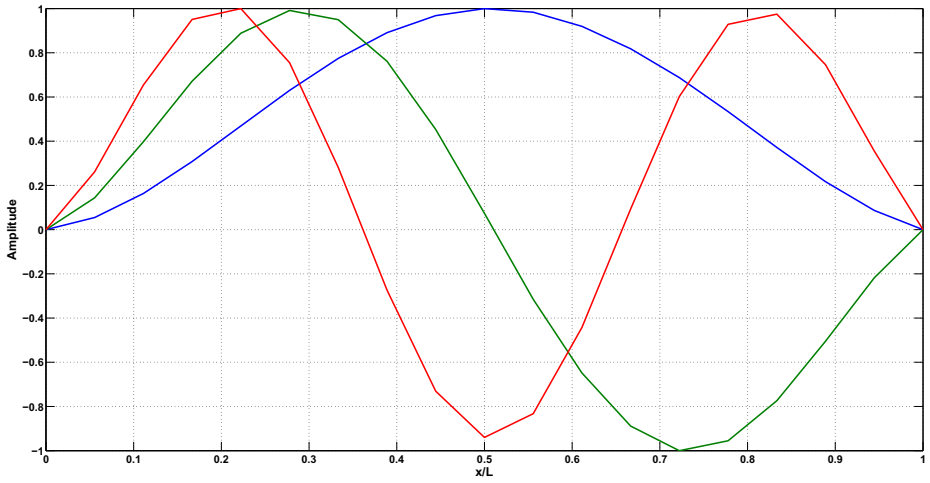

Figure 5.10. Elastic support case mode shapes generated by the FEM.

5.2.3 Beam With Rotational Masses on Both Ends

The third finite element model constructed is the counterpart of the theoretical simply-supported beam with rotational masses on both ends. Given the nature of the experimental setup which will be explained in detail in Chapter 7, a structure was built in such a way that two torque arms were attached to the boundaries so that a boundary-varying structure could be achieved. These arms can be fixed to produce a clamped boundary; or can be let free to produce a pinned boundary. Unfortunately, they add a considerable amount of rotary inertial mass to the boundary, changing the properties of the intended simply-supported configuration. This is the reason why a third model had to be studied. Consider the beam shown in Fig. 5.5. By inspection of the experimental structure shown in Fig. 7.3 the most noticeable similarity between these two pictures is the big attachments at both ends. For the experimental case, it was not very difficult to determine the inertia effect of these elements, as they are produced by plates rotating along their edges. The rotational moment of inertia for this case is,

$$I_0 = \frac{1}{3}mL^2 \tag{5.30}$$

where m is mass of the plate, L is arm length and I_0 is the rotational inertia. The masses of the attachments were estimated through the CAD software used for designing the structure and are $m_1 = 28\ kg$, and $m_2 = 14\ kg$ which will produce two rotational moments of inertia, one for each end, whose units are $kg\ m^2$ which were then transformed to units of inertia per units of rotation by multiplying them by $180/\pi$, and then transformed to the dimensionless rotational moment of inertia constant,

$$I^* = \frac{\rho A L^3}{I_0}. \tag{5.31}$$

For the setup of study, these values are $I_1^* = 54$, and $I_2^* = 27$. The finite element model was constructed using the same number of nodes and elements as the two previously described. An internal condition stating the rotational mass effects was included for each end which will not vary the node and element layouts shown in previous figures. Boundary conditions were set similarly as these cases. The results are shown in Table 5.3.

Table 5.3. FEM frequency comparison for a system with rotational masses on both ends (in Hertz).

Analytical	**FEM**
5.7413	5.7851
13.6967	13.9492
25.0677	25.2683
50.1448	50.3739
93.4043	93.5265

It is evident how close these frequencies are, confirming that this finite element model is correctly constructed. Some differences between the values could be caused

by the difficulty that posed to estimate accurately the type of rotational moment of inertia due to the complexity of the structure. For simplicity this parameter was considered as a rotating plate along its edge, however, some other shapes and off-axis considerations were not taken into account. Fig. 5.11 shows the first three modes of the structure.

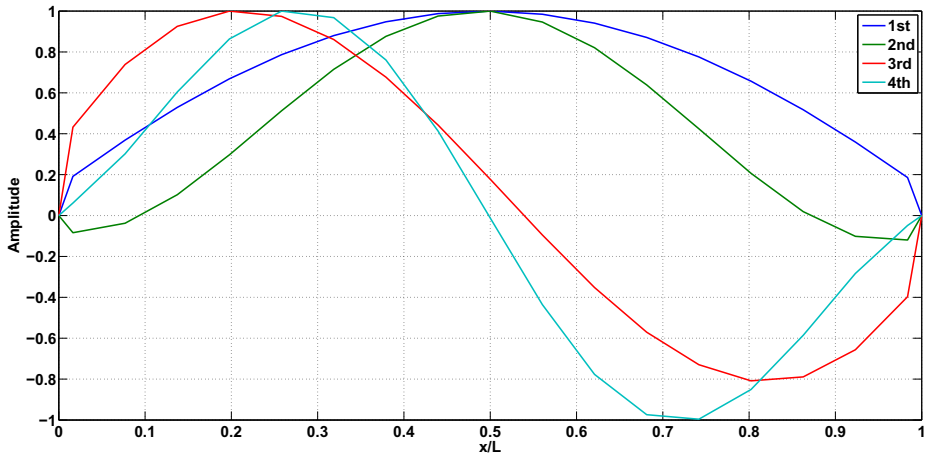

Figure 5.11. Modeshapes of a simply-supported beam with rotational masses on both ends, generated by the FEM.

Three analytical models and three finite element models have been developed. These were chosen as the source of the model space which will be compared with the "unknown" experimental model to determine the closest correlation.

5.2.4 Finite Element Model Details

The finite element formulation used in the present thesis calculates the stiffness and mass matrices from nodal information in which each node has six degrees of freedom. Figure 5.12 shows a detail of the six degrees of freedom for each node. In this figure, plain numbers represent nodes, boxed numbers represent elements, R_1 to R_6 represent the six DOF for the first node; and $R7$ to $R12$, the six DOF for the second node. Therefore, the global mass and stiffness matrices are of size $6n \times 6n$

where n is the number of nodes, and r are the the DOFs constrained by the boundary conditions.

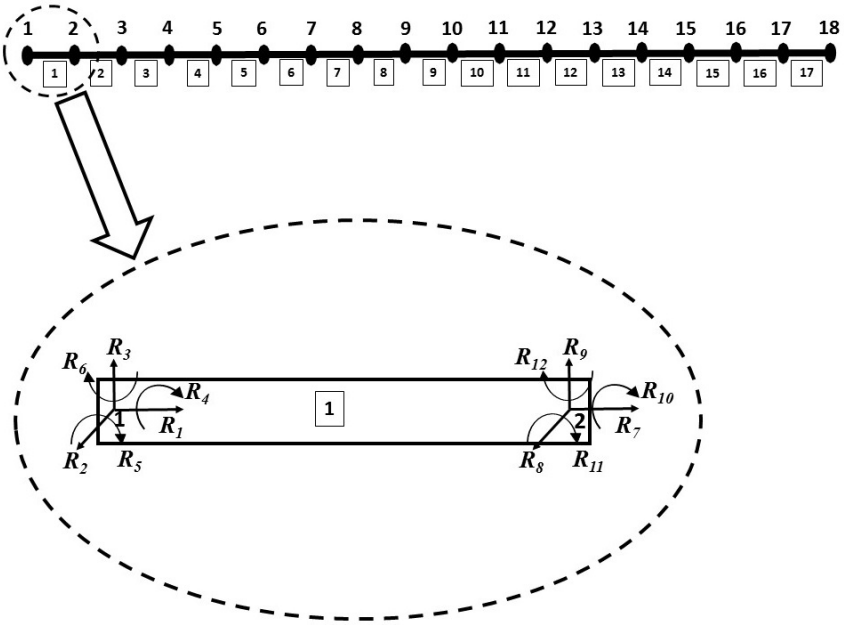

Figure 5.12. Beam element with element coordinates.

Mass and Stiffness Matrices

It is assumed that vibration only occurs in 2D; therefore, the unwanted DOF are constrained in such a way that only the desired directions of movement are characterized by the finite element analysis, reducing the original problem to a 3 DOF per node: one for translation in the vertical z direction, one for translation in the horizontal x direction, and one for rotation around the y direction.

Consider a beam element. The stiffness influence coefficient k_{ij} is the force in DOF i due to a unit displacement or unit rotation in DOF j. From the principle of virtual displacement, the general equation for k_{ij} is:

$$k_{ij} = \int_0^L EI(x)\psi_i''(x)\psi_j''(x)dx \tag{5.32}$$

which can be evaluated analytically for $i, j = 1...6$, resulting in element stiffness matrix:

$$\bar{\boldsymbol{k}_e} = \frac{EI}{L^3}\begin{bmatrix} \frac{L^2A}{I} & 0 & 0 & -\frac{L^2A}{I} & 0 & 0 \\ 0 & 12 & 6L & 0 & -12 & 6L \\ 0 & 6L & 4L^2 & 0 & -6L & 2L^2 \\ -\frac{L^2A}{I} & 0 & 0 & \frac{L^2A}{I} & 0 & 0 \\ 0 & -12 & -6L & 0 & 12 & -6L \\ 0 & 6L & 2L^2 & 0 & -6L & 4L^2 \end{bmatrix} \tag{5.33}$$

where E is the modulus of elasticity, A is the cross-sectional area, I is the area moment of inertia and L is the length.

Similarly, the mass influence coefficient m_{ij} is the force in DOF i due to unit linear acceleration or unit angular acceleration in DOF j. Applying again the principle of virtual displacement, the general equation for m_{ij} is:

$$m_{ij} = \int_0^L m(x)\psi_i(x)\psi_j(x)dx \tag{5.34}$$

which can be evaluated analytically for $i, j = 1...6$, resulting in element mass matrix:

$$\bar{\boldsymbol{m}_e} = \frac{mL}{420}\begin{bmatrix} 140 & 0 & 0 & 70 & 0 & 0 \\ 0 & 156 & 22L & 0 & 56 & -13L \\ 0 & 22L & 4L^2 & 0 & 13L & -3L^2 \\ 70 & 0 & 0 & 140 & 0 & 0 \\ 0 & 54 & 13L & 0 & 156 & -22L \\ 0 & -13L & -3L^2 & 0 & -22L & 4L^2 \end{bmatrix} \tag{5.35}$$

where m is the total mass of the element.

The 6 × 6 element stiffness matrix $\bar{\boldsymbol{ke}}$ and the 6 × 6 element mass matrix $\bar{\boldsymbol{me}}$ are transformed in global element coordinates through an appropriate transformation matrix, $\mathcal{A}$ [85].

$$\boldsymbol{K} = \mathcal{A}\bar{\boldsymbol{k_i}} \tag{5.36}$$

$$\boldsymbol{M} = \mathcal{A}\bar{\boldsymbol{m}}_{\boldsymbol{i}}. \tag{5.37}$$

Finally, the natural frequencies and mode shape vectors are obtained through solving the eigenvalue problem for the eigenvalues and eigenvectors, respectively.

$$\boldsymbol{K}\phi = \omega^2 \boldsymbol{M}\phi \tag{5.38}$$

Interpolation functions

The displacement of the beam element shown in Fig. 5.12 is related to its six DOF through:

$$\sum_{i=1}^{6} u_i(t)\psi_i(x) \tag{5.39}$$

where ψ is the displacement of the element due to unit displacement. The 6 × 6 stiffness and mass matrices of Eqs. 5.33 and 5.35, respectively turn into 4 × 4 local element matrices when eliminating the coefficients associated with axial DOF at each node. Therefore, $\psi_i(x)$ satisfies the homogeneous boundary conditions:

$$i = 1 : \psi_1(x = 0) = 1, \psi_1'(x = 0) = \psi_1(x = L) = \psi_1'(x = L) = 0 \tag{5.40a}$$

$$i = 2 : \psi_2(x = 0) = 1, \psi_2'(x = 0) = \psi_2(x = L) = \psi_2'(x = L) = 0 \tag{5.40b}$$

$$i = 3 : \psi_3(x = L) = 1, \psi_3'(x = 0) = \psi_3(x = 0) = \psi_3'(x = L) = 0 \tag{5.40c}$$

$$i = 4 : \psi_4(x = L) = 1, \psi_4'(x = 0) = \psi_4(x = 0) = \psi_4'(x = L) = 0 \tag{5.40d}$$

Assuming no shear effects, the governing equation for a beam loaded at its ends is:

$$EI\frac{d^4u}{dx^4} = 0 \tag{5.41}$$

whose general solution is of the form,

$$u(x) = a_1 + a_2\left(\frac{x}{L}\right) + a_3\left(\frac{x}{L}\right)^2 + a_4\left(\frac{x}{L}\right)^3. \tag{5.42}$$

After enforcing the boundary conditions of Eqns. 5.40a, constants a_1, a_2, a_3 and a_4 are determined.

$$\psi_1(x) = 1 - 3\left(\frac{x}{L}\right)^2 + 2\left(\frac{x}{L}\right)^3 \tag{5.43}$$

$$\psi_2(x) = L\left(\frac{x}{L}\right) - 2L\left(\frac{x}{L}\right)^2 + L\left(\frac{x}{L}\right)^3 \tag{5.44}$$

$$\psi_3(x) = 3\left(\frac{x}{L}\right)^2 - 2\left(\frac{x}{L}\right)^3 \tag{5.45}$$

$$\psi_4(x) = -L\left(\frac{x}{L}\right)^2 + L\left(\frac{x}{L}\right)^3 \tag{5.46}$$

which can be used as interpolation functions for the finite element model.

Additional Elements

Once the nodal contributions to the global mass and stiffness matrices have been established, the interaction between such nodes was defined through rigid links. Four rigid links were defined at equidistant lengths along the beam; namely, at $x = 0$, $x = L/3$, $x = 2L/3$ and $x = L$. The definition pattern for these rigid links were to fix the node on the front element as master node, and link the corresponding nodes on the other beams as slave nodes. The rigid link diagram is shown in Fig. 5.13, where M refers to master node; and S, to slave node.

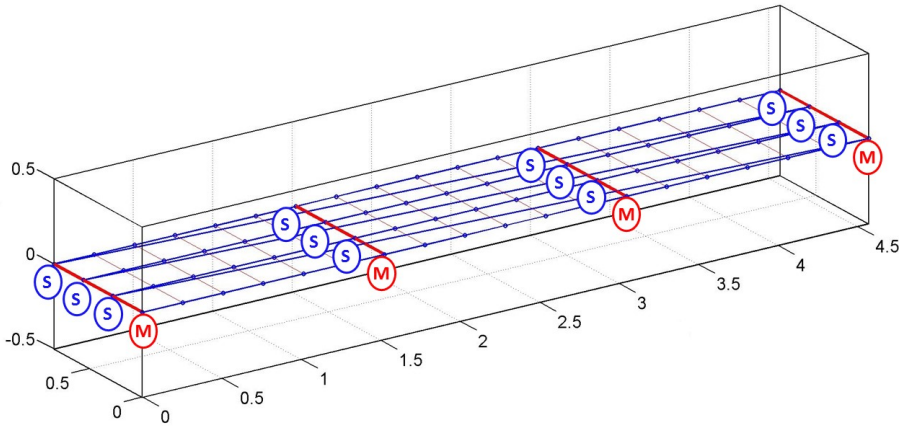

Figure 5.13. Detail of the FEM rigid links.

Notice that these rigid links are not defined as beam elements, therefore they don't have any contribution to the overall mass and stiffness matrices.

The boundary condition definition was briefly explained in Sec. 5.2.1. The finite element toolbox used in the present thesis has the capability to create a boundary condition in the same way as a nodal DOF is defined, that is to say, a vector of six elements (three for translation and three for rotation) is defined with values of zero and one (zero for free and one for constrained). Figure 5.14 depicts an example definition of boundary conditions for a pinned-free beam element. The left side has a pinned boundary with free rotation only around the y axis and all other DOFs constrained; and the right side, has a free translation along the x and z axis, free rotation around the y axis and all the other DOFs are constrained.

Similarly, lumped masses and spring elements are defined by 6-element vector. For the former case, three translational mass-contributions and three rotational inertia-contributions have to be defined; and for the latter, three linear spring stiffnesses and three rotational spring stiffnesses have to be defined.

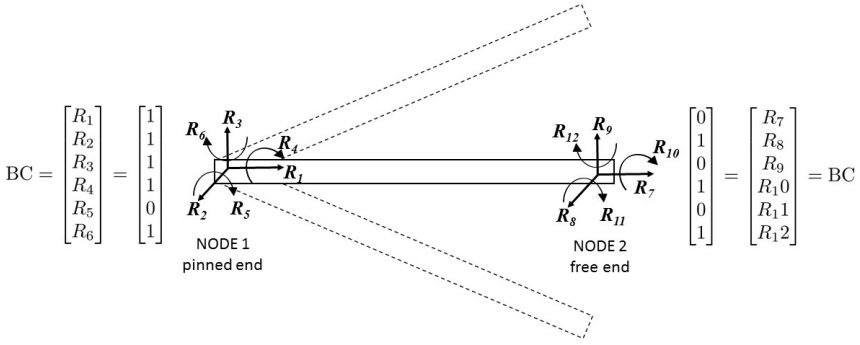

Figure 5.14. Boundary condition definition example.

The rotational mass FEM explained in Sec. 5.2.3, had only one rotational component acting around the y axis, which is consistent with a 2D model. Lumped masses on each nodal point were neglected. The mass definition is shown in Fig. 5.15. On the other hand, the spring supported model had rotational springs acting in the boundary nodes around the y axis, as element that prevented the nodes to rotate freely. As explained in Sec. 5.2.2, springs are conceptualized as boxes having shear resistance across the faces other than the axial face.

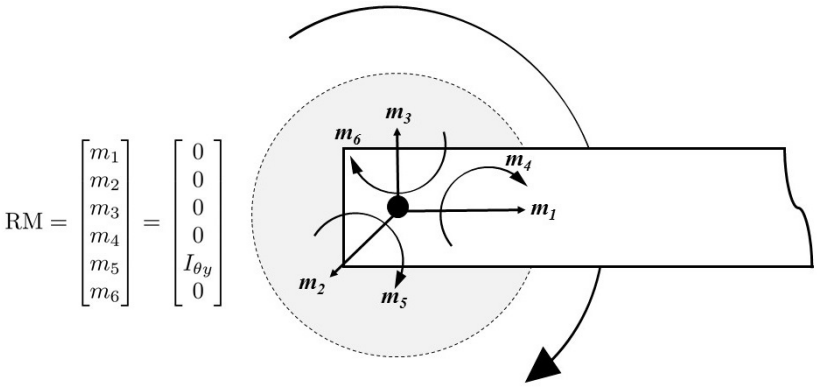

Figure 5.15. Rotational mass definition example.

6. NUMERICAL VERIFICATION

6.1 Introduction

As stated previously, the development of the mathematical models used in this thesis is the first part of a much broader procedure which is the numerical verification of the proposed technique.

A model correlation method has been proposed but before it can be implemented with experimental data, it has to be tested with unpolluted data so that it can prove its reliability. In the present chapter, this verification will be performed in an iterative way so that it can be further implemented with real data. Two sources of data can be used instinctively from the mathematical models already discussed: the analytical and the finite element models. It is expected that for the analytical case, a perfect correlation occurs; whereas for the finite element case, which is an approximation, a close-to-perfect-correlation occurs.

6.2 Methodology

A good approximation of the structural model was made in Sec. 5.2.3. This case will be used to run the correlation procedure against the three developed mathematical models, each one with different parameter values. This constitutes the 'model space', a group of distinct parametrized models to which the experimental case is going to be compared until the best match is determined. The mathematical models to be used are:

1. Simply supported beam with both ends free for rotation.

2. Simply supported with:

- Rotational springs on both ends with three different $k_{\theta i}$ values on one end, and five proportional values going from 20% to 100% of $k_{\theta i}$ on the other end. This gives a total of twenty five cases.
- Rotational inertial mass on both ends, with five different I_{ri} values on one end, and five proportional values going from 20% to 100 % of I_{ri} on the other end. This gives a total of twenty five cases.

3. Clamped boundary on both ends (clamped-clamped beam.)

The described list contains roughly 80 different analytic models to compare from. It is clear that the solution space can be as wide as needed to determine the closest parameter correlation. The procedure to simulate the unknown boundary condition case is deatiled below:

1. Define the number of modes n to be simulated.
2. Obtain the eigenvalues, ω_n and mode shape vectors ϕ_n from the analytical equations or FEM.
3. Aproximate each mode to a state-space model corresponding to the associated degree of freedom.
4. Obtain the response of the system to a simulated input signal for each degree of freedom by solving the equations of motion. This constitutes the simulated data.
5. Apply an identification technique (FFT or ERA) to generated data to obtain the modal parameters. This step is to replicate a similar procedure of experimental modes. Noise or any other disturbance can be added in this step.
6. Compare the obtained mode shapes to those of the analytical models using the correlation method.
7. Plot the correlation matrix in a bar plot to determine the highest value and, therefore, the best model match.

6.3 Model Selection

Figure 6.1 presents five subplots, three for individual and two for combined (stacked) mode shapes. In each subplot, four curves are overlaid which correspond to the simulation, the simply-supported, the clamped-clamped and the rotational mass models. By inspection of this figure, it is evident that there are some lines not matching in all five subplots. In the figure, the red dotted lines with squared markers represent the mode shape of the case study; i.e., the simulation obtained from an analytical equation which is considered the "experiment". The continuous blue lines represent the analytical model of the same case but obtained through the FFT process to recreate the method as close as possible to the real experiment. The dashed black and dashed green lines correspond to the simply-supported and clamped-clamped cases, respectively.

In the first subplot, all four lines are almost coincident and a no conclusions can be made to determine which model is closer to the simulated case. The second subplot shows an almost collinear behavior between the simulation and the rotational mass models, whereas a slight deviation of the simply-supported and clamped-clamped models from that of the simulation. Although a deviation is observed, no conclusions can be made at this point either. The third subplot shows a significant deviation of the simply-supported and clamped-clamped models from that of the simulation and, at the same time, it shows how a consistent convergence between the simulation and the rotational mass analytical model. The last two subplots show a comparison between models but using stacked vectors instead of individual vectors; for these two cases, a consistent collinearity is observed between the rotational mass model and the simulation. Three modes have been used for explaining this step. Depending on the necessity, more mode shapes can be used to have a better convergence, depending on the complexity of the model and the availability of good experimental high mode shapes.

Although the previous step produces a fair amount of information about which model to select, it does not provide a parametric result regarding the boundary conditions of such a model. The goal of this technique is to determine with a great deal of certainty the parameters involved in the chosen model. For example, if a spring-supported model is selected, the method would provide an interval of spring-stiffness values as parameters of the system.

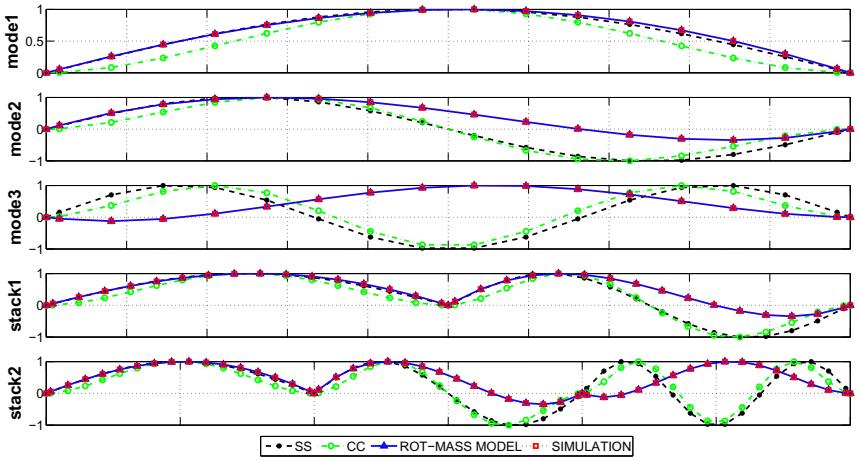

Figure 6.1. Modal vector comparison.

6.4 Correlation Analysis

Once the visual inspection has been conducted, the ultimate mathematical verification is done through the correlation methods described in Chapter 4. Consider again the simulated experiment just detailed in the previous section. Suppose that some given mode shape vectors have been obtained after performing impact testing to a structure. Such vectors are shown in Fig. 6.2. This is going to be the experimental "case study". Suppose also that the only assumption made for this mode shape is that it corresponds to the vibration of a beam of known dimensions and material constants but unknown boundary conditions (which is usually the case); i.e., parameters

M, **C** and **K** have been experimentally obtained. The proposed technique's aim is to compare this case study vector with several analytical model cases to determine which resembles the closest to it.

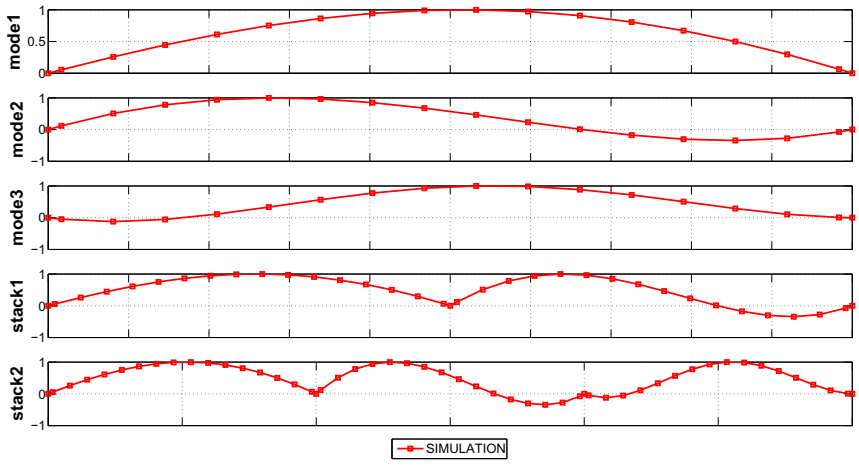

Figure 6.2. Case study.

After comparing this mode shape with the classical boundary-condition models similar to the step described in Sec. 6.3 one can conclude preliminarily that the obtained mode shape corresponds to a beam with rotational masses on both ends. However, this is still a vague conclusion because such a beam could have infinite number of combinations of rotational inertias at its ends; therefore, a refined model updating step is to be performed to determine with an acceptable tolerance, the values of such parameters. As an example, nine rotational-inertia and nine spring-stiffness combinations are going to be used leaving aside the simply-supported and clamped-clamped cases, since these are special cases of the spring-supported beam. The solution space is then composed of eighteen candidates just for this example. These possible models are going to be correlated with the simulated "experimental" case whose model is supposedly unknown. The graphical results are shown in Fig. 6.3, where it is clear that the unknown case (red-colored) is significantly off from any spring-supported model case (dark-green-colored). This will be evident in the bar

plot of the correlation values. On the other hand, when comparing the rotational mass model cases (blue-colored), a much closer relationship is observed. In fact, one of the cases gets really close to the experimental case. For a refined result, the analyst could just add more case combinations to the solution space to get an almost perfect match.

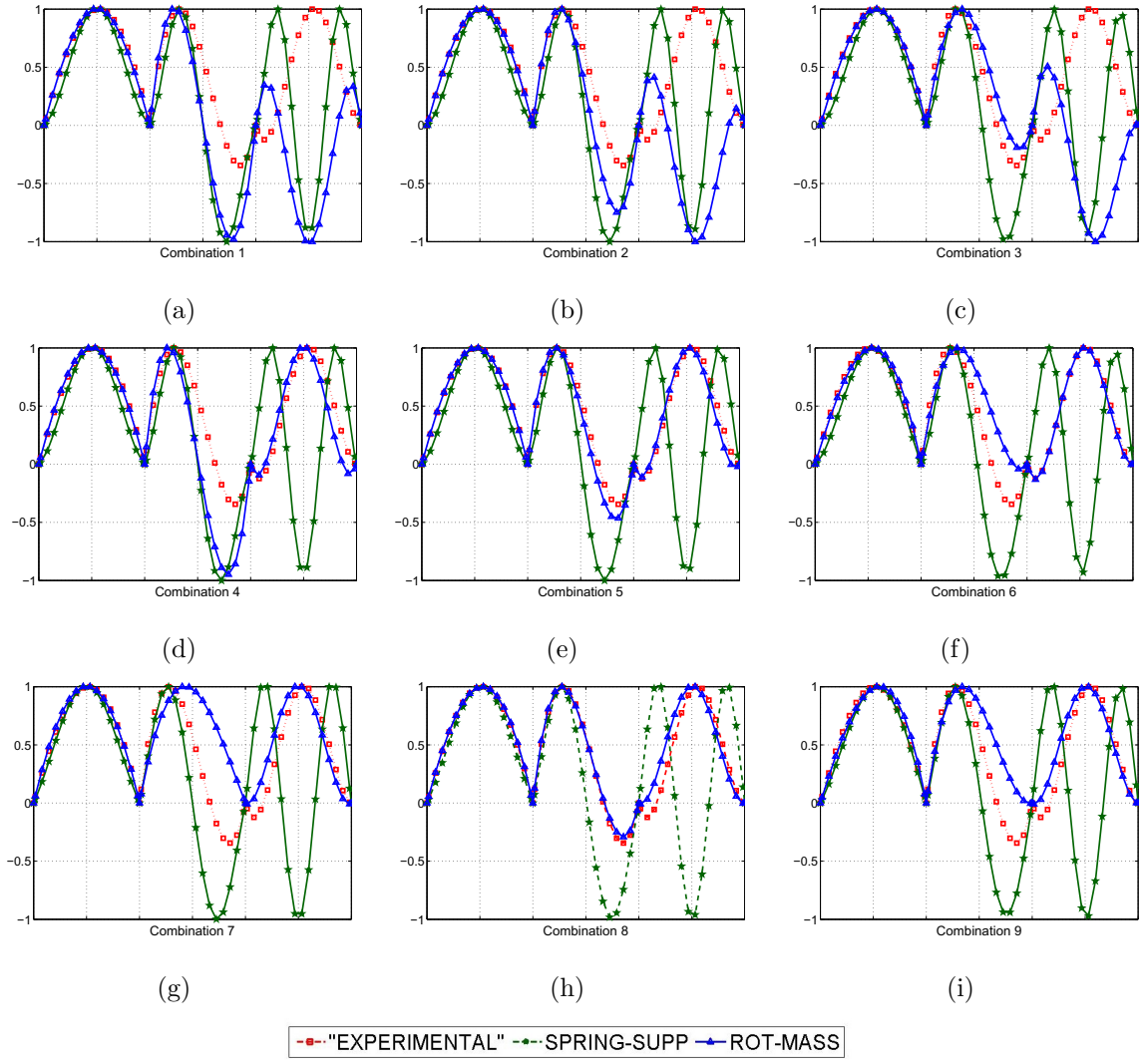

Figure 6.3. Correlation comparison of spring-supported and rotational-mass parameter combinations.

A good preliminary conclusion can be obtained from observation. Indeed, from a quick look to these, it is clear that for cases (e) and (h), very close correlations between

the experimental (red) and rotational mass (blue) models are occurring. However, our aim is to determine which parameters are causing this correlation; therefore, further study shall be performed to obtain such values. The algorithm carries out comparisons between the experimental model and all the models included in the solution space, giving one correlation index for each comparison. Each mode shape vector of the solution space has two additional cells containing the two boundary condition parameters which can be easily extracted after determining the highest correlation index. These results are shown in Fig. 6.4(a) and 6.4(b); the first, corresponding to the spring-supported beam cases; and the second one, to the rotational-inertia cases.

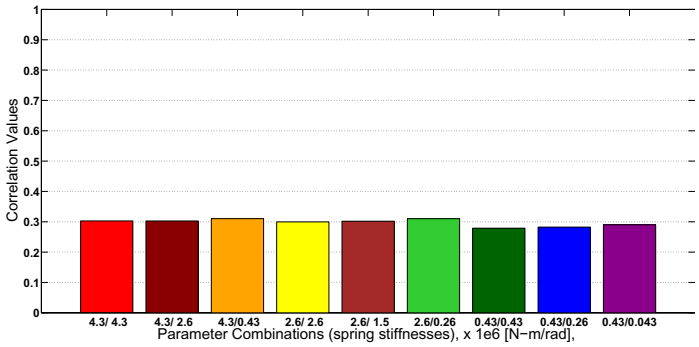

(a) Spring-supported

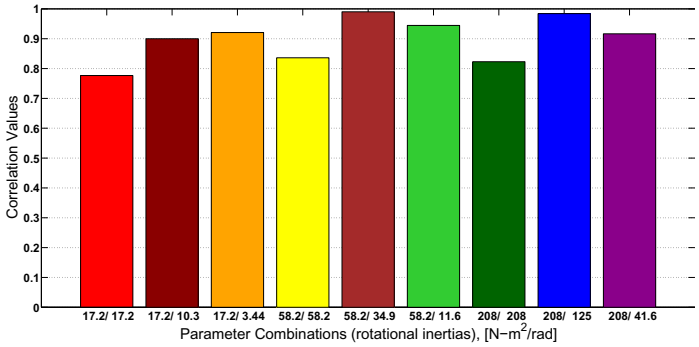

(b) SS w/ rotational masses

Figure 6.4. MAC-based correlation results.

Figure 6.4(b) confirms the preliminary visual conclusion made from Fig. 6.3: that is to say that combinations 5 and 8 are the closest-related models to the experimental one because the lines corresponding to the model and the simulation are mostly

coincident in these two plots. The final result of this example study is the output of the model parameters in the command window of MATLAB, which is shown Fig. 6.5.

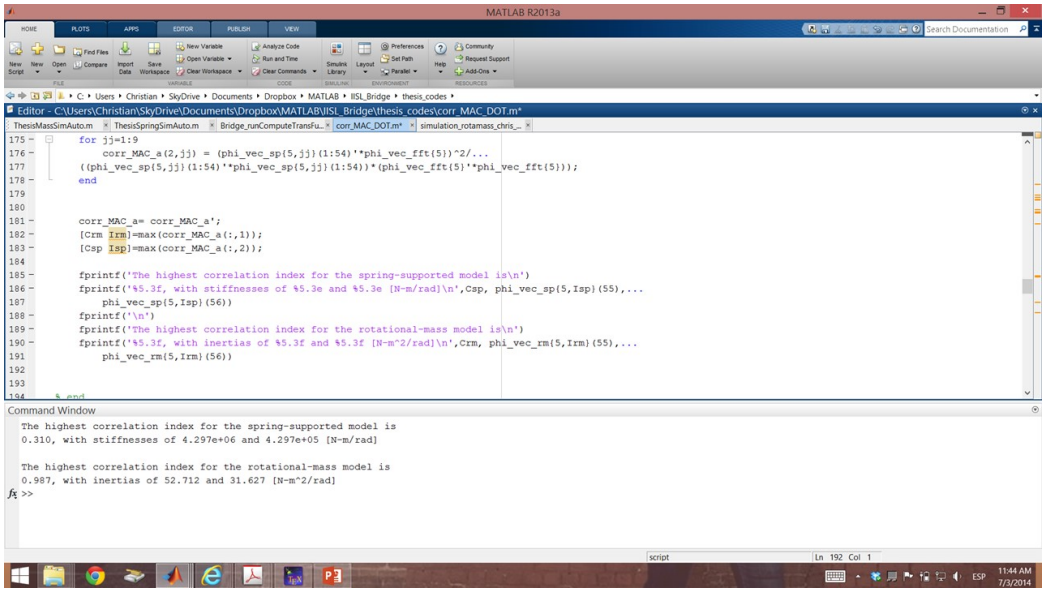

Figure 6.5. MATLAB command window results.

The obtained parameters are $I_1 = 52.712$ Nm^2/rad and $I_2 = 31.627$ Nm^2/rad. The exact values used to simulate the experimental case were $I_1 = 58.213$ Nm^2/rad and $I_2 = 34.982$ Nm^2/rad, which yield errors of 9.44% for I_1, and 6.1% for I_2 and an overall correlation parameter of 0.9987 which is acceptable to adopt this model combination as the correct boundary conditions for this experimental setup.

PART III: EXPERIMENTAL VALIDATION

7. EXPERIMENTAL SETUP

7.1 Introduction

To experimentally validate the proposed method, a special setup was designed and constructed. For designing this structure, standard mechanical design procedures were employed. Not all steps performed will be explained in detail as this is not the scope of this thesis. The steps [82] include:

1. Conceptualization
2. Research
3. Feasibility assessment
4. Establishing the design requirements
5. Preliminary design
6. Detailed design
7. Production planning and tool design
8. Production

7.2 Conceptualization & Design Parameters

Some important requirements and concepts had to be considered in this structure, the most relevant were:

1. The dominant behavior of the structure should be similar to those of a beam. Therefore, a slender and long configuration had to be selected. This condition derives from the premise that a simple structure was to be used for the experimental validation.

2. The structure should allow both vehicular and pedestrian transit for lab analysis; therefore it needed to be wide enough to allow for such traffic.

3. The structure should also allow complete and fast assembly-dissasembly of all its components.

4. The structure had to have the capability to replicate many types of boundary conditions; namely, pinned, fixed, and even spring-supported configurations in a fast and effective way.

5. To contribute to damage detection projects which are an important field studied by the IISL group on a regular basis, the structure should be constructed so that damage conditions might be simulated for future studies.

6. For realistic modal testing, a first natural frequency around 5 Hz was set as a requirement.

7.3 Research

To comply with the requirements listed in Sec. 7.2, existing laboratory structures in similar labs were considered as a reference. Unfortunately, the six conditions described above made this search a difficult task. Nevertheless, a good approximation for the needed setup was found in the Smart Infrastructure Management Laboratory at the University of Florida, which is shown in Fig. 7.1 and whose generous sharing of information was important in the completion of the present work. This structure however, did not meet all the requirements because it is a truss structure and its behavior as a beam was very limited. An additional two structures were considered but unfortunately neither met all the requirements.

Figure 7.1. Scaled truss bridge for SHM. (Courtesy of Dr. Jennifer A. Rice, University of Florida at Gainesville).

7.4 Design and Construction

After having discussed many of the above-listed features with fellow members of the IISL group, a conceptual design was obtained. This design is shown in Fig. 7.2. The design consists of four 3-section beams connected by endplates with bolts and nuts; two boundary assemblies, each consisting of a cylindrical shaft between two pillow block bearings with a pivoting plate connecting the beams with the pin; and two pseudo-stiffening plates such that all four beams of the bridge have synchronized vibrations. These plates are called pseudo-stiffening because they don't provide any significant structural addition to the behavior of the bridge as their purpose is only to enforce synchronized vibration.

As shown in the figure, most of the features are included in the conceptual design: it is a structure that can be modeled as a beam because it does not have any additional structural elements that would make it behave otherwise; it has discontinuities

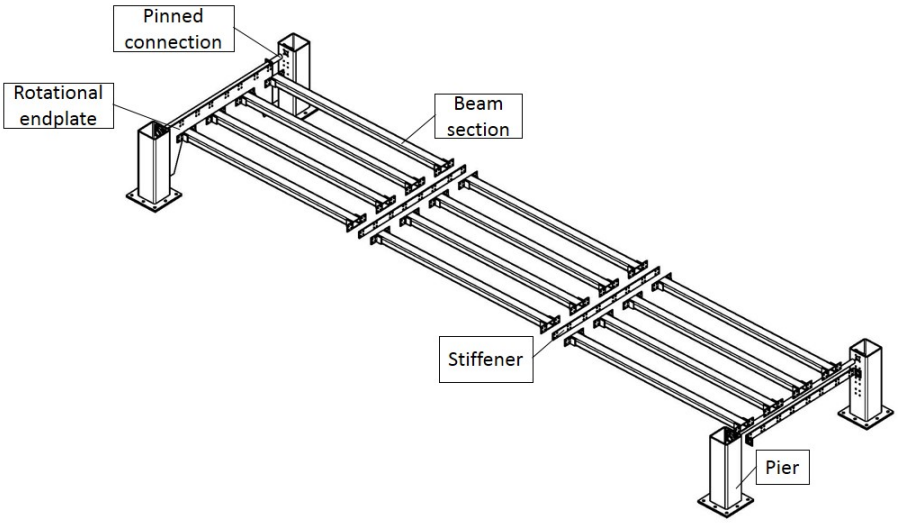

Figure 7.2. Scaled bridge. Conceptual design.

in each beam which could be considered as damage for further studies; and it has different boundary condition configuration features.

A finite element model using SAP2000 was developed to test many commercial steel sections and determine the most suitable one for obtaining the desired first natural frequency. From this analysis, it was determined that a HSS 3" $\times$ 2" $\times$ 3/16" rectangular hollow structural section was the most appropriate. It must be noted that this analysis was made considering uniform continuous beams and no rotational masses at the ends. The frequency obtained from the model was around 7 Hz.

Once the sections were selected, the next step in the design process was to develop detailed drawings. A set of the most relevant details of these drawings is included in the Appendix. The drawings were submitted to the selected machine and welding shop for construction under the supervision of the author. Like any other design,

some problems were present after the initial assembly that needed to be corrected; the most important was a twisting of the structure once assembled, due to the welding process. Manual alignment was performed to correct this issue. Nevertheless, the received work was acceptable according to the desired expectations.

A special connection was designed for changing the boundary conditions. The structure has the ability to pivot at the ends through a pin and bearings. It was expected that the pin can be fixed to the piers through end plate connections whereas the bearings supply almost frictionless rotation.

To replicate damage in the structure, some steel elements can be replaced by a similar section of different material. For such a case, three additional aluminum beam-sections were ordered. Some of the desired effects that these sections provide are discontinuity of structure, change of stiffness and change of distributed loading profiles. Finally, the last element is a deck or platform which is not shown in the figure but will allow safe walking and vehicle traffic over the structure. Vehicle traffic will be limited only to scaled vehicles. The final dimensions of the bridge were:

- Length = 4500 mm
- Width = 1000 mm
- Height = 500 mm
- Beam section length = 1500 mm
- Approximate weight = 250 kg

7.5 Assembly

The designed structure is 100% disassemblable, for setup versatility and storage capability. The duration of assembly was around one working day (eight hours), but

initial adjustments and corrections took this period to almost two weeks. For the joints between beam-sections, bolts and nuts were used and the tightening procedure was performed using a pneumatic power tool to have similar torque in each bolt. Preliminary torquing of the bolts was made manually, but this caused excessive static deflection at midspan. Some pictures of the assembled structure will be shown below: Figure 7.3 depicts the detail of the boundary condition plate. The cylindrical shaft is the pin which rotates freely when the four bolts (marked with a circle) are not secured. When the bolts are secured (as in the picture), the boundary turns into a clamped one. Anchoring of the structure to the floor as well as connections between beams and end plate are partially shown.

Figure 7.3. Detail of mechanism for modifying the boundary conditions: bolted = fixed; unbolted = pinned.

An aerial view of the structure is depicted in Fig. 7.4. The bridge has four beams (from top to bottom of the figure) and each beam has three sections separated by connection flanges (marked with two rectangles). For damage simulation, these con-

nections can be left loose, a section of the beam can be removed without producing significant structural instability, or a section can even be replaced by an aluminum section. The versatility of such a configuration is considerable.

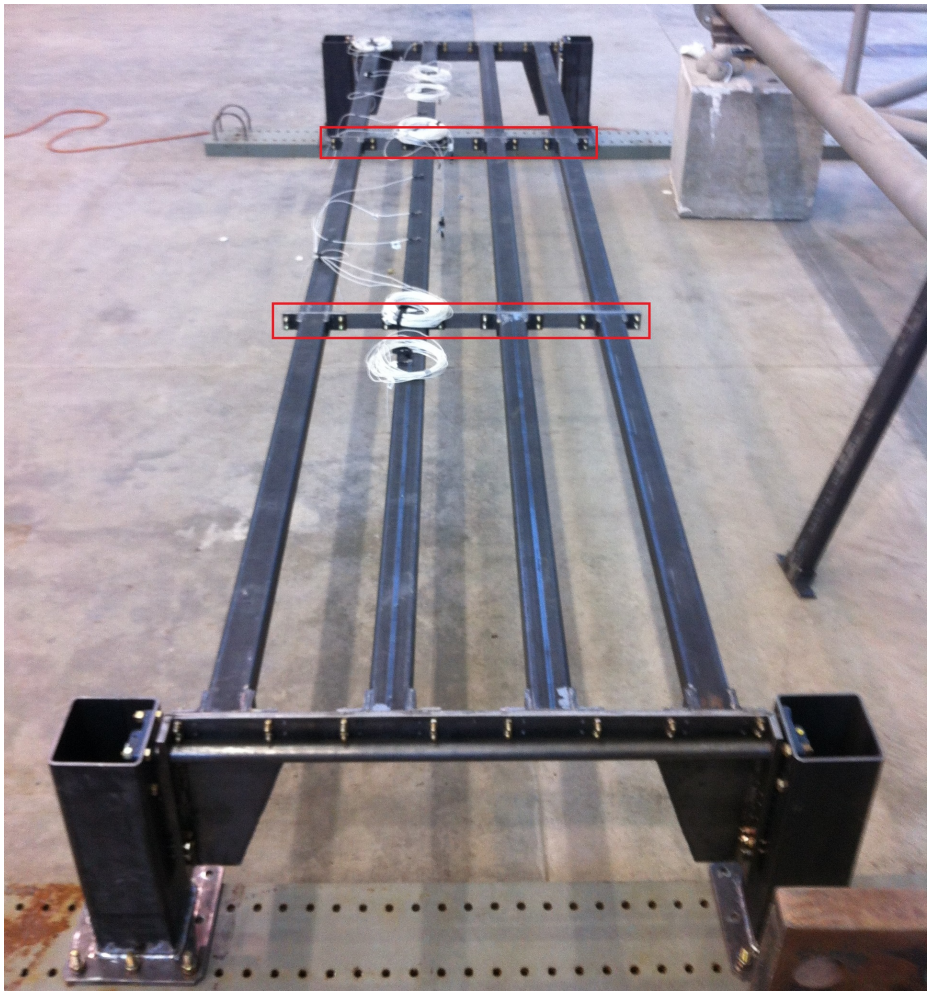

Figure 7.4. Aerial view of the structure.

This section has been intended to be a brief description of the steps taken to have a feasible experimental setup for the project. To provide detailed design calculations and material selection procedures is out of the scope of this thesis.

8. STRUCTURAL IDENTIFICATION AND CORRELATION OF CASE STUDY

8.1 Introduction

Most modeling problems pose a challenge as the results and findings obtained from a model always have to be later correlated with experimental observations. As stated in early chapters, no model is perfect, and paraphrasing George E.P. Box: "All models are wrong, but some are useful."

The proposed models are not the exception and from the earliest phase of the project, this fact was anticipated. Trying to model a complex 3D structure with an Euler-Bernoulli beam model which is essentially a 2D model represents the first, and ultimately, the main obstacle. Nevertheless, with the appropriate adjustments, such a model can be very useful to properly characterize the system's behavior. In this chapter, three identification processes will be applied; namely, one assuming that the bridge is behaving like a simply-supported beam; a second one, assuming the most critical case of an elastically supported beam which is a clamped-clamped case; a third one, updating the first two by introducing rotational masses and springs at both ends accordingly.

The identification will be done by the simple Fast Fourer Transform (FFT) technique, which will be applied to raw data collected from the structure to determine the natural frequencies by peak picking. In Section 8.4, three examples of model selection are developed so that the reader fully understands the mechanics of the method. As repetitive as this section and its sub sections may seem, they are intended to provide clarity towards the first step of the technique which is proposed to be a good model selection. After having understood the previous step, an example with real

experimental data gathered from the constructed structure is performed in Section 8.5, where previous knowledge of the model is used as starting point. In this section, parameter estimation and model refinement are explained. At the end of the chapter, the reader shall fully understand the two steps needed for a correct application of the proposed methodology.

8.2 Experimental Setup

A general experimental setup was assembled for testing the structure. Sixteen PCB PIEZOTRONIC piezoelectric, ceramic shear ICP® accelerometers were used in conjunction with two S+O ANALYZER data acquisition boxes with eight channels per box. Accelerometers were attached to the structure with magnetic mounts in several configurations which are listed in Table 8.1 and schematically described in Fig 8.1. For the case of Table 8.1, z corresponds to the vertical direction, longitudinal refers to vibration along the beam's horizontal x axis, and transversal refers to vibration along the beams transversal y axis. For this thesis, only configurations 2 and 3 will be analyzed to have a case as close as possible to that of a 2D vibrating beam.

Table 8.1. Experimental configurations.

Configuration	**No of sensors**	**Location**	**Figure and symbol**
1	16	beam 1	8.1(a), red dot
2	16	beam 2	8.1(a), blue squares
3	16	beam 3	8.1(a), green triangles
4	16	beam 4	8.1(a), orange diamonds
5	14	nodal pts	8.1(b), yellow sand-clocks
6	4	flange A	8.1(b), purple stars
7	4	flange B	8.1(b), red stars

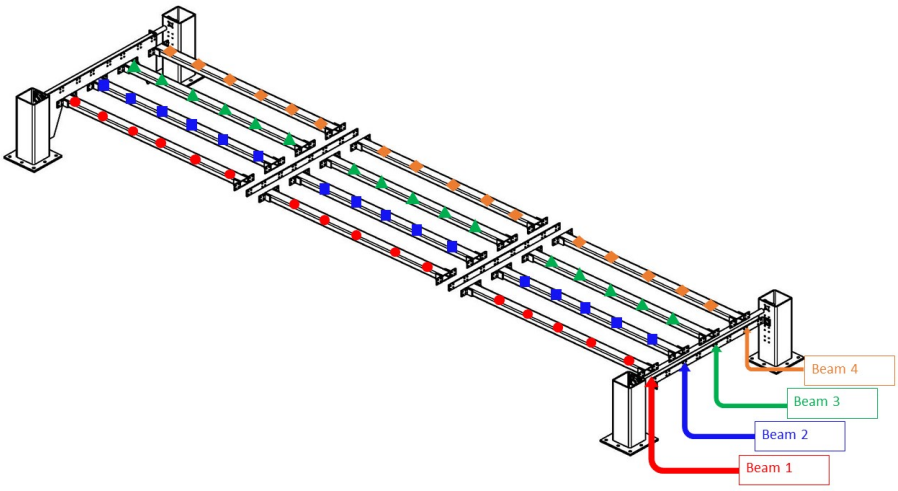

(a) Longitudinal configurations.

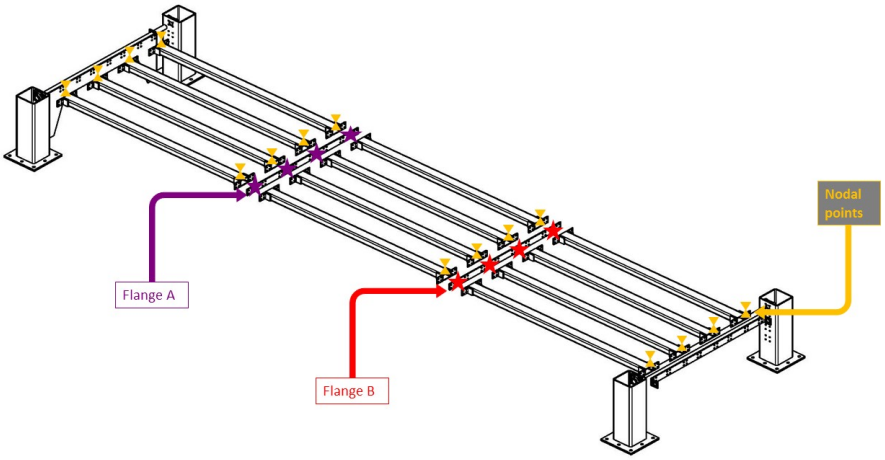

(b) Transversal configurations.

Figure 8.1. Experimental configurations.

Impact hammer testing was performed in each experiment with a sampling frequency of 1024 Hz to obtain useful frequency information up to half that value according to Nyquist-Shannonn theorem, i.e., 500 Hz. The hammer used was a PCB modally tunned hammer with a soft tip for low frequency excitation. Technical details

of all the equipment used in all conducted experiments are included as appendices however, the frequency range of such hammer is shown in Fig. 8.2

The standard experiment is described below:

1. Accelerometer mounting to the structure either using magnetic mounts or wax, depending if the added weight of the magnet is going to induce a parameter modification or it could be neglected. For this experiment, the added mass of accelerometer mounts is negligible.

2. Wiring between sensors, hammer and DAQ boxes. The type of accelerometers used for the experiment work with 10-32 low-noise type coaxial cables.

3. Initial settings in the data acquisition software including number of boxes to be used, active/inactive channels, type of signal (AC,DC), sampling frequency, time frame of each acquisition, data format, sensitivity of instruments, and units of measurement.

4. Impact testing. The structure is hit repeatedly, for around twenty times, leaving time between hits so that it can get back to zero vibration before the next hit (for this structure, usually 10-15 seconds) for around 20 times. The more hits, the better the results due to more averaging of impact response signals

5. After the first impact testing practice, data must be checked to verify its quality, consistency between hits, response form and whether it is meaningful. Only after this step, repeated testing can begin.

6. Post processing. With all the data sets properly stored, processing them with any selected technique can be performed. In this thesis, as mentioned earlier, the fast Fourier transform is used.

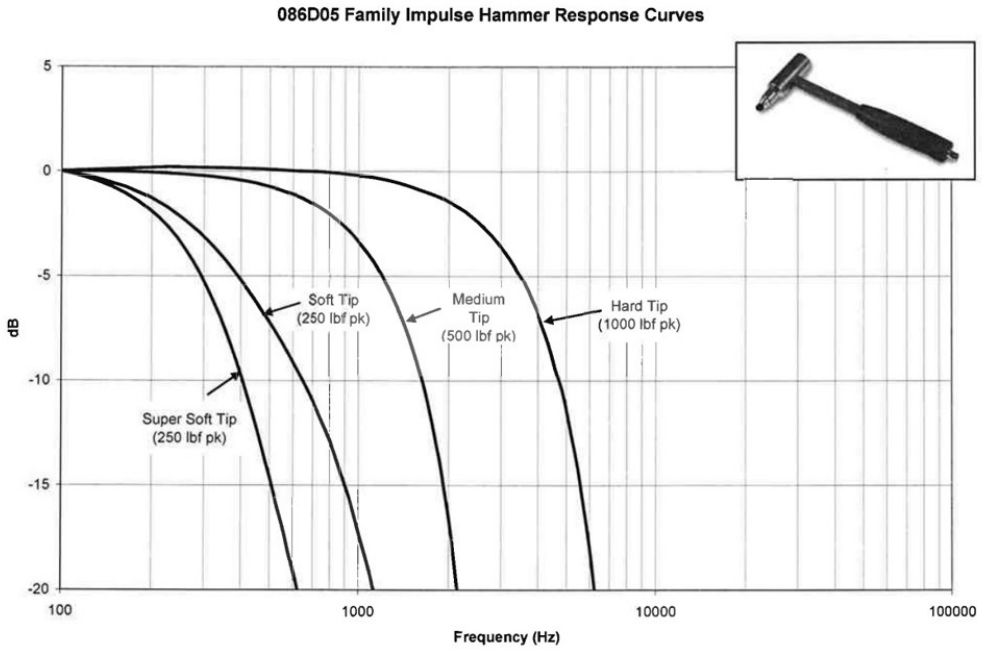

Figure 8.2. Hammer response curves (from PCB Piezotronics).

8.3 Algorithm for Modal Identification Fast Fourier Transform

The goal of modal identification is to obtain modal parameters of a structure such as natural frequencies, mode shapes and damping ratios from experimental data. As explained in Chapter 2, many techniques are available both in the frequency and time domains. Natural frequencies were estimated using the fast Fourier transform of the response acceleration signal of each accelerometer. A MATLAB code was used with inputs of impact signal and response acceleration data, and outputs of frequency response function (FRF or TF), real and imaginary TF, input spectra, and coherence function. Outputs of the code can be conveniently filtered by accelerometer or by hit number to determine specific information pertaining a desired location of the structure. The principal technique used in the code was the fast Fourier transform (FFT), which takes a discrete signal in the time domain and converts it into its discrete frequency-domain representation. This technique is extremely useful for computing modal parameters, as it shows resonant frequencies of a response signal as peaks which

are easy to identify. It is also popular because most of real life structures cannot be tested on a shake table or with a shaker to excite the desired frequencies. An example of the input and output signals for an arbitrary location of the bridge is shown in Fig. 8.3: the top graph is the impact signal, whereas the bottom graph is the acceleration response.

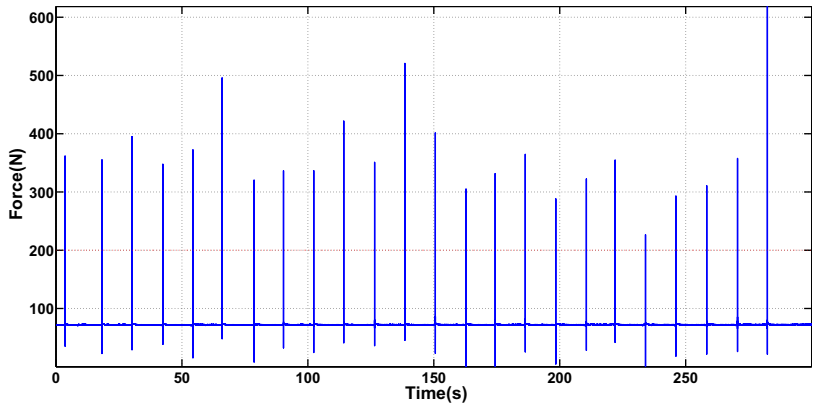

(a) Hammer impact history (input signal).

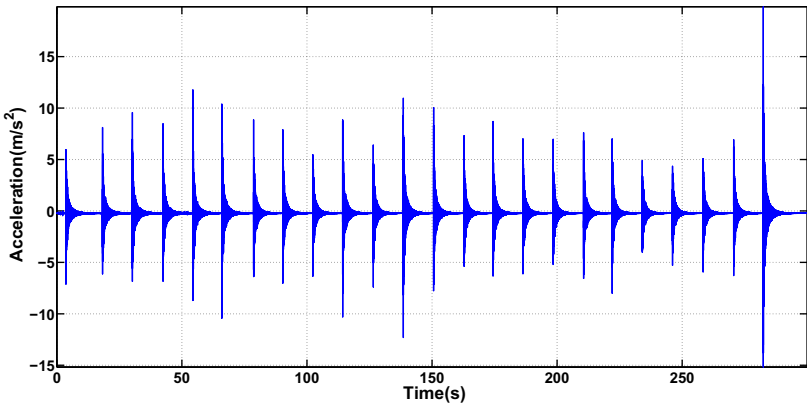

(b) Acceleration history (output signal).

Figure 8.3. Experimental input/output signals.

This constitutes the first step in the algorithm, so the analyst can make sure everything is normal in the input and output.

The next step is to choose which hits are good for analysis and which have to be neglected. As a manual technique, hammer hitting is not free from errors; at first, it

would appear to be an easy task, but it usually takes some time before one becomes experienced with the instrument to obtain the right hit. Figure 8.4 depicts the impact signal for a complete test, in which it is evident that impact peaks 9, 10 and 11 are in the same hit, as well as peaks 14 and 15. For error minimization, these have to be eliminated from the algorithm, to minimize errors.

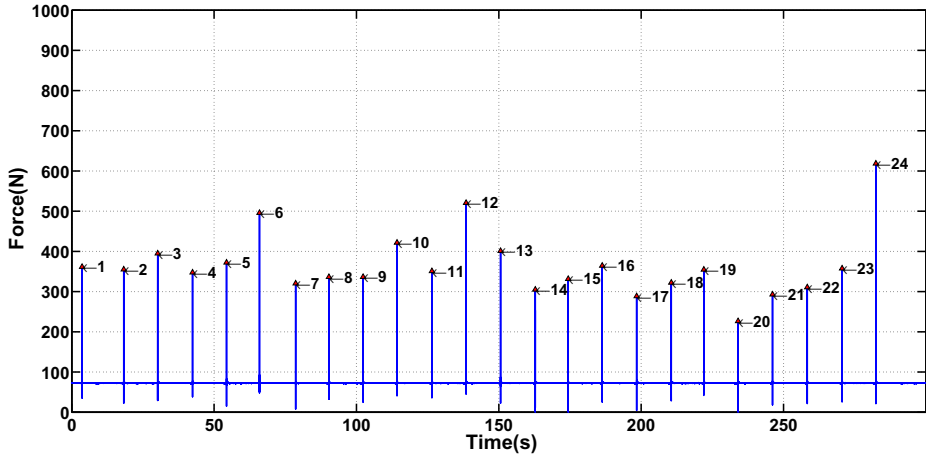

Figure 8.4. Hammer hit peak choosing.

A second check for choosing the right hits is to analyze each hitting interval, i.e., the force versus time of each hit within the chosen input window. There must be only one hit in the window for the algorithm to produce good results. If two or more impacts are observed, the hit has to be discarded as well. Figure 8.5 shows a plot in which all the hits within the chosen window have a single peak, the solid blue line is the window and the superimposed lines are all the hits. As two or more peaks appear, the hit should not be included in the analysis.

The next checkpoint is to determine if the impact signal is large enough to excite all the frequencies of interest. A good technique for this verification is to get the hammer response curve for the experiment, similar to Fig. 8.2. This plot will determine if the chosen tip is suitable for exciting the modes of interest. Of course, this is intended when specific frequencies are to be studied. Nevertheless, time, resources and effort are used in every experiment, and it is not desirable to waste them by not

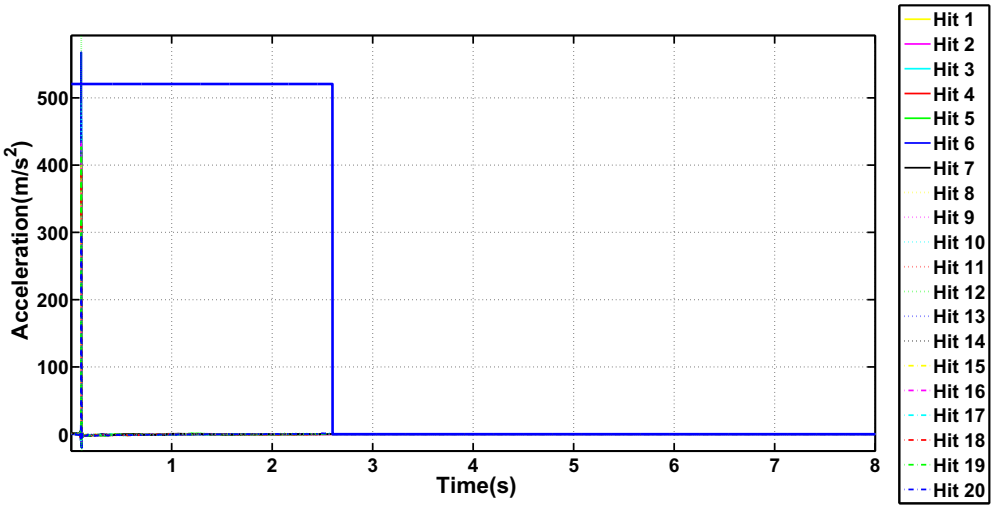

Figure 8.5. Number of peaks within an imput window.

paying attention to all the details.

Just like the input signal needs to be thoroughly analyzed, the output signal must be taken care of as well. One of the most important aspects of impact testing is the use of a good window for the response (different than the input window described above). This resource is necessary due to the fact that a lightly-damped structure, such as the experimental setup, will not cease vibrating within the short time between hits. Even if this time is extended as much as possible, very small amplitude vibrations will remain on the system for rather long time. To overcome this problem, the signal must be forced to decay to zero within a reasonable window width. The most popular impact weighing window used for this purpose is the exponential which is used to "force the data to satisfy the periodicity requirements of the Fourier Transform" [83].

After all these "sanity checks", one is ready to obtain the plots of interest: the FRF, and the imaginary transfer function from which the mode shapes and natural frequencies and damping ratios can be determined.

8.3.1 Modal Analysis Results of Experimental Setup

The MATLAB algorithm output is a set of plots for fully understanding the response of the system in the frequency domain. Some of these plots will be shown herein; specially the two most important: FRF and mode shapes. It should be noted that a preliminary definition of the peak region must be made for the algorithm to determine the exact frequency at which a mode appears. This is done in the program setup and is very useful for modal verification. Figure 8.6 shows the most relevant code outputs:

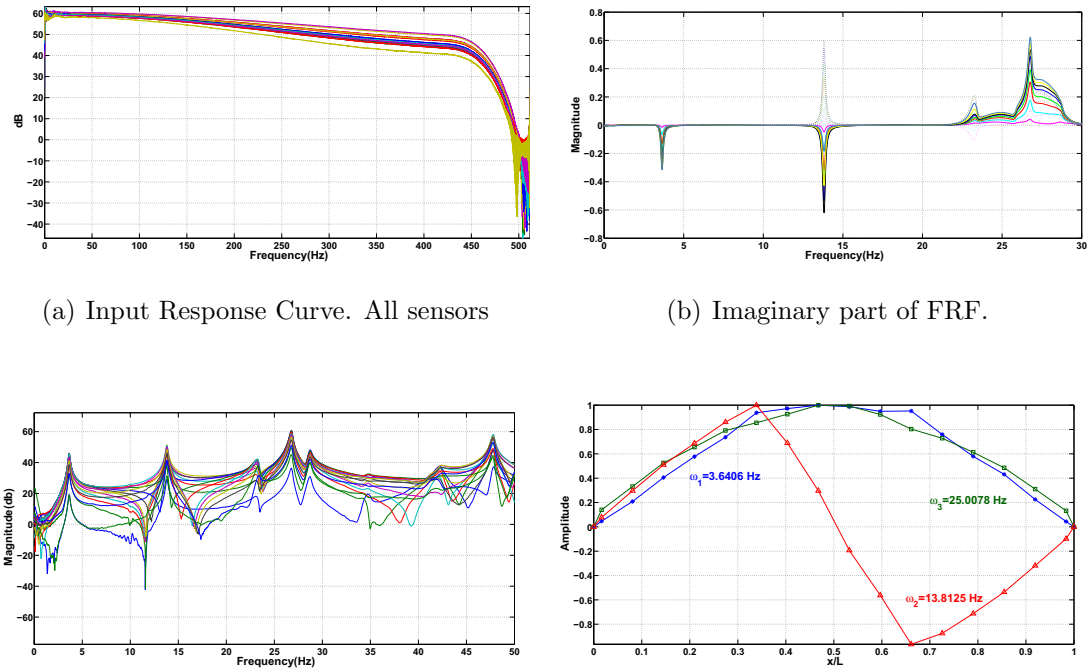

(a) Input Response Curve. All sensors

(b) Imaginary part of FRF.

(c) Transfer Function. All sensors.

(d) First Three Modeshapes.

Figure 8.6. FFT code outputs.

Figure 8.6(a) shows the input response for the chosen hammer tip. This means that frequencies up to 400 Hz can be excited by the hitting action. The imaginary part of the FRF is plotted in Figure 8.6(b). This plot is particularly useful for determining the mode shapes as the phase and relative amplitude of each peak determines the corresponding phase and amplitude of each sensor position. The better the res-

olution (i.e., the number of sensors), the better the mode shape estimation. The resolution issue was addressed at the end of Ch. 4.

In an ideal testing methodology, the complete FRF matrix could be obtained by hitting every sensor location and acquiring and post-process the generated data. Unfortunately, the testing procedure has to be planned considering the time factor and performing n hammer tests would result in a significant consumption of time (n is the number of sensors), this is why only one row or column of the FRF matrix was obtained which provided fairly acceptable mode shape results. Figure 8.6(c) shows the FRF for all the accelerometers where the first four peaks can be clearly distinguished and finally, Figure 8.6(d) depicts the mode shape estimation for the first three modes which were later correlated using the proposed method.

8.4 Correlation to a Simply-Supported Beam

The correlation process has been designed to be fully computational. That is to say that an experimental model should be compared to a group of candidate models automatically to determine the closest relationship which is the updated model. To show the methodology in this thesis, the correlation study will be shown individually for three example cases. In the first case, the model space consists of a unique element corresponding to the simply-supported beam: single mode shape vectors along with stacked vectors are plotted on the same axes, as explained in Chapter 4; and finally, all vectors: single modes and stacked modes are computationally correlated. For demonstration purposes, a group of superimposed plots will be presented in which all three modes are compared separately as well as stacked (similar to Fig. 6.1). The first three normalized mode shape vectors, both in amplitude and in distance of a simply-supported beam with a resolution of sixteen accelerometers (plus two nodes at the ends) are shown in Fig. 8.7, 8.8 and 8.9. Each figure depicts a mode shape column vector with its correspondent graphical representation so the reader can better

understand what a mode shape vector is and looks like. It must be kept in mind that these are the analytical model mode shapes, to which the experimental are going to be compared. This explanation will be made only for the simply-supported case as the procedure becomes repetitive for further models.

$$\psi_1 = \begin{Bmatrix} 0 \\ 0.0060 \\ 0.0297 \\ 0.0522 \\ 0.0725 \\ 0.0898 \\ 0.1035 \\ 0.1129 \\ 0.1178 \\ 0.1178 \\ 0.1129 \\ 0.1035 \\ 0.0898 \\ 0.0725 \\ 0.0522 \\ 0.0297 \\ 0.0060 \\ 0 \end{Bmatrix}$$

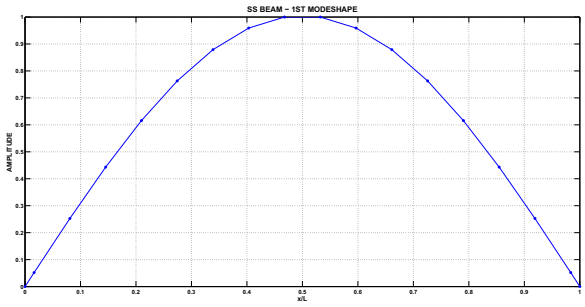

Figure 8.7. First mode shape vector along with its graphical representation. SS model.

These three mode shape vectors will be correlated with the corresponding three experimental mode shapes with the addition of two stacked mode shape vectors. The first stacked mode shape vector and its graphical representation is shown in Figure 8.10. Due to space limitations, the second stacked vector which consists of 54 row-elements will not be displayed, although its graphical representation will be presented in the results section. After this preliminary step, the procedure becomes straightforward: five experimental vectors are going to be compared graphically and iteratively against five analytical vectors to determine the degree of linear relation between them. The procedure, as described in Sec. 4.1, will be applied herein for this model case. Two plots will be presented: a first, corresponding to the mode shape comparison and a second, one corresponding to the correlation matrix.

$$\psi_1 = \left\{ \begin{array}{c} 0 \\ 0.0121 \\ 0.0576 \\ 0.0937 \\ 0.1146 \\ 0.1170 \\ 0.1004 \\ 0.0676 \\ 0.0238 \\ -0.0238 \\ -0.0676 \\ -0.1004 \\ -0.1170 \\ -0.1146 \\ -0.0937 \\ -0.0576 \\ -0.0121 \\ 0 \end{array} \right\}$$

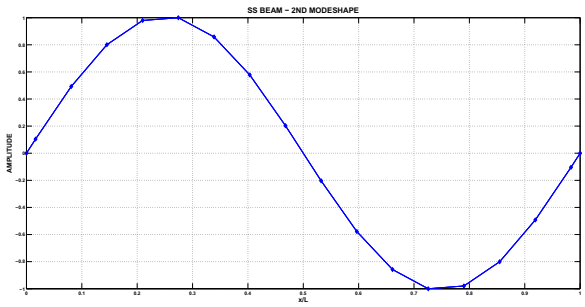

Figure 8.8. Second mode shape vector along with its graphical representation. SS model.

8.4.1 Graphic Results for the Simply-Supported Case

Figure 8.11 shows the graphic relation between five experimental vectors versus five analytic vectors. A close relationship can be observed for the first two modes as the red and black lines are almost collinear; however, for the third mode and subsequent sub-plots, this trend begins to disappear and significant discrepancies between lines are observed.

8.4.2 Correlation Results for the Simply-Supported Case

The correlation matrix is presented graphically in the form of bars. As more mode shapes are added to the result, more decreasing trend is observed. Figure 8.12 shows these results.

From this graphic, many conclusions can be discussed.

$$\psi_1 = \left\{ \begin{array}{c} 0 \\ 0.0182 \\ 0.0817 \\ 0.1160 \\ 0.1087 \\ 0.0625 \\ -0.0060 \\ -0.0725 \\ -0.1129 \\ -0.1129 \\ -0.0725 \\ -0.0060 \\ 0.0625 \\ 0.1087 \\ 0.1160 \\ 0.0817 \\ 0.0182 \\ 0 \end{array} \right\}$$

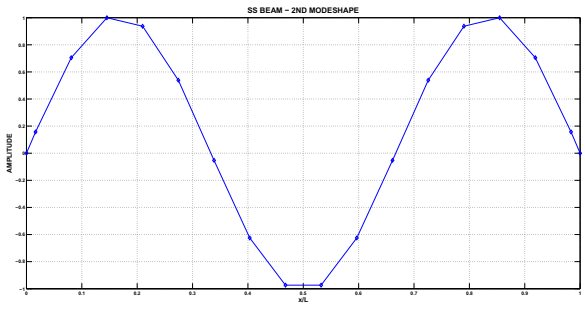

Figure 8.9. Third mode shape vector along with its graphical representation. SS model.

1. An acceptable correlation is observed between mode shapes 1 and 2. This is expected as first and second mode shapes are quite similar for all cases.

2. When comparing between the third mode shape vectors, a dramatic decrease of correlation index is obtained. This is likely to yield a solid conclusion of incorrect model.

3. The overall correlation index, which can be obtained by simply taking the last value of the correlation vector as it shows the linear relationship of all the stacked mode shapes is $CI = 0.3952$, which is rather low for concluding a strong relationship.

4. The correlation vector is presented below:

$$\psi_4 = \left\{ \begin{array}{c} 0 \\ 0.0060 \\ 0.0297 \\ 0.0522 \\ 0.0725 \\ 0.0898 \\ 0.1035 \\ 0.1129 \\ 0.1178 \\ 0.1178 \\ 0.1129 \\ 0.1035 \\ 0.0898 \\ 0.0725 \\ 0.0522 \\ 0.0297 \\ 0.0060 \\ 0 \\ 0 \\ 0.0121 \\ 0.0576 \\ 0.0937 \\ 0.1146 \\ 0.1170 \\ 0.1004 \\ 0.0676 \\ 0.0238 \\ -0.0238 \\ -0.0676 \\ -0.1004 \\ -0.1170 \\ -0.1146 \\ -0.0937 \\ -0.0576 \\ -0.0121 \\ 0 \end{array} \right\}$$

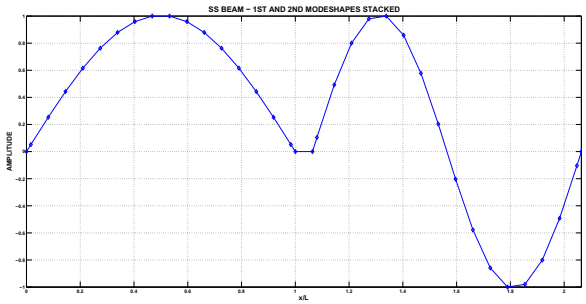

Figure 8.10. Vector of two stacked mode shapes along with its graphical representation. SS model.

$$CM = \begin{bmatrix} 0.9963 \\ 0.9534 \\ 0.0117 \\ 0.9738 \\ 0.3952 \end{bmatrix}.$$

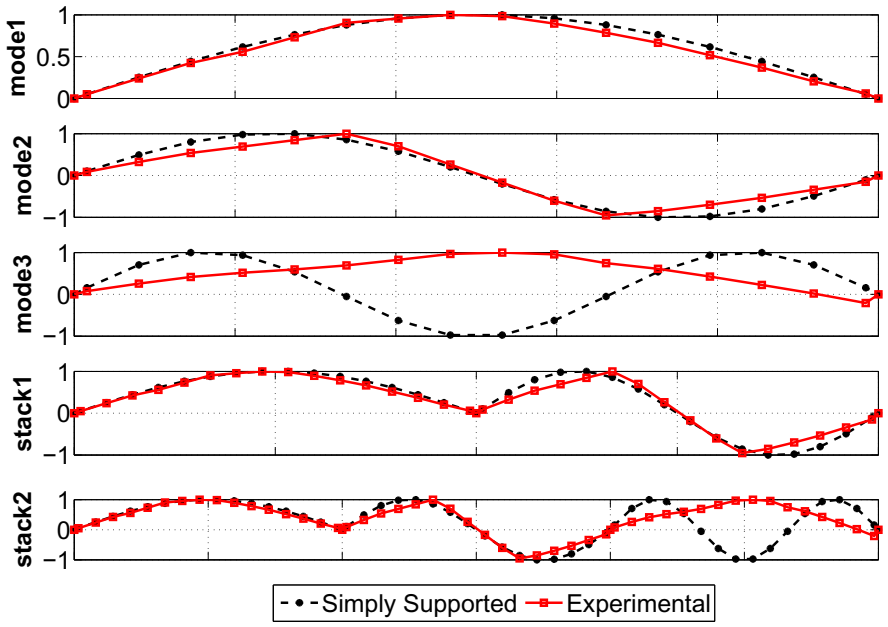

Figure 8.11. Simply-supported vs. experimental mode shapes.

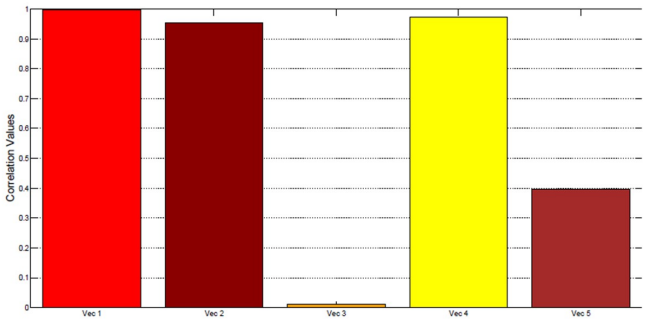

Figure 8.12. Correlation results. Simply-supported model.

8.4.3 Correlation to a Clamped-Clamped Beam

A similar approach to that of the previous section was applied, but using the model of a clamped-clamped beam instead. The reader should recall that the purpose of this algorithm is to look for the higest correlation between the experimental mode

shape and the chosen mathematical ones. For brevity, the mode shape vectors are not presented explicitly, instead, only the three first graphical representations of the mode shapes are shown in Fig. 8.13.

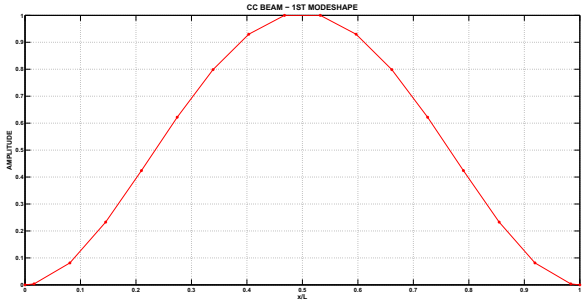

(a) 1st Modeshape.

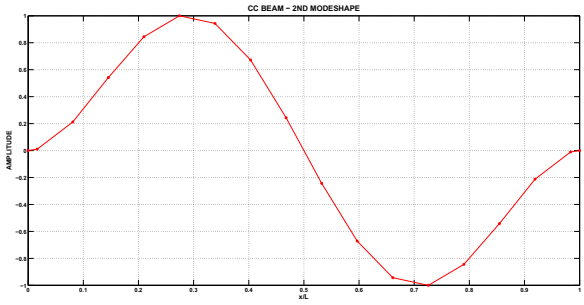

(b) 2nd Modeshape.

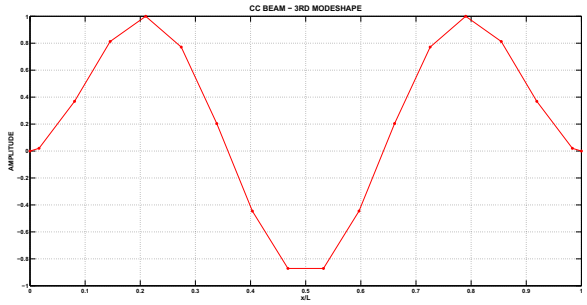

(c) 3rd Modeshape.

Figure 8.13. Modeshapes of a clamped-clamped beam.

Although these look rather similar to those of the simply-supported case, the reader should note a slight difference in the slope at the boundary conditions. Therefore, a second check is to be performed, using the same experimental mode shape vectors.

After performing the correlation check for a second time, the results are shown in Fig. 8.14. The conclusions for this graphic are:

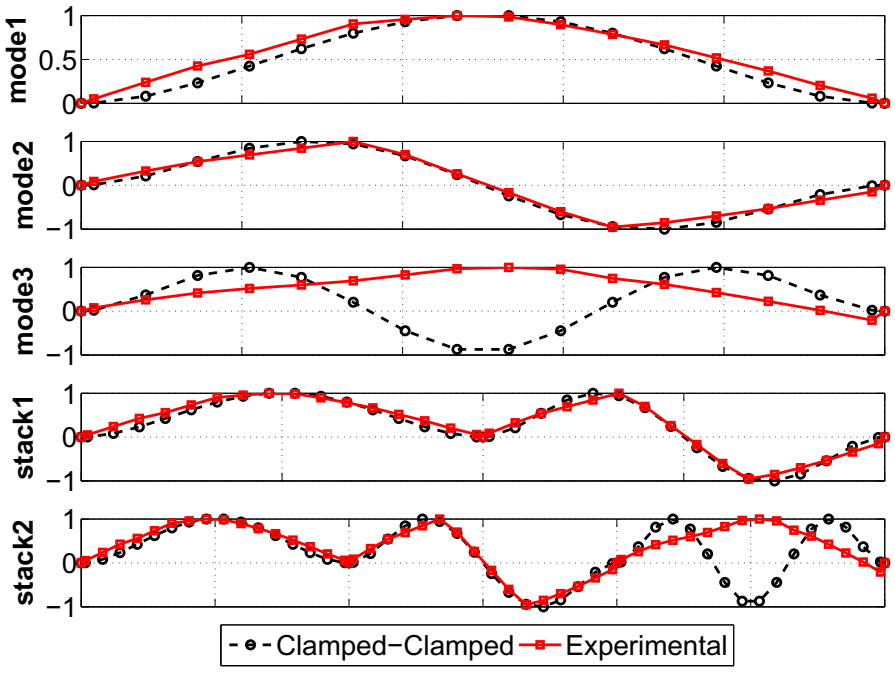

Figure 8.14. Clamped-clamped vs. experimental mode shapes.

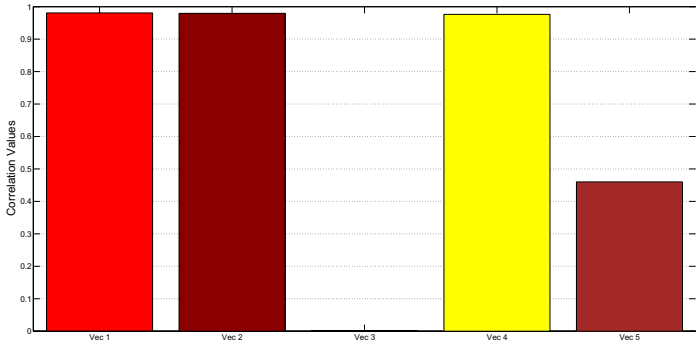

Figure 8.15. Correlation results. Clamped-clamped model.

1. Again, high correlation values appear for mode shape vectors 1 and 2.

2. An even lower correlation value than that of the simply-supported case is observed in mode shape 3.

3. The overall correlation index, is $CI = 0.4598$, a small improvement from the last case, but still too low for a conclusive judgment.

4. The correlation matrix is presented below:

$$CM = \begin{bmatrix} 0.9808 \\ 0.9794 \\ 0.0018 \\ 0.9763 \\ 0.4598 \end{bmatrix}.$$

8.4.4 Correlation to a Beam with Rotational Masses at Both Ends

The third preliminary check is made with a beam with rotational masses at both ends. It is assumed that the mathematical model matches with enough proximity to the real inertia of the bridge's ends. However, this is not going to be always the case and that is expected. The method would have the capability to identify even a difference like that. When a computational run of this algorithm is performed to an unknown structure, it would have to be able to identify its physical parameters such as inertial forces. A beam with rotational masses on both ends was depicted in Fig. 5.5. The three individual mode shapes are shown in Fig. 8.16.

When correlating these modes with those of the experimental model, the results of Fig. 8.17 are obtained. For the case of the rotational mass model, a much more clear coincidence is observed between the experimental and model curves. Nevertheless, this does not mean that the chosen model is correct. This point has to remain very clear for the reader. The proposed methodology only offers a procedure for choosing a

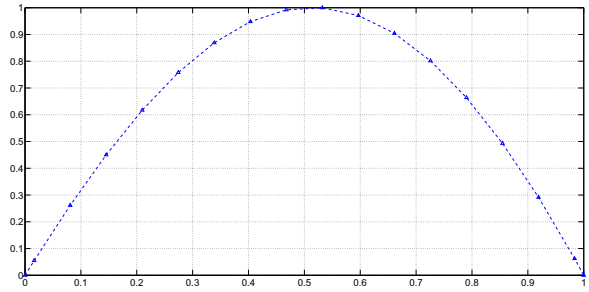

(a) 1st Modeshape.

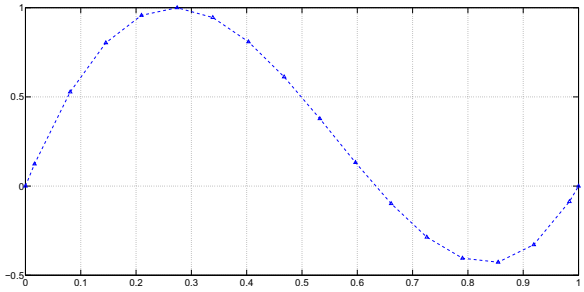

(b) 2nd Modeshape.

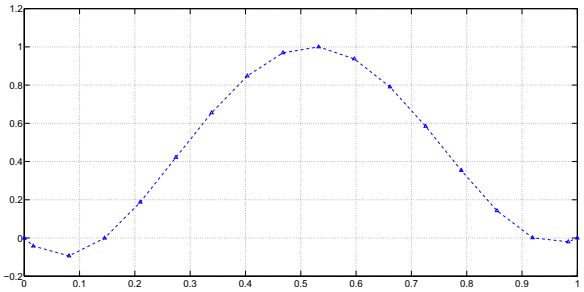

(c) 3rd Modeshape.

Figure 8.16. First three mode shapes of a beam with asymmetrical rotational masses.

model close enough so that the system's behavior can be predicted with such model, but it does not result in a model confirmation technique.

The observations of this third correlation check are summarized in the following list:

1. This is the best result of all three correlation tests.

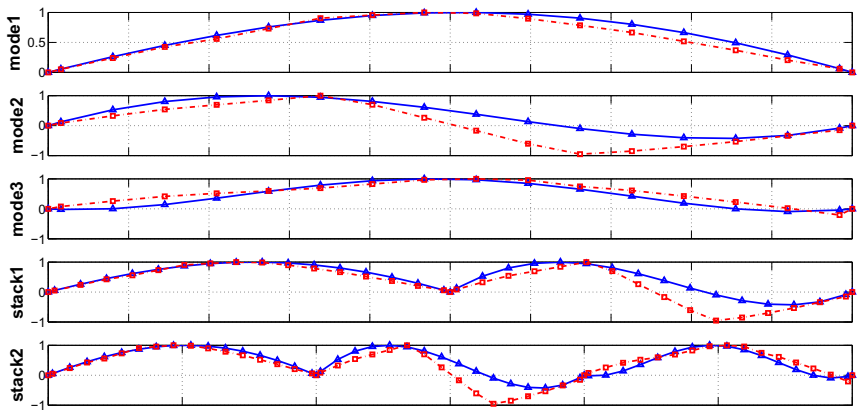

Figure 8.17. Rotational mass vs. experimental mode shapes.

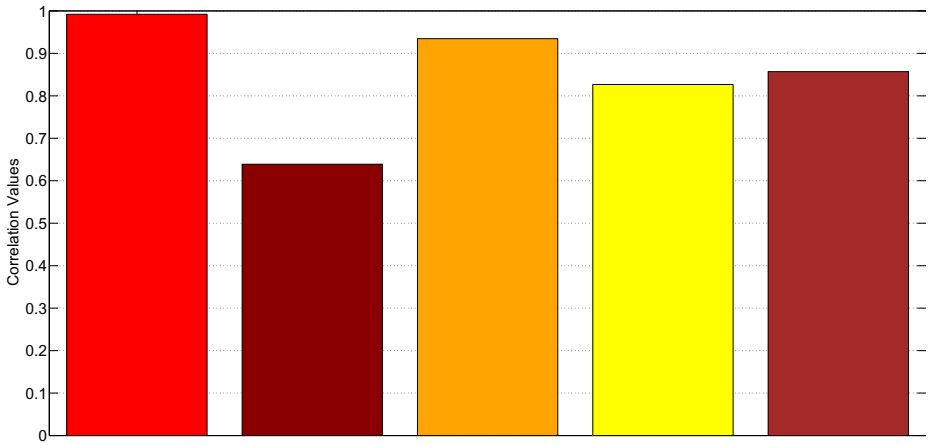

Figure 8.18. Correlation results. Rotational mass model.

2. High correlation values appear in mode shapes 1 and 3. A slightly lower correlation value appears in mode shape 2. This can be obesrved in Fig. 8.17 where curves corresponding to the 2nd mode shape have a small deviation.

3. The overall correlation index, is $CI = 0.8570$, which is significantly higher than the preceding cases. Notice that for a total confirmation of correlation, more modes can be used in the study and no experimental model will have values close to unity due to external factors and uncertainties.

4. The correlation vector is presented below. However, should be noted that the main difference is established by the high correlation of the third mode shape in contrast to the two preceding cases where such value was close to zero.

$$CM = \begin{bmatrix} 0.9920 \\ 0.6389 \\ 0.9346 \\ 0.8267 \\ 0.8570 \end{bmatrix}.$$

8.5 Correlation Algorithm to Determine Model Parameters

The previous three sections were devoted to explaining and demonstrating the visual and general characteristics of the proposed method. A broad model definition was made based on such observations. However, as explained in Sec. 6.4, this is a vague conclusion and does not offer the analyst a solid relationship between the general model and the unknown boundary conditions. To overcome this problem a similar procedure as the one developed in the cited section is done herein with the only difference that instead of using a mode shape set generated with a simulation, a real experimental mode shape set of unknown boundary conditions is considered. Such mode shape set is shown in Fig. 8.6(d). A similar comparison to the eighteen cases utilized in Sec. 6.4 is shown in Fig. 8.19. The solid red line corresponds to the experimental mode shape obtained from hammer testing of the structure, the dashed blue and green lines correspond to the spring-supported and rotational-inertia models, respectively. It is evident that closer correlations of the experimental mode shape with the latter occur, whereas poor correlations with the former, especially in the third mode shape is observed.

Similarly, as in Sec. 6.4, the second part of the analysis is to study the correlation index for each inertia combination which was presented in the form of a bar plot. At

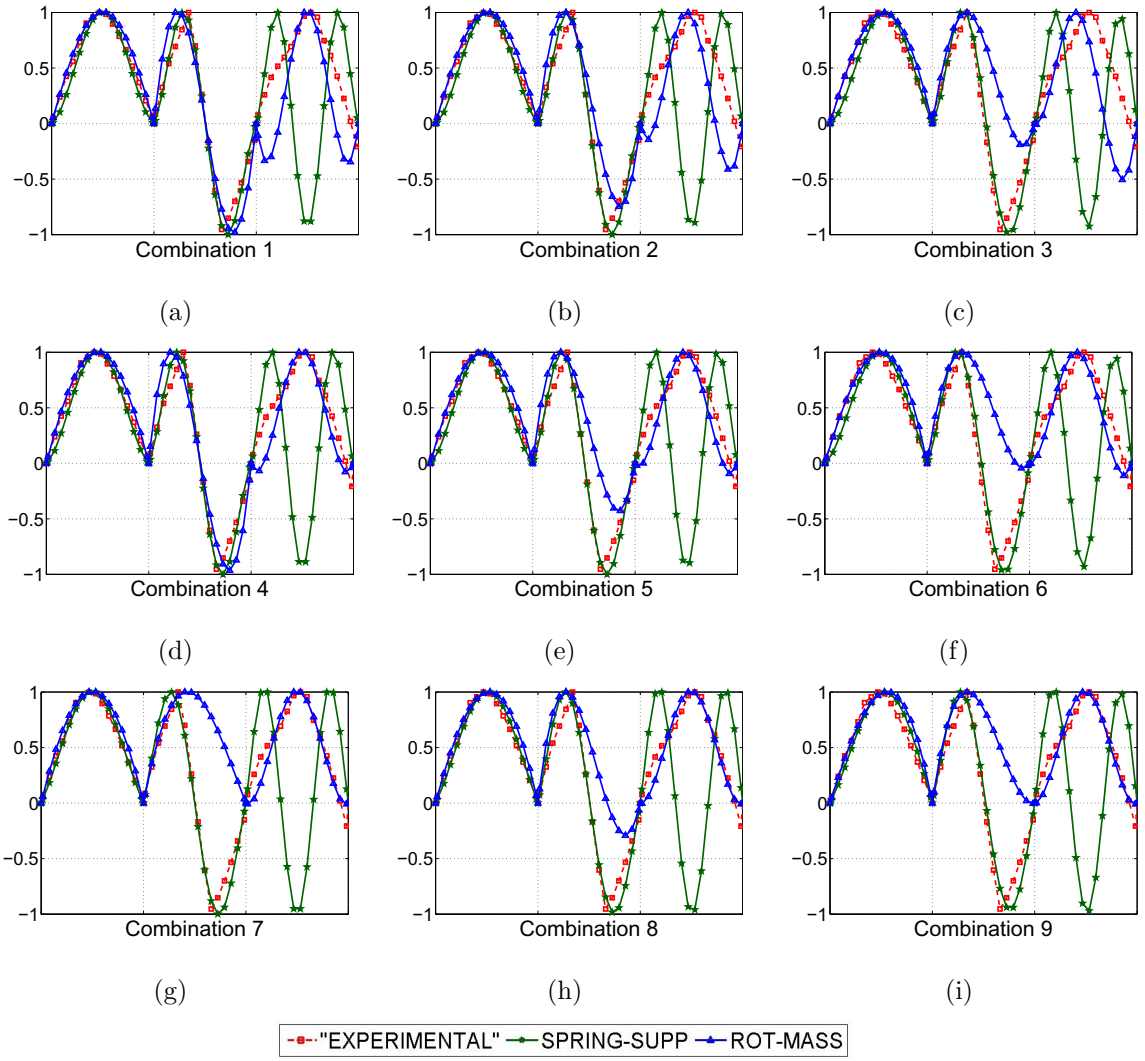

Figure 8.19. Correlation comparison of nine parameter combinations.

this point it is necessary to point out that this technique is intended to facilitate the model updating process but it requires that the analyst also apply good engineering judgment. A certain amount of knowledge of the structure is required beforehand, for instance the general type of boundaries at which the structure is subjected to (e.g., fixed, free, pinned or some combination of these); the general type of loading (e.g., concentrated load, distributed or profiled loading, or some combination of these); and the type of service the structure is intended for (e.g., heavy or light traffic, pedestrian traffic, or some combination of these). A good check of the validity of the chosen

parameters is to compare the natural frequencies with those of the chosen model. If such frequencies are comparable within a range between 10% and 20% (for at least the three first natural frequencies), it could be said that reasonable close model for an unknown system.

The bar plot of the correlation indexes for both rotational inertia and spring-supported model cases are shown in Fig. 8.20. The final results are:

- Simply supported structure with rotational masses on both ends.
- Parameter values are: $I_1 = 52.712$ Nm^2/rad, and $I_2 = 52.712$ Nm^2/rad which produce a correlation index of 0.937.
- The first five natural frequencies compared to those corresponding to the model are listed in Table 8.2

Table 8.2. Final frequency comparison (in Hertz).

Analytical	**FEM**	**Exp.**
5.7071	5.8918	3.6328
13.3434	14.4385	13.8516
22.1749	25.8347	27.8750
49.8844	50.6847	47.8203
93.2855	93.6796	94.2180

8.6 Discussion

Even though choosing the boundary condition combination case with the highest correlation may prove to be enough for selecting a model, this conclusion may not be final as other parameter combinations may present a high correlation value. Consider

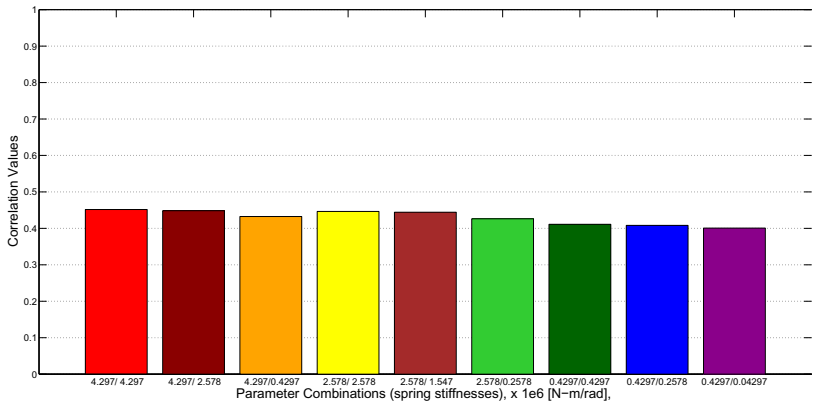

(a) Simply supported with rotational springs

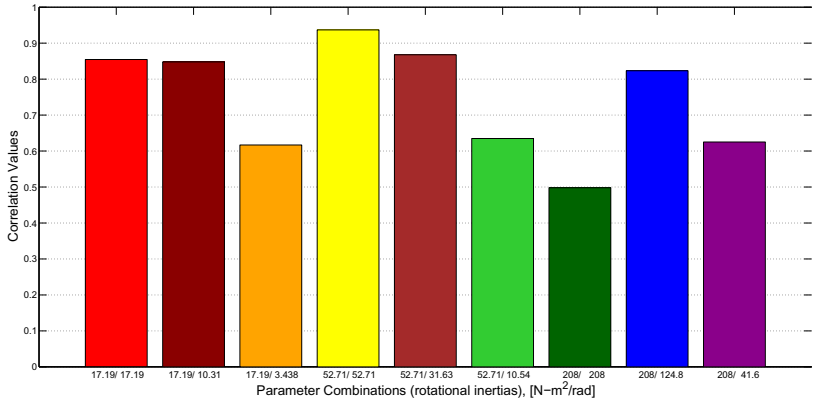

(b) Simply Supported with rotational masses

Figure 8.20. MAC-based correlation results.

for example a case in which two correlation indexes are very close in value. Which one is correct and could a threshold be defined to evaluate this quantitatively? This constitutes an important design question. Certainly one could choose to use more mode shape vectors. Indeed, when using only the first mode shape vector, almost all the indexes are approximately equal to one. When the second mode shape is added, some indexes reduce considerably but still several are close to one. If the third mode shape is added, a bar plot similar to Fig. 8.20 can be observed. In this case, the yellow and maroon bars are pretty close. By adding a fourth mode shape vector, it is

expected that the leading trend of a parameter combination is maintained, confirming such as the best match.

Low correlation values as those depicted in Fig. 8.20(a) are a clear indication of insufficient model space size. A poor correlation index average value is signal of the wrong model selection. Moreover, if by adding more mode shape vectors the trend does not change, a different model must be selected and added to the correlation algorithm.

An alternative to the previously mentioned problem is the fact that each modal contribution's weight is different in the total response of the system. Indeed, the first mode has a bigger contribution than the second mode, which has a bigger contribution than the third mode, and so on. From this standpoint, one could think about applying a weighting function to each mode so that the stacked mode shape vector varies by sections instead of in an overall way. This approach could represent a much more accurate correlation algorithm.

Another good alternative is to modify the resolution of the experiment in such a way that a variable resolution is obtained. In sections of the structure where the mode shape behavior is fully understood and predicted, fewer sensors can be installed in exchange of zones of the structure in which more understanding of the behavior is needed. This technique could be linked to the weighting approach described above in the sense that a higher number of sensors can be used when trying to identify higher modes.

8.7 Implementation of the Methodology

The correlation technique developed in this thesis is an intermediate step between experimental data and updated model. For full implementation of the method in a real structure, a diagram with all the suggested steps is presented in Fig. 8.21, this diagram is a summary of what an analyst must do to implement this technique in any structure.

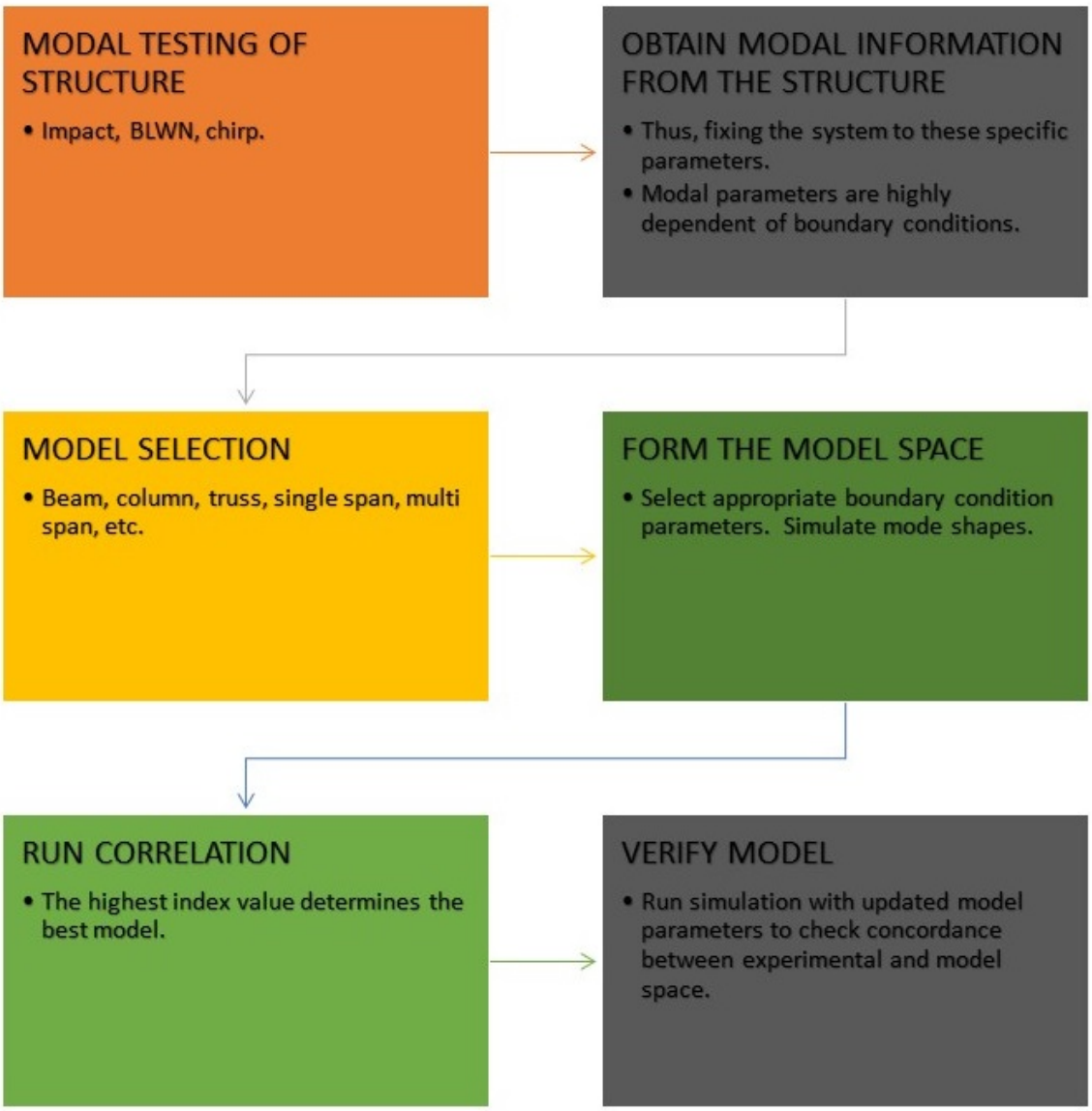

Figure 8.21. Correlation method. Implementation

9. CONCLUSIONS

A novel methodology for establishing an accurate model for predicting the behavior of the vibrations in a beam has been developed, in which a linear correlation equation is applied to compare the degree of linearity between an experimentally obtained mode shape vector and a group of suitable analytical mode shape vectors extracted from selected model candidates (model space). The procedure is performed iteratively comparing one by one until the highest correlation index is achieved.

After performing the proposed methodology, if deviations are still present in the model, classical model updating techniques can be further applied to tweak the response to a most accurate state. However, the correlation technique should be enough.

Finding natural-frequency correlations may not yield the most accurate model as mode shape correlations. However, a good extra check for the analyst is to compare mode shapes in a first step; and natural frequencies in a second step to approximate the model as much as possible to the real structure.

Almost all the classical models along with the non-classical combination cases studied give a high correlation for the first mode shape and fairly high values for the second mode shape. When analyzing from the third mode shape onwards, is when correlation study can be clearly distinguished. Therefore, a good result is obtained when constructing a vector of at least the three first mode shapes stacked together. Correlation cannot be studied when comparing individual mode shapes as many of these are similar from one model to another.

An updated model in which the manipulable parameters are those corresponding to the boundary conditions instead of structural or material parameters, is a much more realistic model to work with. The main source of model discrepancies should be looked for in the most unknown aspect of a structural system which precisely are its boundary conditions. This also holds for model variations over lifespan, as boundary conditions are the most likely aspect of a system to change due to use and wear.

The proposed methodology can be used as a supplementary or complementary technique. The former, for cases where computational costs and time requirements are not a big issue; and the latter, where high accuracy of the updated model is required. Nevertheless, once a model has been narrowed enough with the correlation method, computational costs can drop significantly if compared to applying the traditional model updating techniques for the whole process.

Model spaces can be constructed either from analytical equations, or finite element models; the method does not require a closed-form solution of any model equation, but only a mode shape vector, which makes the methodology much more user-friendly and straightforward.

Deviations of the observed natural frequencies from those of the predicted by the updated model are expected for higher modes. Indeed, Table 8.2 shows good concordance for the first three modes and an increasing deviation for higher modes due to noise implications and system uncertainties.

The most visible uncertainty of the experiment was welding torsion which was not included in the model. Probably this is the reason of some of the deviations described above. This particular uncertainty is likely to be the cause of having the same rotational inertia value in both sides when these values are not symmetric in reality.

10. RECOMMENDATIONS AND FUTURE DIRECTIONS

1. Many features could be enhanced for future testing. One of the main issues encountered is the torsion of the beam-sections due to welding. It is well known that any welding process will inflict residual stresses due to excessive heat produced. It is recommended a close monitoring of the manufacturing procedure to minimize such a problem. An industrial procedure known as matrix manufacturing may be used where a pattern is set up beforehand to constrain the elements that are going to be welded so the stresses won't twist them in the process.

2. For experiments with a large amount of accelerometers (> 5), it is highly recommended the use of wire identifiers. The task of identifying cables among many similar-looking ones can be very time consuming.

3. If finite element modeling is selected as the source of the elements of the model space, careful attention must be paid to filter computational modes.

4. It is not necessary to have a big amount of elements in the model space. The experimental comparison of Ch. 8 was made with six cases for one of the boundary conditions, and fractions of 1, 0.6, 0.4, 0.2 and 0.1 of that value for the other boundary condition. This set of combinations yielded 36 elements in the model space. It is recommended to start looking for the extreme cases (2 elements), and then include a couple in between. Once the model has been narrowed, more elements can be added as needed.

5. A logic future direction of this research project is to explore simple structures different than a beam; say, a one or two story structure.

6. The present thesis used only mode shape vectors as the comparison elements. Natural frequencies were not included in the analysis but only as posterior check points. It is recommended to include natural frequencies as a weighting element in the methodology for further accuracy of the method.

7. The structure used in this project has the capability of replicating many types of boundary conditions. Though, only a simply-supported configuration with rotational masses at both ends was used. Another logic future step is to explore different boundary conditions in the same structure and to apply the methodology in these.

8. Another possible approach for dealing with the problem of more than one high correlation index would be to explore the possibility of applying a weighting factor to each mode, proportional to the contribution of such mode to the total response of the structure.

LIST OF REFERENCES

LIST OF REFERENCES

[1] Wikipedia contributors, "Structural Health Monitoring," Wikipedia, The Free Encyclopedia, http://en.wikipedia.org/w/index.php?title=Structural_health_monitoring\&oldid=612319780 (accessed July 23, 2014).

[2] Wikipedia contributors, "Modal Analysis," Wikipedia, The Free Encyclopedia, http://en.wikipedia.org/w/index.php?title=Modal_analysis\&oldid=618123843 (accessed July 23, 2014).

[3] Wikipedia contributors, "Finite Element Updating," Wikipedia, The Free Encyclopedia, http://en.wikipedia.org/w/index.php?title=Finite_element_updating\&oldid=594129961 (accessed July 23, 2014).

[4] Caicedo, J. M. "Two Structural Health Monitoring Strategies Based on Global Acceleration Responses: Development, Implementation, and Verification." MSc. Thesis, Washington University at Saint Louis, 2001. Department of Civil Engineering, 2001.

[5] Meirovitch, L. "Fundamentals of Vibrations". International Edition, McGraw-Hill, 2004.

[6] Karnovsky, I. A., O. I. Lebed. "Free Vibrations of Beams and Frames". New York: McGraw-Hill, 2004.

[7] Gorman, D.J. "Free Vibration Analysis of Beams and Shafts". New York: Wiley, 1975.

[8] Blevins, R. D., and R. Plunkett. "Formulas for Natural Frequency and Mode Shape." Journal of Applied Mechanics 47 (1980): 461.

[9] Hibbeler, R. C. "Free Vibration of a Beam Supported by Unsymmetrical Spring-Hinges." Journal of Applied Mechanics 42, no. 2 (1975): 501-502.

[10] Hibbeler, R. C. "Erratum: Free Vibration of a Beam Supported by Unsymmetrical Spring Hinges. (Journal of Applied Mechanics, 1975, 42, pp. 501 502)." Journal of Applied Mechanics 48, no. 2 (1981): 449-449.

[11] Goel, R. P. "Free Vibrations of a Beam-Mass System with Elastically Restrained Ends." Journal of Sound and Vibration 47, no. 1 (1976): 9-14.

[12] Rao, C. K. and S. Mirza. "A Note on Vibrations of Generally Restrained Beams." Journal of Sound and Vibration 130, no. 3 (1989): 453-465.

[13] Chun, K-R. "Free Vibration of a Beam With one End Spring-Hinged and the other Free." Journal of Applied Mechanics 39, no. 4 (1972): 1154-1155.

[14] Lv, B., W-L. Li, J. Dai, H-J. Zhou, F-X. Guo, and Z-B. Gao. "Vibration Analysis of Beams with Arbitrary Elastic Boundary Conditions." Applied Mechanics and Materials 66 (2011): 1325-1329.

[15] Kang, K-H., and K-J. Kim. "Modal Properties of Beams and Plates on Resilient Supports with Rotational and Translational Complex Stiffness." Journal of Sound and Vibration 190, no. 2 (1996): 207-220.

[16] Register, A. H. "A note on the vibrations of generally restrained, end-loaded beams." Journal of Sound and Vibration 172, no. 4 (1994): 561-571.

[17] Yen, T. C., and S. Kao. "Vibration of Beam Mass System with Time-dependent Boundary Conditions." ASME Journal of Applied Mechanics 26 (1959): 353-356.

[18] Laura, P. A., J. L. Pombo, and E. A. Susemihl. "A Note on the Vibrations of a Clamped-Free Beam With a Mass at the Free End." Journal of Sound and Vibration 37, no. 2 (1974): 161-168.

[19] Maurizi, M. J., R. E. Rossi, and J. A. Reyes. "Vibration Frequencies for a Uniform Beam with One End Spring-Hinged and Subjected to a Translational Restraint at the Other End." Journal of Sound and Vibration 48, no. 4 (1976): 565-568.

[20] Maurizi, M. J., D. V. Bambill de Rossit, and P. A. Laura. "Free and Forced Vibrations of Beams Elastically Restrained Against Translation and Rotation at the Ends." Journal of Sound and Vibration 120, no. 3 (1988): 626-630.

[21] Maurizi, M. J., R. E. Rossi, and J. A. Reyes. "Comments on A Note of Generally Restrained Beams." Journal of Sound and Vibration 147, no. 1 (1991): 167-171.

[22] Greif, R., and S. C. Mittendorf. "Structural Vibrations and Fourier Series." Journal of Sound and Vibration 48, no. 1 (1976): 113-122.

[23] Li, W. L. "Free Vibrations of Beams with General Boundary Conditions." Journal of Sound and Vibration 237, no.4 (2000): 709-725.

[24] Wang, J-S., and C-C. Lin. "Dynamic Analysis of Generally Supported Beams Using Fourier Series." Journal of Sound and Vibration 196, no. 3 (1996): 285-293.

[25] Yayli, M. O., M. Aras, and S. Aksoy. "An Efficient Analytical Method for Vibration Analysis of a Beam on Elastic Foundation with Elastically Restrained Ends." Shock and Vibration, vol. 2014, Article ID 159213, 7 pages, 2014. doi:10.1155/2014/159213

[26] Lin, Y. K. "Free Vibrations of a Continuous Beam on Elastic Supports." International Journal of Mechanical Sciences 4, no. 5 (1962): 409-423.

[27] Lai, H-Y., J-C. Hsu, and C-K. Chen. "An Innovative Eigenvalue Problem Solver for free Vibration of Euler-Bernoulli Beam by using the Adomian Decomposition Method." Computers & Mathematics with Applications 56, no. 12 (2008): 3204-3220.

[28] Mao, Q. "Free Vibration Analysis of Elastically Connected Multiple-Beams by Using the Adomian modified Decomposition Method." Journal of Sound and Vibration 331, no. 11 (2012): 2532-2542.

[29] Failla, G., and A. Santini. "A solution Method for Euler-Bernoulli Vibrating Discontinuous Beams." Mechanics Research Communications 35, no. 8 (2008): 517-529.

[30] Bilello, C., and L. A. Bergman. "Vibration of Damaged Beams Under a Moving Mass: Theory and Experimental Validation." Journal of Sound and Vibration 274, no. 3 (2004): 567-582.

[31] García-Garino C., A. E. Mirasso, M. A. Storti, and M. E. Tornello. "Vibraciones de Vigas y Pórticos Ante la Presencia de Fisuras. Implementación del Problema Inverso." Mecánica Computacional no. XXXII (2013): 1715-1735.

[32] Wang, J-L., and P-Z. Qiao. "Vibration of Beams with Arbitrary Discontinuities and Boundary Conditions." Journal of Sound and Vibration 308, no. 1 (2007): 12-27.

[33] Ratazzi, A. R., D. V. Bambill, and C. A. Rossit. "Free Vibrations of Beam System Structures with Elastic Boundary Conditions and an Internal Elastic Hinge." Chinese Journal of Engineering, vol. 2013, Article ID 624658, 10 pages, 2013. doi:10.1155/2013/624658

[34] Courant, R. "Variational Methods for the Solution of Problems of Equilibrium and Vibrations." Bull. Amer. Math. Soc 49, no. 1 (1943): 1-23.

[35] Huebner, K. H., and E. A. Thornton. "The Finite Element Method for Engineers, 1982." Wiley, New York.

[36] Zienkiewicz, O. C., and R. L. Taylor. "The Finite Element Method for Solid and Structural Mechanics". Butterworth-Heinemann, 2005.

[37] Salgado da Silva Oliveira, J. M. "Análise Modal Experimental Aplicada a um Componente Estrutural Automóvel." (2012). `http://hdl.handle.net/1822/22703`

[38] Fu, Z-F., and J-M. He. "Modal Analysis". Butterworth-Heinemann, 2001.

[39] Visser, W. J. "Updating Structural Dynamics Models Using Frequency Response Data." PhD Dissertation., University of London, 1992.

[40] Brown, D. L., and R. J. Allemang. "The Modern Era of Experimental Modal Analysis." Sound and Vibration 41, no. 1 (2007): 16-33.

[41] Mendes Maia, N. M., and J. M. Montalvão e Silva. "Theoretical and Experimental Modal Analysis". Taunton: Research Studies Press, 1997.

[42] Ewins, David J. "Modal Testing: Theory and Practice". Vol. 79. Letchworth: Research Studies Press, 1984.

[43] Fu, Z-F, and J-M He. "Modal Analysis". Butterworth-Heinemann, 2001.

[44] Cooley, J. W., and J. W. Tukey. "An Algorithm for the Machine Calculation of Complex Fourier Series." Mathematics of Computation 19, no. 90 (1965): 297-301.

[45] Mendes Maia, N. M. "Modal Identification Methods in the Frequency Domain." In Modal Analysis and Testing, pp. 251-264. Springer Netherlands, 1999.

[46] Bishop, R. E. D. "An Investigation into the Theory of Resonance Testing." Philosophical Transactions of the Royal Society of London. Series A, Mathematical and Physical Sciences, no. 1055 (1963): 241-80.

[47] Kennedy, C. C. "Use of Vectors in Vibration Measurement and Analysis." Journal of the Aeronautical Sciences (Journal of the Aeronautical Sciences) 14, no. 11 (1947): 603-625.

[48] Dobson, B. J. "Modal Analysis Using Dynamic Stiffness Data." 3rd International Modal Analysis Conference, Orlando, FL. (1985): 279-285

[49] Dobson, B. J. "A Straight-Line Technique for Extracting Modal Properties from Frequency Response Data." Mechanical Systems and Signal Processing 1, no. 1 (1987): 29-40.

[50] Mendes Maia, N. M. "Extraction of Valid Modal Properties from Measured Data in Structural Vibrations." PhD Dissertation, Imperial College London (University of London), 1988.

[51] Gaukroger, D. R., C. W. Skingle, and K.H. Heron. "Numerical Analysis of Vector Response Loci." Journal of Sound and Vibration 29, no. 3 (1973): 341-353.

[52] Ewins, D. J., and P. T. Gleeson. "A Method for Modal Identification of Lightly Damped Structures." Journal of Sound and Vibration 84, no. 1 (1982): 57-79.

[53] Brittingham, J. N., E. K. Miller, and J. L. Willows. "Pole Extraction from Real-Frequency Information." Proceedings of the IEEE 68, no. 2 (1980): 263-273.

[54] Schmerr, L. W. (1982), "A New Complex Exponential Frequency Domain Technique for Analysing Dynamic Response Data, Proceedings of the 1st International Modal Analysis Conference (IMAC I), Orlando, Florida, USA, 183-186.

[55] Juang, J-N., and H. Suzuki. "An Eigensystem Realization Algorithm in Frequency Domain for Modal Parameter Identification." Journal of Vibration, Acoustics Stress and Reliability in Design 110, no. 1 (1988): 24-29.

[56] Richardson, M. H., and D.L. Formenti. "Parameter Estimation from Frequency Response Measurements Using Rational Fraction Polynomials." In Proceedings of the 1st International Modal Analysis Conference, vol. 1, pp. 167-186. 1982.

[57] Fillod, R., G. Lallement, J. Piranda, and J. L. Raynaud. "Global Method of Modal Identification." In Proceedings of the 3rd IMAC Conference, Orlando, Florida, pp. 1145-1151. 1985.

[58] Zhang, L. and H. Kanda. "The Algorithm and Application of a New Multi-Input-Multi-Output Modal Parameter Identification Method." Shock and Vibration Bulletin, (1986): pp. 11-17

[59] Coppolino, R. N. "A Simultaneous Frequency Domain Technique for Estimation of Modal Parameters from Measured Data". No. 811046. SAE Technical Paper, 1981.

[60] Link, M., and A. Vollan. "Identification of Structural System Parameters from Dynamic Response Data." Zeitschrift fur Flugwissenschaften und Weltraumforschung 2 (1978): 165-174.

[61] Klosterman, A. L. "On the Experimental Determination and Use of Modal Representations of Dynamic Characteristics". Order No. 7216547, University of Cincinnati, 1971. http://search.proquest.com/docview/302560639? accountid=13360

[62] Leuridan, J., and J. Kundrat. "Advanced Matrix Methods for Experimental Modal Analysis-A Multi-Matrix Method for Direct Parameter Extraction." In Proceedings, International Modal Analysis Conference (1982): 192-200.

[63] Juang, J-N., and Richard S. Pappa. "An Eigensystem Realization Algorithm for Modal Parameter Identification and Model Reduction." Journal of Guidance, Control, and Dynamics 8, no. 5 (1985): 620-627.

[64] Spitznogle, F. R., and A. H. Quazi. "Representation and Analysis of Time-Limited Signals Using a Complex Exponential Algorithm." The Journal of the Acoustical Society of America 47, no. 5A (2005): 1150-1155.

[65] Vold, H., and G. T. Rocklin. "The Numerical Implementation of a Multi-Input Modal Estimation Method for Mini-Computers." In International Modal Analysis Conference Proceedings (1982): 542-548.

[66] Ibrahim, S. R., and E. C. Mikulcik. "A Time Domain Modal Vibration Technique." The Shock & Vibration Bulletin, vol. 46(5) (1976): 187-196.

[67] Gersch, Will. "Estimation of the Autoregressive Parameters of a Mixed Autoregressive Moving-Average Time Series." Automatic Control, IEEE Transactions on 15, no. 5 (1970): 583-588.

[68] Gersch, W., N. N. Nielsen, and H. Akaike. "Maximum likelihood estimation of structural parameters from random vibration data." Journal of Sound and Vibration 31, no. 3 (1973): 295-308.

[69] Leuridan, J., and H. Void. "A Time Domain Linear Model Estimation Technique for Multiple-Input Modal Analysis." In Modal Testing and Model Refinement: Presented by the Winter Annual Meeting of the American Society of Mechanical Engineers, Boston, Massachusetts, November 13-18, (1983): 51. American Society of Mechanical Engineers, 1983.

[70] Juang, J-N, and M-Q. Phan. "Identification and Control of Mechanical Systems". Cambridge University Press, 2001.

[71] Allemang, R. J. "The Modal Assurance Criterion-Twenty Years of Use and Abuse." Sound and Vibration 37, no. 8 (2003): 14-23.

[72] Lieven, N. A. J., and D. J. Ewins. "Spatial Correlation of Mode Shapes, the Coordinate Modal Assurance Criterion (COMAC)." In Proceedings of the 6th international Modal Analysis Conference, vol. 1 (1988): 690-695.

[73] Heylen, W., and S. Lammens. "FRAC: a Consistent Way of Comparing Frequency Response Functions." In Proceedings of the Conference on Identification in Engineering Systems, (1996): 48-57.

[74] Fotsch, D., and D. J. Ewins. "Application of MAC in the Frequency Domain." ROLLS ROYCE PLC-REPORT-PNR (2000).

[75] Heylen, Ward, and Theo Janter. "Extensions of the modal assurance criterion." Journal of Vibration and Acoustics 112, no. 4 (1990): 468-472.

[76] Brechlin, E., K. Bendel, and W. Keiper. "A New Scaled Modal Assurance Criterion for Eigenmodes Containing Rotational Degrees of Freedom." In Proceedings of the International Seminar on Modal Analysis, vol. 3, (1999): 1175-1182. Katholieke Universiteit Leuven

[77] Messina, A., I. A. Jones, and E. J. Williams. Proceedings of Conference on Identication in Engineering Systems, Swansea, U.K., 67/76. "Damage detection and localisation using natural frequency changes"

[78] Messina, A., T. Contursi, and E. J. Williams. "Multiple Damage Evaluation Using Natural Frequency Changes." Proceedings of the 15th International Modal Analysis Conference 1, (1997): 658-664

[79] Koh, B. and S. J. Dyke. "Structural Health Monitoring for Flexible Bridge Structures using Correlation and Sensitivity of Modal Data. Computers & Structures, (3-4), (2007): 117-130.

[80] Pandey, A. K., and M. Biswas. "Damage Diagnosis of Truss Structures by Estimation of Flexibility Change." Modal Analysis-The International Journal of Analytical and Experimental Modal Analysis 10, no. 2 (1995): 104-117.

[81] MATLAB Release 2013a, The MathWorks, Inc., Natick, Massachusetts, United States.

[82] Wikipedia contributors, "Engineering Design Process," Wikipedia, The Free Encyclopedia, `http://en.wikipedia.org/wiki/Engineering\_design\_process`

[83] Avitabile, P. "Modal Space-In Our Own Little World." Experimental Techniques 37, no. 2 (2013): 3-5.

[84] Chazi, Eleni. "Identification Methods for Structural Systems." Course Lectures. `http://www.vvz.ethz.ch/Vorlesungsverzeichnis/dozentPre.do?semkez=2014S&dozide=10005329&ansicht=2&lang=en` Eidgenössische Technische Hochschule Zürich, 2013.

[85] Chopra, Anil K. Dynamics of structures. Vol. 3. New Jersey: Prentice Hall, 1995.

VITA

VITA

CHRISTIAN E. SILVA

CAREER OBJECTIVE

A Master of Science in Mechanical Engineering with concentration in Structural Dynamics & Vibrations, and Control Systems.

EDUCATION

Purdue University Master of Science in Mechanical Engineering. Candidate August 2014. Grade Point Average 3.43 on a 4.00 scale

Escuela Superior Politécnica del Litoral, Ecuador. Mechanical Engineer. February, 2002. Grade Point Average 7.11 on a scale of 10.

WORK EXPERIENCE Ecuasteel S. A., Guayaquil-Ecuador August 2004 - July 2012

- Industrial machinery construction project management.
- General management tasks for manufacturing department and administrative areas.

IIASA-CAT, Guayaquil-Ecuador August 2002 - August 2004

- Engine Technical Department Supervisor.

HONORS AND ACTIVITIES

- Ecuadorians at Purdue University Association - President 2014 - Present.
- Secretaría Nacional de Ciencia, Tecnología e Innovación, Ecuador (National Secretary of Science Tecnology, and Innovation Ecuador) - Universities of Excellence Scholarship Program. Grantee, Aug 2011.